4. SEA ICE AND SNOW MEASUREMENTS

Melinda Webster[1], Benjamin Lange[2], Gerit Birnbaum[3], Felix Linhardt[4], Amy Macfarlane[5], Mallik Mahmud[6], Ilkka Matero[3], Ian Raphael[7], Julia Regnery[3], Aikaterini Tavri[8], Luisa von Albedyll[3], Evgenii Salganik[9], Igor Sheikin[10], Madison Smith[11], Marcel Nicolaus[3] (not on board), Don Perovich[7] (not onboard), Gunnar Spreen[12] (not on board)

[1]U. Alaska Fairbanks
[2]NPI
[3]AWI
[4]CAU Kiel
[5]WSL/SLF
[6]U. Calgary
[7]Dartmouth College
[8]U. Victoria
[9]NTNU
[10]AARI
[11]U. Washington
[12]U Bremen

Grant-No. AWI_PS122_00

A comprehensive summary of the sea ice and snow measurements during all 5 cruise legs can be found in Nicolaus et al., 2022.

The snow and sea ice measurements during PS122/4 continued the MOSAiC sea ice program of the previous three legs, with an expansion of the optics component and the addition of cross-team activities (see Table 4.1). These measurements were carried out by a team of 14 scientists beginning on 13 June with an ice station en route to the MOSAiC Central Observatory.

***Tab. 4.1**: The Leg 4 ICE Team Program*

Subchapter	Component of the Leg 4 Sea Ice Program
4.1	Ice Coring
4.2	Snow and Surface Characterization
4.3	Helicopter (ALS and EM-bird)
4.4	Terrestrial Laser Scanner
4.5	Transect
4.6	ROV
4.7	Optics
4.8	Stakes
4.9	Ridges
4.10	Ice Dynamics
4.11	Remote Sensing
4.12	Melt ponds
4.13	Freshwater Lens
4.14	Supporting Observations

Upon arrival to the Central Observatory on 17 June, the fortress floe was selected for the reinstallation of the field program. The floe consisted of level, first-year ice and sediment-laden, second-year ice, both of which enabled comparative time-series measurements of both ice types during the summer melt season. Due to some time-series sites (e.g., second-year ice coring) having fractured and drifted away at the end of Leg 3, new time-series sites were established at the beginning of the camp reinstallation period.

Between 17 June and 31 July, sea-ice and weather conditions were characterized by stable ice dynamics, persistent fog, and extensive melt. The initial state of the surface was a ripened snowpack with pools of melt water underneath. Melt ponds were present, but in the early stage of development. The melt ponds grew rapidly in depth and coverage, creating challenging conditions for on-ice work and infrastructure maintenance. Between 7 and 17 July, major drainage events occurred across the Central Observatory, providing an opportunity to measure the effects of heightened freshwater input, including freshwater lens and false bottom formations. The combination of poor visibility, ship motion, and frequent polar bear visits disrupted on-ice activities and caused power outages, but these had minimal effects on the ability to accomplish core measurements in the weekly plan. In the final week at the floe, on-ice measurements and instrument recovery were conducted in parallel until 30 July, one day before the floe broke apart. The remainder of the program was dedicated to instrument recovery at L- and M-sites in the Distributed Network.

For an overview of the ICE program accomplishments and selected measurement summaries during Leg 4, please see Figures 4.1 and 4.2.

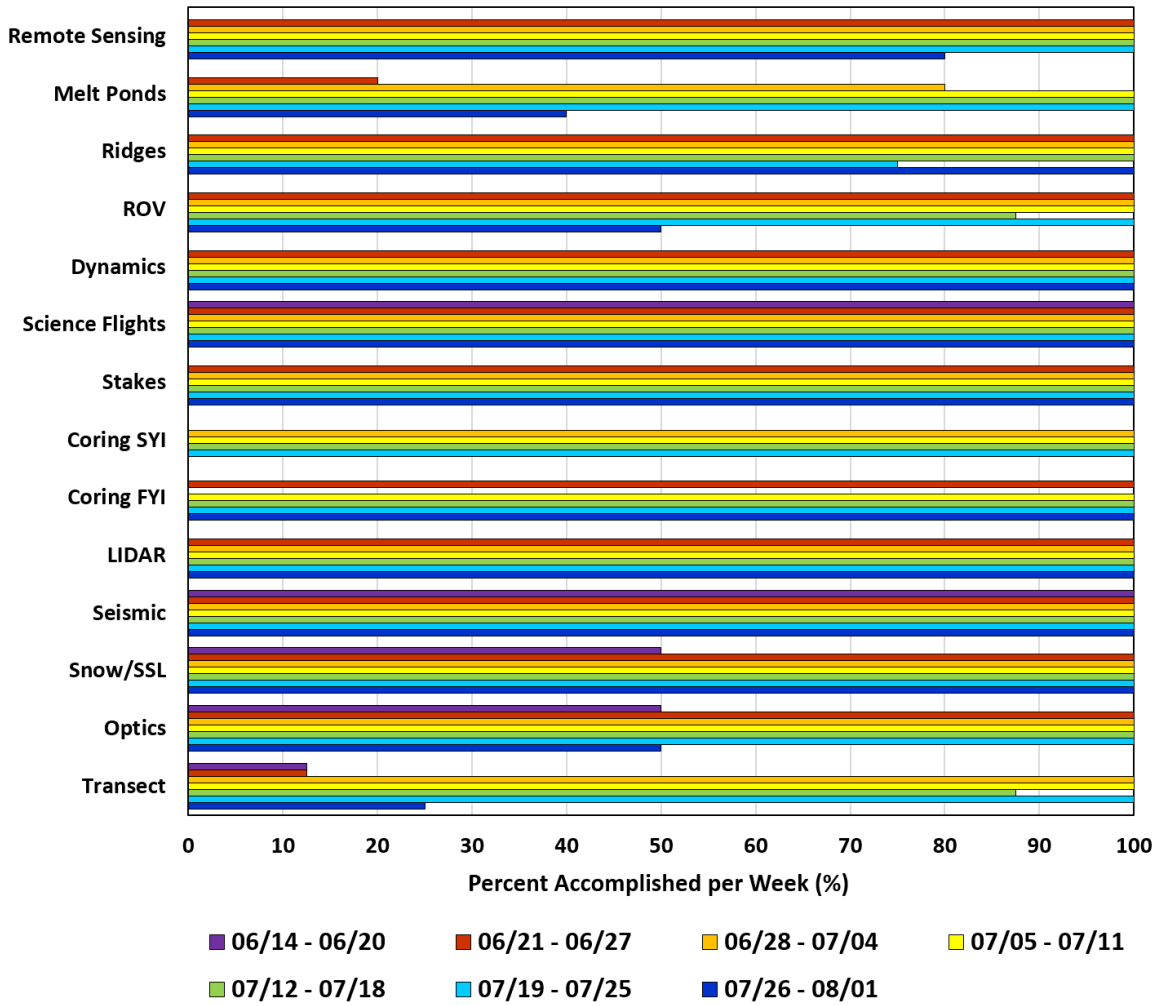

Fig. 4.1: *The percent accomplished of each (ICE Team) science task per week based on the weekly plan. The field camp was fully established during week 21-27 June and evacuated on week 26 July – 1 August. Frequent polar bear encounters, poor visibility, and ship motion had minimal impact on the ICE Team science program during Leg 4.*

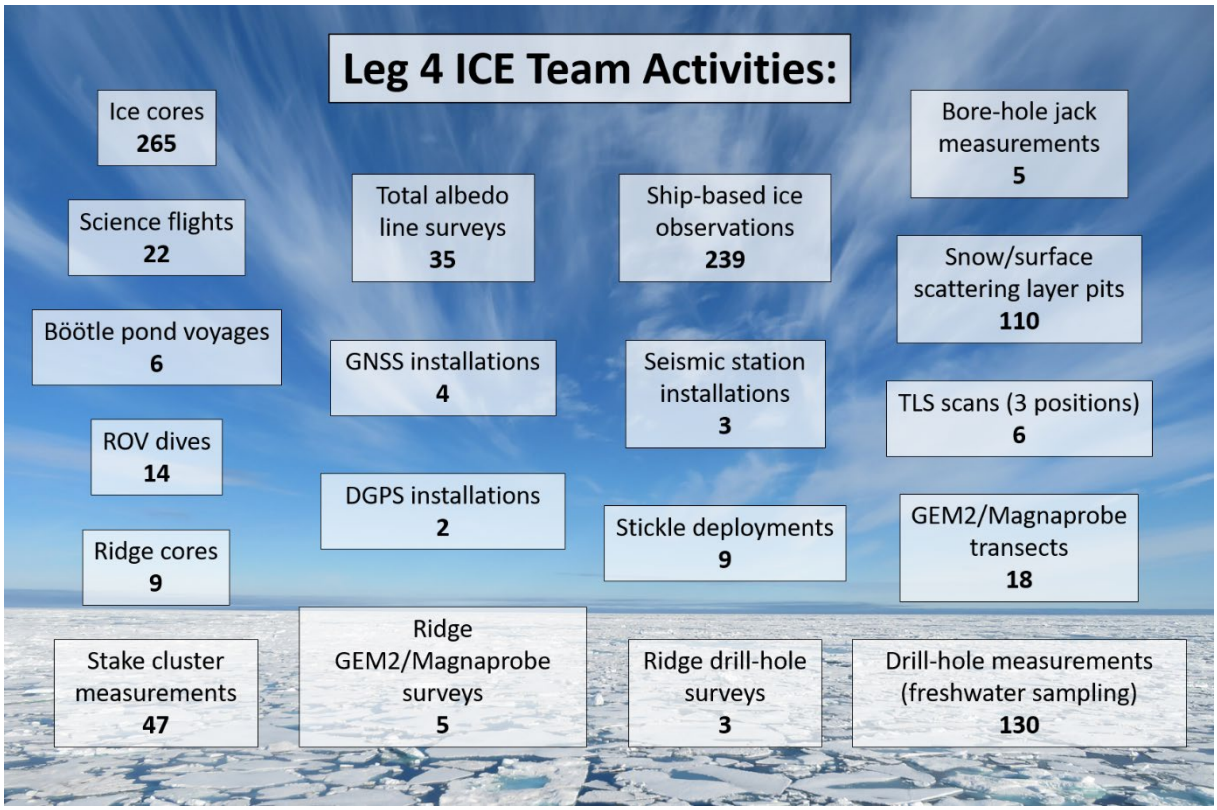

Fig. 4.2: *Measurement summaries from the science tasks of the Leg 4 ICE Team. Background photo: Luisa von Albedyll.*

References

Nicolaus, M, Perovich, DK, Spreen, G, Granskog, MA, Albedyll, LV, Angelopoulos, M, Anhaus, P, Arndt, S, Belter, HJ, Bessonov, V, Birnbaum, G, Brauchle, J, Calmer, R, Cardellach, E, Cheng, B, Clemens-Sewall, D, Dadic, R, Damm, E, de Boer, G, Demir, O, Dethloff, K, Divine, DV, Fong, AA, Fons, S, Frey, MM, Fuchs, N, Gabarró, C, Gerland, S, Goessling, HF, Gradinger, R, Haapala, J, Haas, C, Hamilton, J, Hannula, H-R, Hendricks, S, Herber, A, Heuzé, C, Hoppmann, M, Høyland, KV, Huntemann, M, Hutchings, JK, Hwang, B, Itkin, P, Jacobi, H-W, Jaggi, M, Jutila, A, Kaleschke, L, Katlein, C, Kolabutin, N, Krampe, D, Kristensen, SS, Krumpen, T, Kurtz, N, Lampert, A, Lange, BA, Lei, R, Light, B, Linhardt, F, Liston, GE, Loose, B, Macfarlane, AR, Mahmud, M, Matero, IO, Maus, S, Morgenstern, A, Naderpour, R, Nandan, V, Niubom, A, Oggier, M, Oppelt, N, Pätzold, F, Perron, C, Petrovsky, T, Pirazzini, R, Polashenski, C, Rabe, B, Raphael, IA, Regnery, J, Rex, M, Ricker, R, Riemann-Campe, K, Rinke, A, Rohde, J, Salganik, E, Scharien, RK, Schiller, M, Schneebeli, M, Semmling, M, Shimanchuk, E, Shupe, MD, Smith, MM, Smolyanitsky, V, Sokolov, V, Stanton, T, Stroeve, J, Thielke, L, Timofeeva, A, Tonboe, RT, Tavri, A, Tsamados, M, Wagner, DN, Watkins, D, Webster, M, Wendisch, M. 2022. Overview of the MOSAiC expedition: Snow and sea ice. *Elementa: Science of the Anthropocene* 10(1). DOI: https://doi.org/10.1525/elementa.2021.000046

4.1 Ice Coring

Evgenii Salganik[1], Benjamin Lange[2], Allison Fong[3], Igor Sheikin[4], Giulia Catellani[3], Emelia Chamberlain[5], Jessie Gardner[6], Oliver Muller[7], Deborah Bozzato[8], Mats Granskog[2] (not onboard), Sønke Maus[1] (not onboard)

[1] NTNU
[2] NPI
[3] AWI
[4] AARI
[5] USCD
[6] UiT
[7] UiB
[8] RUG

4.1.1 Objectives

Within the general coring objectives (see 8.5 Coring – *NOT AVAILABLE*), the ICE Team is responsible for the ice physics properties analysis (temperature, salinity, density, and microstructure).

4.1.2 Work at sea

Each general coring event consisted of two teams with four scientists each, made up of members from the ICE, ECO, and BGC Teams. Once per week, when weather and ice conditions allowed, these teams would sample from the old „Dark Site First Year Ice“ (FYI) and newly established „Dark Site Second Year Ice“ (SYI) sites. Between 26 and 30 (21 and 22), cores were collected each week from the FYI (SYI) site, depending on the processing capability of the different teams each week. Team ICE planned for 8-9 cores each week, with 4 high priority cores: temperature (TEMP), salinity and oxygen isotopes (SALO18), density (RHO), and microCT (CT).

On week 45, coring sessions at the FYI coring site encountered melt pond formation, which necessitated the move of the sampling area across the site to bare ice areas. Melt pond formation and drainage additionally led to the formation of a freshwater lens and false bottom layers under the FYI, making thickness measurements challenging. At the beginning of Leg 4, the average FYI thickness was 1.60 m, while during the last week of measurements, it was 1.10 m, yielding ~0.1 m of ice loss per week due to melt. The new SYI coring site was moved close to Alli’s Ridge because the original SYI coring site was inaccessible from the main floe. The SYI thickness remained nearly constant during Leg 4 in the range of 2.1-2.2 m except in week 47, when the SYI thickness was 2.6 m, presumably due to local-scale heterogeneity.

Upon returning from coring in the field, the microCT samples were centrifuged and imaged using an x-ray computed tomography (CT) technique within 24 hours. Cores for the MOSAiC repository, backup, texture, plastic, sediment, optics, and the upper part of the CT core were sealed in plastic sleeves and stored at -20 °C. Density was measured at -15 °C by densitometry in paraffin in the freezer lab using a Kern EMB-V scale. Salinity and bulk salinity were measured on the melted samples and remaining water, respectively, with a conductivity probe Mettler Toledo SevenGo by the ICE Team. After the ECO Team melted salinity samples (SALO18 core) for nutrient analysis, the samples were measured for salinity using a conductivity probe YSI 30 by the ICE Team and bottled for future isotope measurement. According to the initial work plan, texture cores were supposed to be processed into horizontal and vertical thin sections onboard. This was not done due to time and personnel constraints. However, texture cores were taken from both sites each week and stored at -20 °C for future analysis.

4.1.3 Preliminary (expected) Results

The ice coring team of Leg 4 successfully continued – and expanded – the coring activity at the FYI and SYI sites. Due to an increased interest in core samples from the ECO and BGC teams over prior legs, Leg 4 had more people available for coring and was able to visit both sites simultaneously each week. Coring events on week 49 were cancelled due to bad visibility, but the FYI coring was successfully performed later that week. During week 50, the MOSAiC ice floe was already broken into several floes and inaccessible. Out of the six working weeks of Leg 4 (which do not include transition, handover and pack-up), the Dark Sites were visited on six occasions: three times to both FYI and SYI sites, twice to just FYI, and once to just SYI. In addition to the Dark Site coring, team ICE was able to core four times at the Jaridge and once at the Alli's ridge. Table 4.1.1 presents a list of cross-disciplinary and ICE team coring sessions together with the total number of recovered ice cores.

Tab. 4.1.1: *Cross-disciplinary and ICE team coring events at Dark Sites and other sites around the CO during Leg 4.*

Date of Coring	Activity Week	Site	MCS Action # for 9cm Corer (7cm corer)	# of Recovered Cores
13.06.2020	4_44	Ice Station	42 (-)	9
14.06.2020	4_44	Ice Station	58 (59)	3
22.06.2020	4_44	FYI	134 (135)	26
30.06.2020	4_45	SYI	29 (30)	22
03.07.2020	4_45	Jaridge	131 (-)	4
06.07.2020	4_46	FYI	18 (19)	29
06.07.2020	4_46	SYI	20 (21)	21
10.07.2020	4_46	Jaridge	178 (179)	5
11.07.2020	4_46	Remote Sensing	100 (-)	4
13.07.2020	4_47	FYI	16 (17)	27
13.07.2020	4_47	SYI	18 (19)	21
15.07.2020	4_47	Alli's Ridge	157 (158)	3
18.07.2020	4_47	Jaridge	199 (245)	4
20.07.2020	4_48	FYI	23 (24)	30
20.07.2020	4_48	SYI	25 (26)	21
24.07.2020	4_48	Jaridge	229 (277)	5
27.07.2020	4_49	FYI	102 (-)	1
27.07.2020	4_49	SYI	101 (-)	1
27.07.2020	4_49	Remote Sensing	- (103)	1
29.07.2020	4_49	FYI	34 (35)	28

The last reported average FYI thickness during Leg 3 was 162 cm (04.05.2020). At the FYI coring site, the ice melted from 159 cm to 107 cm over 5 weeks between the first coring of Leg 4 (22.06.2020) and the last coring of Leg 4 (29.07.2020). Similar to the old SYI coring site, the SYI at the new coring site consisted of a refrozen melt pond about 70 cm to 120 cm thick with new ice that formed below and was located in an area with rafted ice (see profiles for 13.07.2020). Figure 4.1.1 below shows the evolution of the salinity, temperature, and density profiles acquired from the FYI and SYI sites.

Due to warm weather, FYI started to deviate from the C-shape salinity profiles before the start of the Leg 4. Both the top and bottom sections of FYI cores were losing salt due to gravity drainage. After week 44, the FYI area started forming melt ponds, which increased rates of top gravity drainage and led to the formation of a freshwater lens underneath the FYI coring site.

The salinity of this lens was 6 ppt during week 47. The presence of this lens changed the salinity of the brine in the bottom part of the FYI coring site and increased rates of bottom desalinization until week 49. Several false bottom layers were observed and collected from weeks 45 to 49 (see also section 4.13 Freshwater Lens and False Bottom).

Salinity profiles for SYI were almost unchanged during Leg 4, with low salinities (under 0.5 ppt) in the upper 140 cm and linearly increasing salinities with decreasing depth to 3-4 ppt (Fig. 4.1.1).

The coring sessions of Leg 4 had 1 m air temperatures close to 0°C. Due to already high sea ice temperatures, the FYI temperatures slowly approached 0°C near the surface, while the bottom temperatures approached the freshwater lens temperatures in the range of 0-0.5°C. The temperatures of SYI remained mostly constant during Leg 4.

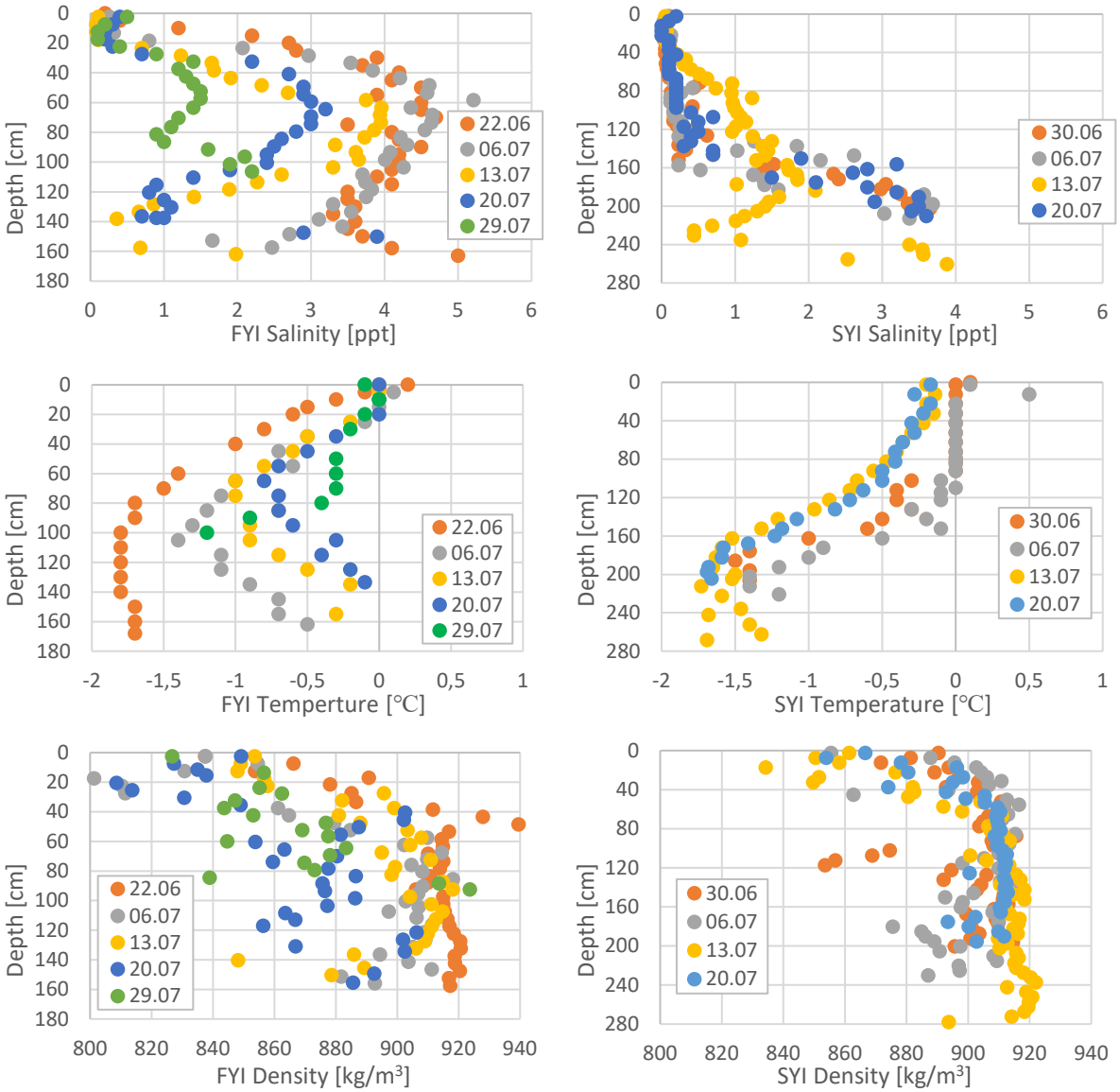

Fig. 4.1.1: *Evolution of salinity, temperature and density profiles over a 5-week (4-week) period of observations during Leg 4 for first-year ice (second-year ice).*

In the framework of the MOSAiC HAVOC project, ridge coring was conducted twice during Leg 4 on activity weeks 4_45, 4_46, 4_47, and 4_48. Given the inaccessibility of the Sea Ice Ridge Observatory (SIRO) Fort Ridge, ECO Ridge “Ridgey McRidgeFace”, and significant distance to Alli’s ridge, a new ridge was selected for coring and given the name “Jaridge.” The goal for the coring was to locate water-filled gap layers in the ice where seawater could be pumped and later analyzed by the ECO Team. The ICE Team took cores during both weeks for temperature, salinity/isotope analysis, and density. Alli’s Ridge was visited twice for ice physics cores and thickness drilling, which was further supported by thickness transect, snow pit, and surface characterization measurements. Further work at ridges in the CO during Leg 4 is described in Section 4.9.

4.1.4 Data Management

All data are handled, documented, archived and published following the MOSAiC data policy (see APPENDIX). All data related to each coring event are located on the MCS within the folder of the device operation corresponding to the deployment of the corer Kovacs Mark II, 9 cm. A scanned copy of the field notes and laboratory book have also been included in these folders. The exhaustive list includes:

- Primary data (when available) for each ICE, ECO, and BGC core transcribed into a spreadsheet (section depths, ice thickness, ice draft, weather, date and time, etc.)
- Salinity and density measured on board within 2-5 days of the coring
- Tomographic imagery of two bottom-most 5-cm ice sections of microCT cores together with 0-5 cm and 15-20 cm depth sections of density cores are available on the MCS within a separate subfolder contained in the folder of the X-ray tomographer Scanco90.

Data will be stored at the PANGAEA data repository: World Data Center PANGAEA Data Publisher for Earth & Environmental Science www.pangaea.de. All data are handled, documented, archived and published following the MOSAiC data policy. DOIs will be communicated to PANGAEA for later access via the future MOSAiC Data Portal.

4.2 Snow and Surface Characterisations

Amy Macfarlane[1], Aikaterini Tavri[2], Maddie Smith[3], Mallik Mahmud[5], Chris Polashenski[4] (not onboard), Martin Schneebeli[1] (not onboard)

[1] WSL/SLF
[2] UVictoria
[3] UW Seattle
[4] Dartmouth
[5] CA.UCalgary

4.2.1 Objectives

The overarching goal of the snow measurements and surface characterisations is to document the spatially and temporally varying porous medium of the snow cover and surface scattering layer. This is conducted with the view of improving models and in support of all MOSAiC inquiries from the ATMOS, BGC, and ECO Teams, as well as the Optics and Remote Sensing programs of the ICE Team. We refer to the cruise reports of Legs 1, 2 and 3 for details. Core parameters are divided into physical; depth, temperature, snow water equivalent, density, specific surface area and chemical: see below subheading Chemical sampling.

4.2.2 Work at sea

Conducted work can be structured in the following sub-tasks:

1. Pits and transects
2. Snow chemical sampling
3. Terrestrial Laser Scanning (TLS) of the snow surface (see TLS section)
4. Lab work

4.2.2.1 Snow pits

The snowpit locations on the central MOSAiC floe (commonly known as the Fortress on previous legs) are shown in Figure 4.2.4. All events are documented in DSHIP as device "snowpit." Physical surface analysis was conducted alongside the following activities:

- Remote sensing
- Optics
- Ridges
- Coring
- Transects

In total, 110 snowpit events were realized on Leg 4. This included 7 A-, 21 B-, 7 C-, 11 D- and 64 uncategorized pits.

The A-pits were conducted weekly or bi-weekly, B-pits were conducted when there was a limitation in time and the snowpit team consisted of one person, C-pits were conducted early in the leg as later the SnowMicroPen (SMP) was not useful when capturing the Surface Scattering Layer (SSL), the new ‘D’ pit included microCT (uCT) sampling and was set-up for opportunistic ‘special samples.’ The 64 uncategorized mainly included near infrared (NIR) images and MicroComputerTomograph (µCT) samples and were frequently done alongside optics measurements. These uncategorised pits also include Aikaterini Tavri’s snowpits at Remote Sensing conducted once or twice daily. See section 4.11 on Remote Sensing.

Due to limitations in undisturbed areas around the floe resulting in fewer A-pits, chemical transects were one way to understand the chemical distributions around the floe. Two transects along the Leg 4 Transect Loop, one Jaridge Ridge transect and one optics transect were executed on Leg 4.

Returning to old sites was extremely difficult due to the equipment and logistical demands of 'floe hopping.' This was only possible once at Snow2-A2, twice at the radiation station on Northern Transect Loop, and twice at the second-year ice (SYI) optics albedo line from Leg 3 between ROV and the radiation station on the Northern Transect Loop. This was due to their locations being situated on neighbouring floes. The first-year ice (FYI) coring site was the only remaining site from Leg 3 on the central floe. This site was only accessible after a melt pond had drained.

Each snowpit measures about 1 m in width. The spatial variability of the physical properties within a meter-scale was not large. However, on a 5 m scale, a melt pond was often encountered.

We did not use and suggest to skip the following measurements in A-pits: SLF-density and wetness sensor (salinity and uneven snow surface affects readings) and InfraSnow (prototype not available). Snow wetness was estimated traditionally using the snow water equivalent (SWE) ETH tube and a permittivity probe at the remote sensing site.

Throughout Leg 4, the MOSAiC floe went through the following changes which affected the observed surface structures:

- Arrival at the beginning of summer, when snow melt-crystals dominated the landscape.
- Level areas with extensive melt ponding and slushy snow with high liquid water content. Surface characterisations were only possible on ridged sites.
- Observed large drainage events as the ice structure became more porous and melt ponds became inter-connected. Drainage removed much of the surface water, which corresponded to a large reduction in melt pond area.
- Structures of drained melt pond bottoms started to appear (Fig. 4.2.1). Areas of the floe started to darken as the sediment appeared due to surface melt.

Fig 4.2.1: *NIR image of a drained melt pond bottom on second-year ice. Photo: A. Macfarlane.*

- Slight undulations in the topography were enhanced as islands and melt ponds became distinct features.
- Conducted some snow on/off experiments, which confirmed that the surface we were seeing was the surface scattering layer. See figure 4.2.2.

Fig 4.2.2: *snow on/off experiment.*

- A few sunny days and the melt ponds started to deepen and melt undercut the pond edges shown in figure 4.2.3. The floe rapidly reduced in thickness due to bottom melt.

Fig 4.2.3: *Melt ponds with undercut edges on first-year ice. Photo: A. Macfarlane*

The drainage events were extremely important for surface characteristics and understanding the surface scattering layer and albedo on FYI. After the drainage events occurred, the previously submerged ice surface re-appeared. When the ice surface is exposed to temperatures close to 0°C and there is good drainage, it becomes extremely porous and small pillar-like structures on the ice surface emerge. This structure is the SSL and has a large influence on the albedo.

The specific surface area (SSA) of the SSL is spatially heterogenous, and NIR-box surface imaging resulted in more consistent and relevant results than point sampling. The 44 mm diameter µCT sample holder was never used, except for individual high-resolution snow structures. Due to the fragility of the SSL, the surface was almost always sampled using the 88 mm diameter and the bulk profile was sampled with 68 mm.

SYI ridge sites, or areas with high snow accumulation, experienced different changes on the surface. The snow at these sites quickly rounded, which was a high contrast to the depth hoar during previous legs. These rounded grains remained until quite late in the leg and depending on the drainage of these areas, different structures formed, including ‘jewel snow.’

Tab. 4.2.1 *Details of each unique snowpit ID.*

	Snowpit ID	Comments
1	AlisRidge-Transect-Left	SMP transect.
2	AlisRidge-Transect-Middle	SMP transect.
3	AlisRidge-Transect-Right	SMP transect.
4	Chemical-perimeter-transect	Joined the Leg 4 Transect Loop team and stopped every 100 Magnaprobe measurements for a select number of samples.
5	DS-A7*	A regular timeseries. Missed a few weeks due to a large melt pond spanning the area. After this drained, the site was visited weekly alongside FYI coring team.
6	Jaridge	A-pit and 'mini A-pits' conducted along a transect.
7	Jaridge-transect	SMP transect.
8	Met-City-Ridge	Revisited after fresh snow in the first few weeks and often visited for A-pits.
9	optics-ECO	An on/off pit experiment conducted next to ECO lodge. NIR and µCT alongside L-Arm and ASD albedo measurements. A level FYI area but the ice thickness was not uniform.
10	optics-LDL	A key timeseries for albedo measurements. Visited weekly with the NIR camera. Images were taken every 20 m along the 200 m albedo line.
11	optics-METcity	Visited during the 24-hour sampling period and in the final week for destructive sampling alongside Kipps and ASD measurements.
12	optics-RB	Destructively sampled in final week alongside Kipps and ASD measurements.
13	optics-stern	Visited during the 24-hour sampling period, but erosion of ice edge lead to its termination at the end of PS122/4_47.
14	optics-transect-ROV	µCT samples conducted early in the leg, but not revisited frequently.
15	optics-transect-SYI	Visited in week PS122/4_47 for radiation station snowpit and recovery operation, managed to visit final two points on same floe. Unfortunately the rest has broken away.
16	Port	Conducted on transit.
17	Port-transect	Conducted on transit.
18	radiation-stn	B-pit as a continuation from the timeseries from Leg 3.
19	RS5-A1	Remote Sensing pit A1.
20	RS5-A2	Remote Sensing pit A2
21	RS5-A3	Remote Sensing pit A3
22	RS5-A4	Remote Sensing pit A4
23	RS5-K	Remote Sensing pit K
24	RS5-K1	Remote Sensing pit K1
25	RS5-K2	Remote Sensing pit K2
26	RS5-K3	Remote Sensing pit K3
27	RS5-K4	Remote Sensing pit K4
28	RS5-transect	Destructive sampling in front of L-Scat during final week.
29	Snow2-A2	Visited once during a clean-up mission for µCT samples.
30	Special-MicroCT	Dship events are now required for opportunistic µCT samples - this is the event ID for these 'special samples'.
31	Starboard-transect	Conducted on transect.
32	SYI-behindAlisRidge	When FYI site was ponded, the site was visited with the SYI coring team in weeks 45 and 46.

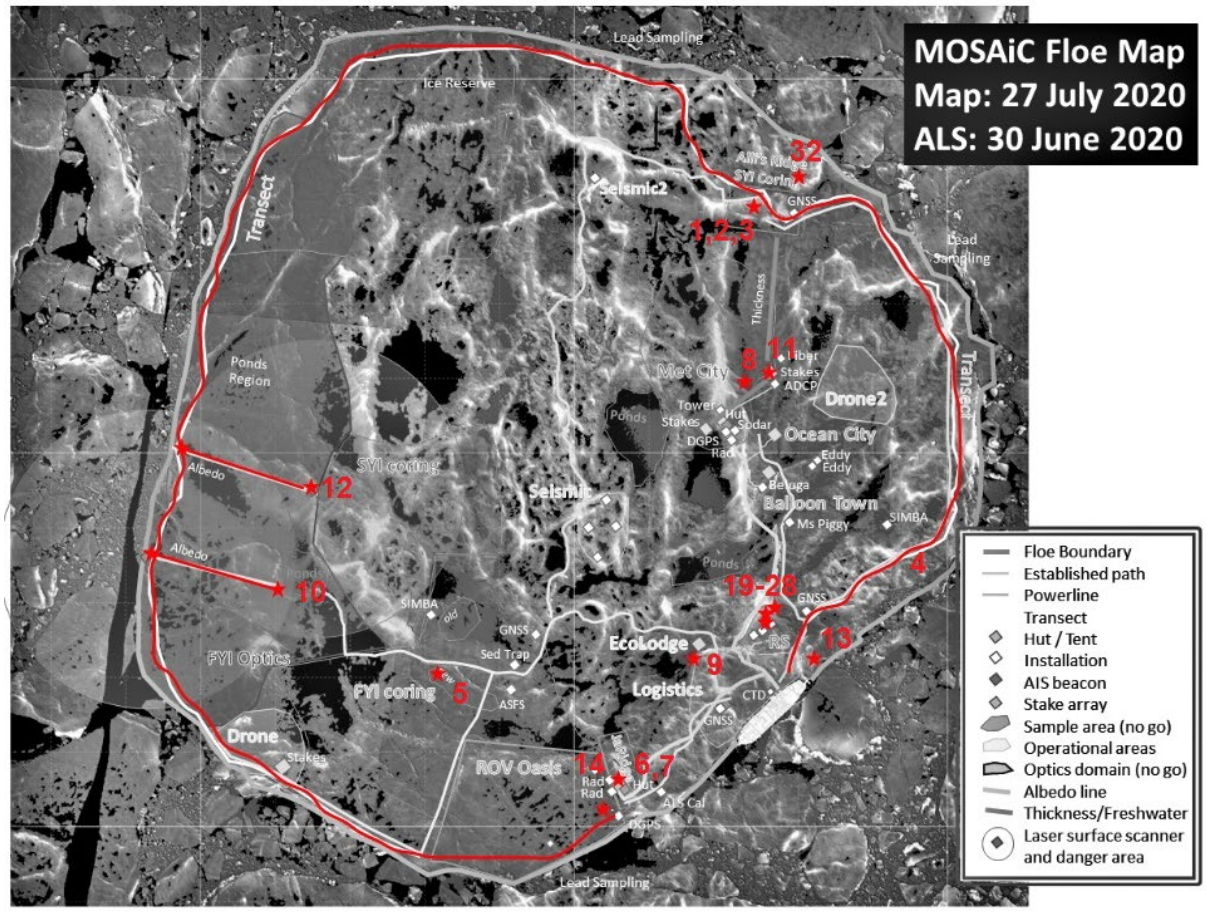

Fig. 4.2.4: *Floe map (state 2020-08-06) with locations of the snow pits and snow transect. See Table 4.2.1 for unique location identifier.*

4.2.2.2 Remote sensing

Remote sensing pit ($RS5$) began quickly as remote sensing was set-up in week PS122/4_44. The snowpit was relocated a few times due to space limitations, equipment manoeuvres and melt pond development in the site. An overview of the snowpit locations can be seen in Figure 4.2.5. Remote sensing was visited once, sometimes twice daily. This was mainly for temperature, traditional density and permittivity measurements and twice a week for a B-pit. Due to $RS5$ being located in close proximity to the logistics area, an initial A-pit was conducted to act as a 'dirty' reference for chemical samples. In the final days of the MOSAiC floe, an SMP and NIR transect was taken as part of a $RS5$ SSL on/off experiment in front of L-scat.

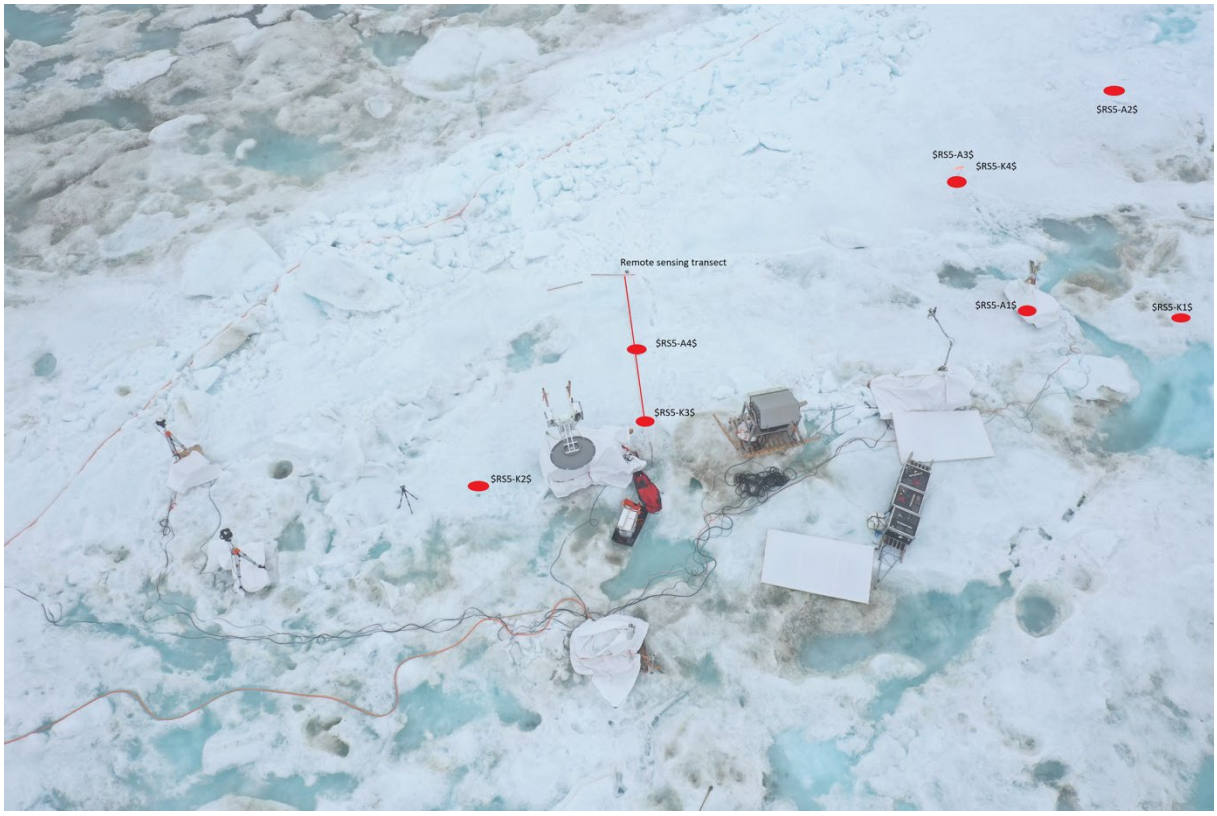

Fig 4.2.5: *An aerial image of the remote sensing site. Photo: J. Hamilton.*

4.2.2.3 Optics

The following event IDs consisted of surface characterisations alongside optics:

- Optics-LDL: Lemon drop line on FYI. To reduce site disturbance, the measurements were not conducted directly under the ASD and Kipps measurement area, but off to the side in a similarly covered area.
- Optics-transect-ROV: FYI above ROV optics grid. µCT samples taken just outside the ASD footprint
- Optics-stern: A mix of FYI and SYI. A main focus for the 24h sampling period- included two on/off surface experiments and one SYI drained melt pond.
- Optics-METcity: A SYI site. Visited twice, the final was destructive as NIR was in the footprint of the ASD and KIPPS.
- Optics-transect-SYI: SYI site. Visited by kayak, unfortunately only the final two markers remained on the same floe.

- Optics-ECO: Rafted FYI area. An on/off surface experiment visited multiple days in a row alongside L-arm and ASD.
- Optics-RB: FYI area. Optics Root Beer Barrel albedo line was destructively sampled at the end of the leg.

Fig 4.2.6: *The NIR in action. This was used vertically to characterise the NIR reflectivity of the SSL. Photo: A. Macfarlane.*

4.2.2.4 Ridges

The ridges sampled during Leg 4 were:

- Remote sensing
- Jaridge
- Alli's ridge
- MET city ridge

An A-pit was conducted whenever possible, however hard icy layers and icy blocks made measurements extremely hard in the early weeks. Jewel snow in poorly drained areas was a problem for SMP measurements, A few weeks later, after a lot of surface melt, the surface scattering layer provided easier chemical sampling and the previously snow-covered ridges became 'blocky.'

4.2.2.5 Coring

FYI was the focus for Leg 4 to continue the time-series from previous legs. However, when the FYI area was ponded for two weeks, surface characterisations were done alongside the SYI coring team.

4.2.2.6 24H sampling period

Every 6 hours: NIR and µCT at optics-stern consisting of three 'library point measurements.'

Every 6 hours: Remote sensing B-pit.

4.2.2.7 Transects and Chemical Snow Sampling

Each week, a chemical sampling task was conducted. Due to time, personnel and ice constraints, not all requests listed could be fulfilled. Furthermore, some sampling was requested only for e.g. 2-weekly, monthly or only after snowfall. However, snow samples were taken for the following purposes (in parentheses: sample coordinator)

- Black Carbon (AWI/Daniela Krampe)
- Halocarbons (BGC/Katarina Abrahamsson)
- Ice Nucleating Particles (INPs) (Jessie Creamean)
- Iodide (Uni Grenoble/Hans-Werner Jacobi)
- Major Ions and Water Isotopes (AWI Glaciology/Maria Hörhold)
- Major Ions, Bromide, INPs, 34S (SO4), Salinity, S-Isotopes (BAS/Markus Frey)
- Major Organic Compounds (PSI/Julia Schmale)
- Microplastics (AWI/SLF)
- Salinity (ICE)- discontinued after all surface samples had zero salinity.
- Sugars (TROPOS)
- Micro-CT samples
- Melted snow was used for d18O samples (NPI)

The rocket traps were not installed due to the ice surface having a high liquid water content, resulting in no wind-blown snow.

Unlabelled sample vials were pre-labelled by us before going into the field and, for each sample, the corresponding snow pit and location within the profile have been documented.

After sampling, the bags and vials were stored either in the -20°C freezer in the F-Deck or in the -20°C AWI sea ice physics freezer at the bow - either in prepared boxes by the institutes who conducted the sampling requests or in one of the SLF skufa boxes.

4.2.2.8 Terrestrial LiDAR Surveys (TLS)

TLS snow accumulation maps could not be calculated prior to snowpit measurements, and the implementation of the stratigraphy-based directed sampling was not possible. To cover spatial variability, NIR transects were conducted in the footprint of the TLS scans (optics-Lemon Drop albedo line, optics-Root Beer Barrel albedo line, DS-A7*) and SMP measurements across ridges. The TLS scans were conducted by Ian Raphael for Leg 4.

This snow-related task is described separately in Section 4.4.

4.2.2.9 Snow Lab

We processed samples cored in the field for µCT analysis (see Figure 4.2.8 as an example scan). 104 snow samples and 45 ice cores were scanned. For details on the coring procedure, refer to the SOP 'snow coring' and the SOP / cheat sheet for the µCT 90 on the MCS. There were no µCT problems with partial reconstruction or missing slices.

Opportunistic sampling:

- Platelet ice
- SSL
- Jewel snow
- Pucks (false bottoms)
- Rotten ice

Special attention was taken to scan the surface and the interface between snow/SSL and ice. The majority of these interface scans were taken using the 88 mm diameter holder. A surface scan of the surface scattering layer can be seen in figure 4.2.8

No samples were cast in the field due to the excellent performance of the uCT. 4 samples were cast in the lab for further thin section analysis.

Data are stored on MCS automatically in the correct folder using a script developed on Leg 2 (see 4.2.4 Data management).

A change was made for 'special samples'. In contrast to previous legs, these now need an event ID in D-ship, they are now organised exactly the same as other samples taken.

Snow salinity was measured in Trockenlabor 3, with the salinity sensor provided by U. Fairbanks, the same used for the physical measurements of the ice cores. The 20 ml sample vials for d18O from NPI were suitable for the melted volumes of snow from salinity measurements. At the end of the leg, these were replaced with glass vials.

4.2.3 Preliminary results

We could measure most core parameters for snow regularly, at least weekly. Adjustments had to be made due to alternative requirements for the surface scattering layer

All key devices for measurements of the surface worked without major issues.

Wetness of the surface had a large influence on measurements. An initial SWE plot in comparison to the previous legs is shown in figure 4.2.7 and shows the large difference in the conditions that were measured on Leg 4.

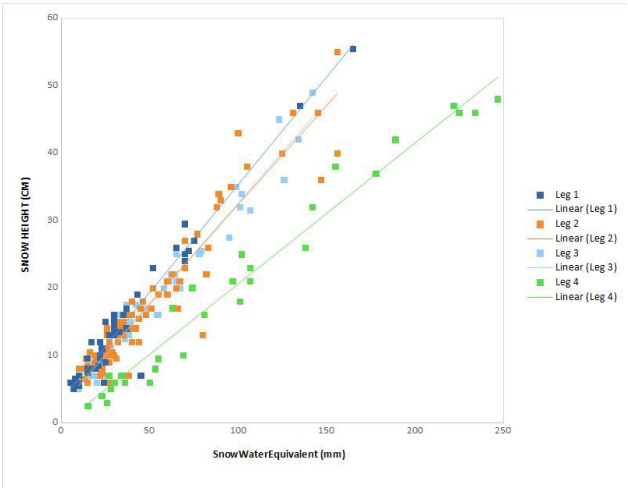

Fig 4.2.7: *The development of the Snow Water Equivalent (SWE) from Legs 1 to 4.*

The microCT operated very well throughout the leg, this is shown by the quantity of samples collected throughout the 3 months. Whenever possible a microCT was taken of the surface to better understand the microstructure and development of certain formations seen on the floe. Some scans included; SSL (Figure 4.2.8), 'jewel snow', platelet ice, pucks (or false bottoms)

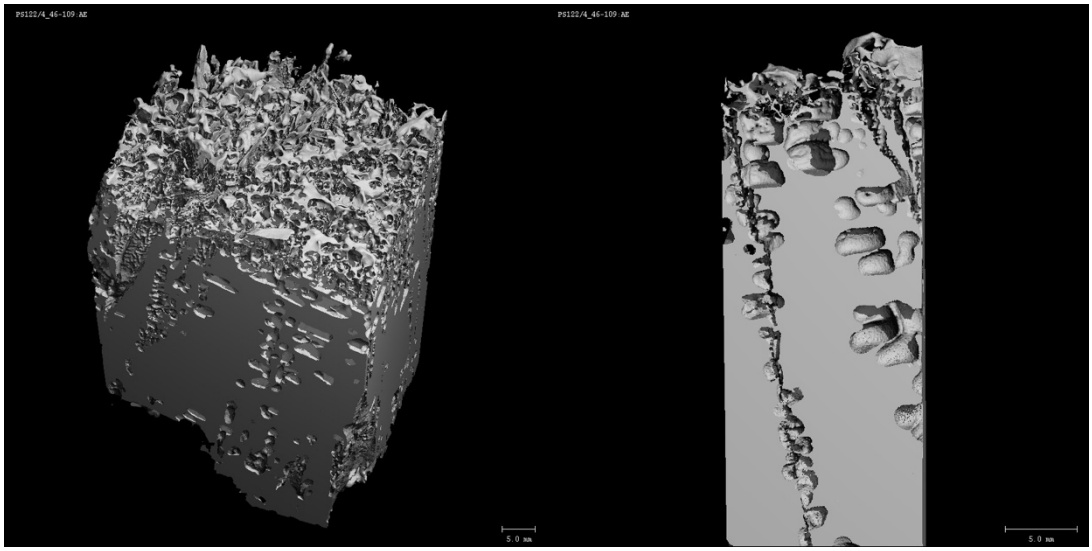

Fig. 4.2.8*: µCT image of SSL (left) and a cross-section of a melted brine channel (right).*

Instrument difficulties experienced in the field are listed below.

- SMP- jewel snow and ice in ridges caused a lot of lateral motion on the tip. A very thin SSL often resulted in skipping measurements. The sensor was replaced on SMP49.
- Density- problems with icy blocks in ridges being too hard to use the cutter. Very loose jewel snow provided similar problems to depth hoar in winter and getting a volume in the cutter that was an accurate representation of the snowpack was extremely challenging. A very thin SSL could not be measured with the density cutter. Layers with high liquid water content (slush), for example at interface were unmeasurable.
- NIR- worked very well in all conditions- difficult to travel with it on a kayak but this was made possible a few times! Vertical (of the surface) and horizontal (of the snowpit wall) images were taken and will provide extremely useful in the data analysis, especially for grain size alongside optics and wetness alongside remote sensing.

- uCT sampling- sometimes taken with liquid nitrogen, sometimes just carefully sampled removing the area around the sample area with a spatula. This required patience and careful transportation of the samples back to the vessel.
- Temperatures in the snowpack didn't drop below -0.5°C, a thermometer with a higher resolution was used at remote sensing and this should be used for all pits in Leg 5.

4.2.4 Data management

All data are handled, documented, archived and published following the MOSAiC data policy (see APPENDIX). All device operations were logged in DSHIP and all sensor raw data files are stored in platforms/packice/snowpit section of the MCS. Final geophysical parameters will be made available via the workspace section of the MCS and archived in the PANGAEA data repository according the MOSAiC data policy.

The set-up of the MCS raw data was continued from Leg 3. Any "special samples" that were collected now require a D-Ship eventID. SOPs and field tasks were updated for the handover to Leg 5. Protocol sheets for the different snowpits were very useful and used throughout Leg 4, transects and snowpits alongside optics measurements required unique protocols. All protocols and field note books were scanned and stored on MCS. Detailed documentation is all in the MCS/workspace/snowpits directory.

4.2.5 Environmental Impact

- Flags
- Running the cold container- energy consumption and how it is cooled
- Sampling bag tops fly away
- Storing samples in plastic vials- one use
- Nitril gloves

4.3 AIRBORNE SEA-ICE SURVEYS (HELI)

Gerit Birnbaum[1], Luisa von Albedyll[1], Stefan Hendricks[1] (not on board), Niels Fuchs[1] (not on board), Robert Ricker[1] (not on board), Arttu Jutila[1] (not on board), Jan Rohde[1] (not on board), Jennifer Hutchings[2] (not on board)

[1]AWI
[2]Oregon SU

4.3.1 Objectives

The objectives of the helicopter-borne sea-ice surveys during MOSAiC have been described in the Helicopter Observational Plan, the Expedition Programme and the cruise reports for PS122.1, PS122.2 and PS122.3. Here we provide a short summary for PS122.4, which took place during summer season:

1. With respect to the overarching MOSAiC Science Plan questions, we mainly contribute to: How does sea ice formation, drift, deformation and melting couple to atmospheric, oceanic and ecosystem processes?
2. With respect to the overarching MOSAiC Science Plan goals, we especially contribute to: What are the spatial variability and temporal evolution of the snow and sea ice cover?
3. What is the spatial distribution of sea ice freeboard and surface roughness within the distributed network (DN)? How do these parameters evolve during the melt season?
4. What is the surface roughness upwind of the meteorological installation at the central observatory (CO)?
5. What is the sea ice thickness distribution within the distributed network and beyond? How does it evolve during the melt season?
6. What is the spatial distribution of melt pond fraction and melt pond properties (e.g., size distribution, shape, depth) within the distributed network? How do those parameters evolve during the melt season?
7. What is the temporal evolution of floe size distribution within the distributed network?

In the present report, we focus on the helicopter measurement programme performed by Team ICE during PS122.4. Further helicopter-borne surveys were performed with the HELiPOD system, work that is funded by the DFG-project “ALEXIA - Analysis Linking Arctic Methane, Carbon Release, Heat Fluxes and Sea Ice from Local to Sub-Regional Scales by Airborne Measurements”. On PS122.4, HELiPOD work was part of the Team BGC research programme (see Chapter 7).

4.3.2 Work at sea

4.3.2.1 Sensors

The following sensors/instrumentation have been operated during PS122.4 on the D-HARK helicopter (ALS&CAM configuration):

- Airborne laser scanner (ALS)
- 2 RGB cameras: 14 mm wide-angle lens and 8 mm fisheye lens (CAM)
- Hyperspectral camera AisaEagle
- Data Management System including operation of radiation thermometer KT-19 and upward and downward looking pyranometers CMP22

The following sensors/instrumentation have been operated during PS122.4 on the D-HAPS helicopter:

- EM-Bird
- 2 GoPros

4.3.2.2 Mission types

There were five different mission types during Leg 4:

- Floe grid – D-HARK (ALS&CAM) & D-HAPS (EM-Bird)
- L-Site survey – D-HARK (ALS&CAM)
- Butterfly survey – D-HAPS (EM-Bird)
- Out and return transect – D-HARK (ALS&CAM) & D-HAPS (EM-Bird)
- Test flight or calibration manoeuver

Between 11 June and 7 August 2020, we performed 3 test flights and 22 survey flights (Table 4.3.1). However, 1 test flight and 5 survey flights had to be aborted after a certain time due to deteriorating weather conditions (ceiling became too low). In the following, the different mission types are explained in more detail.

For the D-HARK ALS&CAM configuration (16 flights), flight altitude and ground speed were adjusted to ceiling and mission goals for every flight. Due to frequent low ceiling, the standard flight parameter of 1000 ft altitude above ground level (employed on Legs 1-3, see cruise reports) was applied only three times (in combination with 80 kn ground speed). The flight altitude in all other cases was 500 ft or lower. For floe grid flights with a special focus on melt pond properties, we operated at 200 ft and 10 kn ground speed over the floe.

With the D-HAPS EM-Bird configuration (9 flights), we carried out all surveys on 40 ft operational bird altitude above ground level and 80 kn air speed.

Floe grids

Floe grid surveys followed a mow-the-lawn pattern more or less centered over the CO floe with a target side-length of about 5 km. Floe grid surveys at 200 ft altitude were only carried out over the CO floe itself.

L-Site Surveys

Real-time coordinates from the three L-Sites (snow buoys) had been used since Leg 1 to span three triangles. The primary objective of this type of mission during Leg 4 was to map changes in surface roughness, floe freeboard, floe size distribution and melt pond properties in the distributed network. As a secondary objective, these surveys served as an opportunity to monitor the ice conditions at the L-Sites.

In an ideal case, the survey lines contain the spines from Polarstern to all L-Sites as well as the outer triangle between the L-Sites, e.g.: PS > L3 > L2 > PS > L1 > L3 > PS > L1 > L2 > PS.

In total, three L-site surveys could be performed on Leg 4 between 30 June and 14 July 2020.

Butterfly surveys

During Leg 4, the EM-Bird butterfly pattern introduced on Leg 3 was continued. It was defined by *Polarstern* (PS) as the starting point and 4 iSVP buoys (P90, P217, P92, P124) as corner waypoints. As the buoys drifted apart and the distances to *Polarstern* increased during Leg 4, not all butterfly surveys consisted of two triangles (Table 4.3.1).

Transect surveys

During Leg 4, we carried out 6 transect flights up to 60 nm away from *Polarstern*, in order to cover the largest possible area. This flight pattern was not linked to buoy positions.

Pyranometer calibration pattern

Two radiation squares were flown on 22 July 2020 under clear sky conditions.

4.3.3 Preliminary (expected) results

Airborne laser scanner

We continued the routine workflow and quick-view processing of the airborne laser scanner data during PS122.4. On flights at altitudes between 200 ft and 500 ft, we used a high-resolution configuration of the laser scanner settings. Hence, processing the data all the way to the final level-4 gridded product took about twice as long as on Legs 1-3 (up to 2 days). During processing, we increased the spatial resolution of the quicklooks to 25 cm. For the first floe survey on 16 June, *Polarstern* was not yet drifting with the floe, which is why we used minutely GPS position from a flux station that was located on the surveyed ice for the drift correction. The CO floe grid survey's merged product was the basis and background for the annotated and constantly updated floe map of the CO. Figure 4.3.1 shows a comparison of three ALS maps of the CO floe obtained during Leg 4. Main changes in surface topography during PS122.4 were introduced by the formation and drainage of melt ponds. Sea ice deformation resulted in weak erosion of the floe edges, but left the interior of the floe unchanged.

RGB cameras with 14 mm wide-angle and 8 mm fisheye lens

During the ALS flights, we operated two downward looking nadir cameras (14 mm wide-angle and 8 mm fisheye lens) collecting high-resolution images of the ice surface. We use a processing chain based on the images from the 14 mm lens camera to retrieve orthomosaics and eventually a digital elevation model (DEM). During the melt season, the main goal was to derive melt pond fraction and melt pond properties like pond size distribution and shape of ponds. Figure 4.3.2 shows a comparison of two orthomosaic of the CO floe.

Hyperspectral camera

The hyperspectral camera was primarily operated to derive melt pond depth. Since AisaEAGLE cannot be used for every combination of flight altitude and ground speed, we employed the hyperspectral camera only on two selected flights (07 and 17 July 2020) over the CO floe to determine melt pond properties. Processing of the AisaEagle data is complex and could not be done with the resources available onboard.

Pyranometers

From the pyranometer data, area averaged albedo will be calculated for flights in the two ideal cases: clear-sky and overcast. The necessary attitude post-processing will be done after the expedition.

EM-Bird

EM-Bird surveys were carried out in order to map the total sea ice thickness distribution at the floe-size scale and at larger scales beyond the L-sites. Note that total thickness refers to here as snow+ice thickness. The butterfly pattern creates a drifting reference scheme in which ice that underwent similar thermodynamic and dynamic changes can be monitored over time. This time series will be used to study the impact of dynamic and thermodynamic processes on the temporal evolution of the ice thickness distribution. During Leg 4, we extended this time series by two full triangles, flown on 21 June, 22 June and 1 July 2020 (Figure 4.3.3).

A second goal is to upscale the ground-based EM ice thickness measurements from the GEM-2 on the Leg 4 Transect Loop located along the perimeter of the CO floe. For this purpose, we conducted a floe-grid pattern in the vicinity of *Polarstern* with several overflights over the floe (Figure 4.3.4).

4.3.4 Data management

All data are handled, documented, archived and published following the MOSAiC data policy (see APPENDIX). All device operations were logged in the AWI sensorweb portal and all sensor raw data files are stored in platform section of MCS. Data will be stored at the PANGAEA data repository (World Data Center PANGAEA Data Publisher for Earth & Environmental Science www.pangaea.de). Final geophysical parameters will be made available via the workspace section of MCS and archived in the PANGAEA data repository according the MOSAiC data policy. Data from the data acquisition system of Polar Research Aircraft (DMS) can be accessed after registration at https://dship.awi.de/exportdisplay/.

Tab. 4.3.1: *Overview of all helicopter sea ice surveys from Polarstern during PS122.4. TO and LDG designate take-off and landing times in UTC respectively. Grey shades indicate D-HARK surveys with the ALS&CAM configuration.*

Flight ID	Device Operation	TO	LDG	Aircraft	Mission Type
20200611_01	PS122/4_44-27	13:20	14:18	D-HARK	Test flight (during transit)
20200615_02	PS122/4_44-65	12:13	13:44	D-HARK	Test flight (during transit)
20200616_01	PS122/4_44-78	09:22	10:57	D-HARK	CO floe grid*
20200619_01	PS122/4_44-95	08:45	10:10	D-HAPS	Transect
20200621_01	PS122/4_44-127	08:39	10:51	D-HAPS	Butterfly (2 triangles)
20200621_02	PS122/4_44-128	13:47	15:52	D-HAPS	Butterfly (1 triangle) + Transect
20200622_01	PS122/4_44-130	08:45	10:10	D-HAPS	Butterfly (1 triangle) + Transect
20200628_01	PS122/4_44-238	09:00	09:30	D-HARK	Test flight (CO)*
20200629_01	PS122/4_45-33	14:36	14:58	D-HARK	CO floe grid (parts)*
20200630_01	PS122/4_45-36	07:39	09:21	D-HARK	CO floe grid
20200630_02	PS122/4_45-37	09:33	11:05	D-HARK	L-Site triangles
20200630_03	PS122/4_45-38	17:43	19:43	D-HAPS	N-S Transect
20200701_01	PS122/4_45-54	15:02	17:13	D-HAPS	Butterfly (2 triangles)
20200704_01	PS122/4_45-112	08:47	10:42	D-HARK	CO floe grid (parts)
20200707_01	PS122/4_46-36	08:57	11:06	D-HARK	CO floe grid
20200707_03	PS122/4_46-39	12:28	14:40	D-HARK	L-Site triangles
20200707_04	PS122/4_46-40	15:43	17:43	D-HAPS	CO floe grid

20200711_01	PS122/4_46-97	11:20	12:20	D-HARK	L2 floe grid*
20200714_01	PS122/4_47-21	12:01	13:46	D-HARK	L-Site triangles*
20200717_01	PS122/4_47-96	15:22	17:24	D-HARK	CO floe grid
20200722_01	PS122/4_48-69	15:15	17:32	D-HARK	Calibration + CO floe grid
20200806_01	PS122/4_50-32	08:53	10:53	D-HARK	S-N Transect
20200806_02	PS122/4_50-37	15:03	17:04	D-HAPS	Transect
20200807_01	PS122/4_50-45	08:35	10:37	D-HARK	E-W Transect
20200807_02	PS122/4_50-47	13:44	14:27	D-HAPS	Transect*

*aborted due to deteriorating weather conditions (ceiling became too low)

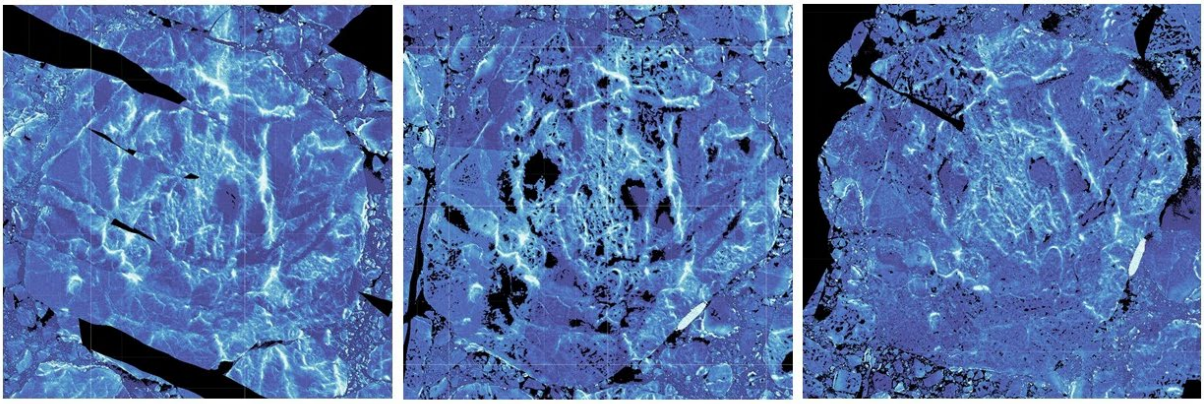

16 June 2020 30 June 2020 17 July 2020

***Fig. 4.3.1**: Comparison of three ALS maps of the CO floe (north is up). The maps give an impression of the surface topography, but also the seasonal transition of surface conditions during melt. For example, the stages of the melt pond evolution are clearly seen in the last two maps, which show the after-effects of melt pond drainage.*

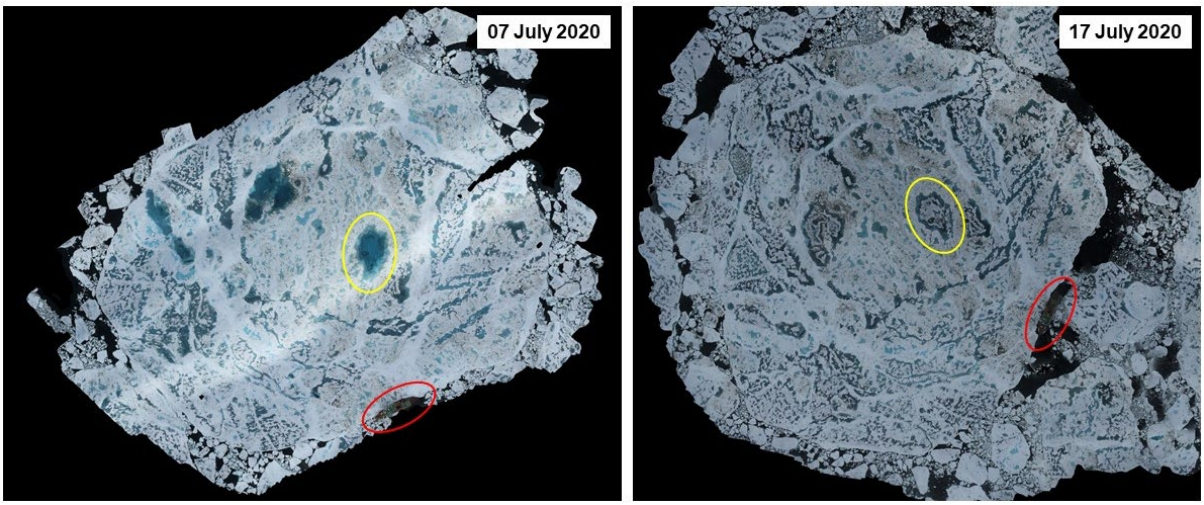

Fig. 4.3.2*: Orthomosaic of the CO floe on 7 and 17 July 2020. The red circles indicate the location of Polarstern. The yellow circles show the location of Mystery pond that drained in the period between the two flights.*

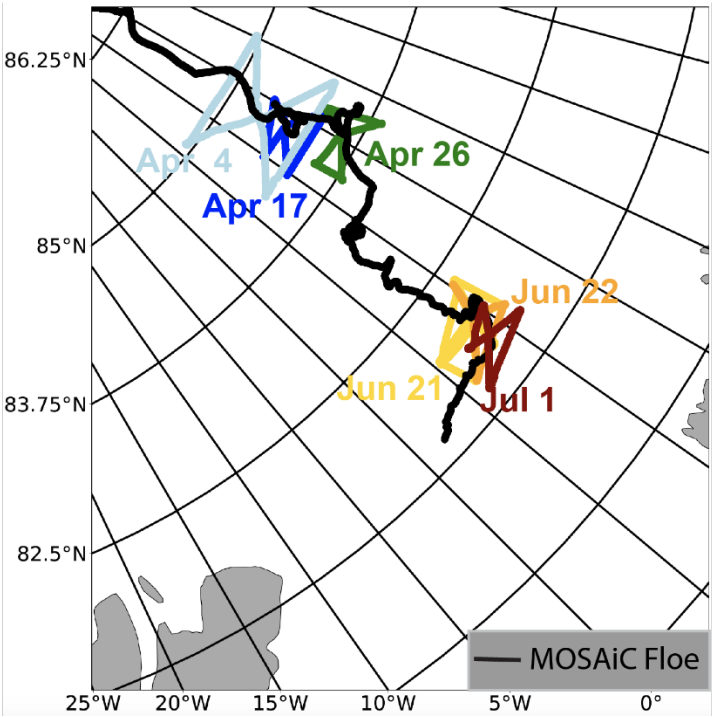

***Fig. 4.3.3**: Summary of Butterfly HEM surveys between April and July 2020 along the MOSAiC floe drift track.*

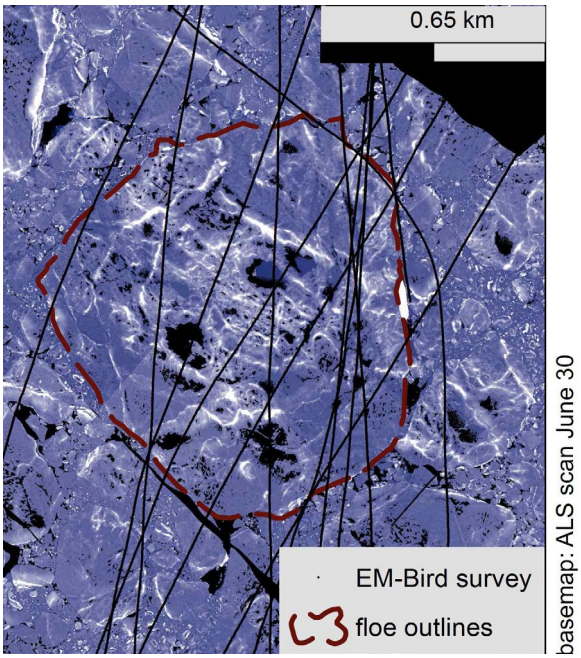

***Fig. 4.3.4**: EM-Bird Floe survey. ALS scan from 30 June overlaid with tracks of the HEM Survey on 07 July 2020 (not drift corrected).*

Tab. 4.2.2 *Overview on all measured parameters for the three defined snow pit types during Leg 3.*

Type A: Parent snow pit	Type B: Quick snow pit	Type C: SMP	Type D: uCT
Complete sampling of physical and chemical properties	Complete physical sampling	Super quick measurements	Special sample
• 10 m - SMP transect, 1 m spacing • Pictures for snow surface and ice surface roughness (SfM) • µCT sampling • Density (volumetric) • Temperature • Salinity • Snow samples for chemical and physical properties **All Type B measurements**	• SMP • NIR photography (SSA) • SWE (ETH tube) • µCT sampling • Site overview photos	• SMP	• uCT

See the DSHIP action log extract file for an overview of the snowpits conducted for Legs 1, 2, and 3

4.4 TERRESTRIAL LASER SCANNING

Ian Raphael[1], Chris Polashenski[1,3] (not on board), Martin Schneebeli[2], Don Perovich[1] (not on board), David Clemens-Sewall[1] (not on board)

[1]Dartmouth College
[2]SLF
[3]USACE/CRREL

4.4.1. Objectives

Surface morphology controls many sea ice processes, including snow catchment and preservation, pond formation and evolution, ice mass balance, and surface atmospheric turbulence. Terrestrial Laser Scanning (TLS) helps us bridge the gap between micro-scale surface characterization, e.g. snow pits and micro-CT measurements, and regional-scale Aerial Laser Scanning (ALS) measurements. Repeated TLS surveys provide a time series of surface evolution at cm-precision over a 0.5 km-scale scan area. Our primary goals on Leg 4 were to:

- Map and quantify the evolution of snow and ice surface roughness
- Observe snow and ice surface ablation
- Observe pond formation, extent, and evolution

4.4.2 Work at sea

Our primary scan fields that were established and maintained on earlier legs separated from our new CO floe prior to our arrival in June. Due to the difficulty and uncertainty of accessing these sites regularly, we established a new scan field on the new CO floe. The new scan field was limited to a remote sector of the floe due to the safety hazards addressed later in this section. The field was collocated with the first-year ice (FYI) optics sites, as well as several pond measurement sites. See Figure 4.4.1 for a site overview.

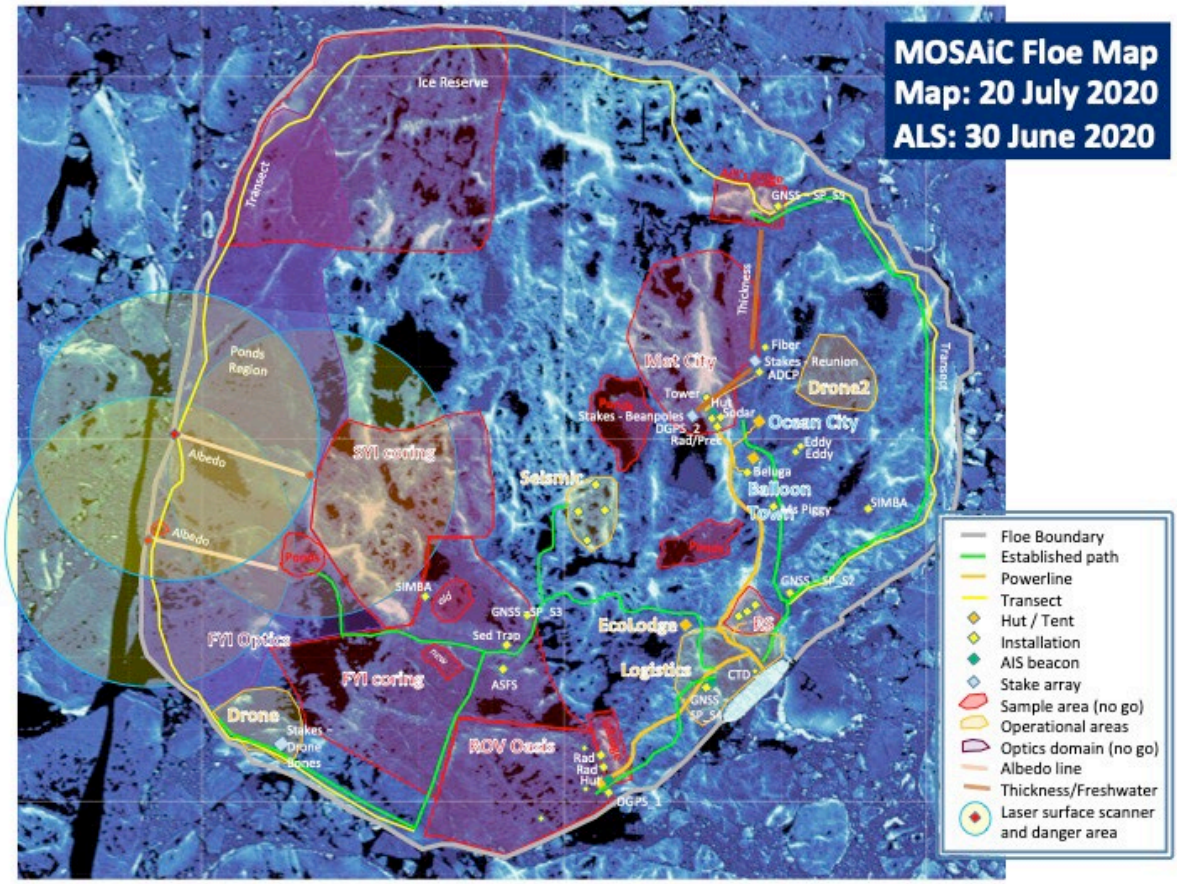

Fig. 4.4.1: *Map of Lidar Fields and Features as of 20200727. The footprint of a single scan is a ~350-m radius around the scan position. The yellow disks indicate our safety field, and have a 200-m radius. Our scan field covered ~400 m x 400 m.*

TLS during the Leg 4 was particularly difficult due to the ice and weather conditions. On previous legs, we installed an array of reflectors frozen permanently into the scan area. We used these reflectors as a fixed reference grid, which allowed us to 1.) tie individual scans together to create daily scan sets, and 2.) directly compare and difference whole scan sets from multiple days. During Leg 4, we could not prevent the reflector posts from melting out between scan days. We therefore reinstalled the posts for each scan day, preventing us from establishing a fixed frame of reference throughout the leg.

Melt also frequently affected individual scans. During individual scans, the tripod melted into the surface, often shifting enough to yield a substantial offset in the scan data. This gave rise to errors in the scanner's own coordinate system, making it difficult to register the scan into the project coordinate system with other scans from the same day.

Furthermore, due to the high attenuation of NIR light in liquid water, the wet snow/ice surface rendered the eye-safe VZ1000 Lidar (URN: *pack_ice:ice_ps:tls-vz1000*) unusable during the melt season. We elected to use the higher-power, but non-eye-safe, VZ6000 (URN: *pack_ice:ice_ps:sn_tls600* [sic]). We managed the safety hazard by clearing a 200m people-free safe zone around the scanner, and using laser safety glasses for the bear guard and instrument operators. Additionally, we notified all scientists and crew not to look into the scan area using any optical magnification device, e.g. cameras and binoculars.

However, because the VZ6000 specifically yields higher returns from wet surfaces, the scanner is much more sensitive to humidity and precipitation. This meant that scanning on foggy, misty, or rainy days was not possible.

The combination of these factors, as well as the 45-minute scan period of the VZ6000, meant that our scan volume was reduced from Legs 1-3. In total, we were able to scan at three scan positions over a total of six scan days.

4.4.3 Preliminary (expected) results

At the beginning of Leg 4, we noted the presence of a snowpack, especially in ridged areas of the floe. The snowpack quickly melted, giving way to the surface scattering layer (SSL). Surface roughness in the scan area generally diminished as snow structures, such as drift aprons and sastrugi, melted, leaving more homogenous ice and SSL surfaces. Later in the leg, preferential melt of sediment-laden ice left hummocked areas, again increasing surface roughness.

Because of the strong reflectivity contrast between ice and pond surfaces, we expect to be able to map the evolution of melt ponds in the scan area as they formed, grew, and finally drained.

4.4.4 Data management

All data are handled, documented, archived and published following the MOSAiC data policy (see APPENDIX). All device operations were logged in the AWI sensorweb portal and all sensor raw data files are stored in platform section of MCS. Final geophysical parameters will be made available via the workspace section of MCS and archived in the PANGAEA data

repository according the MOSAiC data policy. DOIs will be communicated to PANGAEA for later access via the future MOSAiC Data Portal.

4.5 TRANSECT

Melinda Webster[1], Luisa von Albedyll[2], Ian Raphael[3], Polona Itkin[4,5] (not on board), Stefan Hendricks[2] (not on board)

[1]University of Alaska Fairbanks
[2]Alfred Wegener Institute
[3]Dartmouth College
[4]University or Tromsø
[5]Colorado State University

4.5.1 Objectives

A new transect route was established on Leg 4 for monitoring the changes in snow depth, sea ice thickness, and melt pond depth during the melt season. Surveys began when a snow cover was still present and ended immediately prior to floe break-up, when the surface was snow-free and covered in drained melt ponds. The data from the nearly month-long time-series from Leg 4 will be valuable for better understanding the:

- Mass balance of snow and sea ice during the melt season.
- Development of melt ponds and their summer evolution.
- Widespread transition of the snow cover to a surface scattering layer.
- Persistence of snow drifts in ridged areas.
- Scalability between ground, airborne, and satellite sea thickness distributions.

4.5.2 Work at Sea

4.5.2.1 The Leg 4 Transect

The Leg 4 Transect Loop covered approximately three kilometers in distance and went in a counter-clockwise pattern along the floe edge and incorporated ~200 m of the original Northern Loop (approximately between Areas 2 and 3 in Figure 4.5.2). The first half of the transect route was predominantly second-year ice, while the second half was mostly first-year sea ice. The transect route was established in segments beginning on 27 June and was fully marked on 29 June, the day of the first complete transect survey. From 29 June onward, transect data were nominally collected four times per week. The last date of a complete survey was 26 July, yielding 18 complete surveys over nearly one month's time.

4.5.2.2 Instrumentation

Unique to Leg 4, the transect work involved measuring both snow and melt pond depths as the surface conditions transitioned snow-covered to snow-free during the melt season. To accommodate both types of measurements when snow and melt ponds were both present, the snow basket of the Magnaprobe was outfitted with foam on its upper portion to provide buoyancy in melt ponds. The bias associated with this addition was ~0.25 cm. For each pond depth surveyed, the measurement counter number was recorded and summarized in accompanying ReadMe files.

Magnaprobe-anja was the primary instrument for all transect surveys except on 16 July, when Magnaprobe-kathrin was used as a temporary replacement.

For total (snow + ice + pond) thickness surveys, Geophex GEM-2 Broadband Electromagnetic Induction Sensor 556 was used until 21 July. On 20 July, problems with the GEM-2 556 were encountered and proved unresolvable. On 21 July, we switched GEM-2 instruments (from 556 to 512) and continued using GEM-2 512 for the remainder of the Leg 4 transect work. For the corresponding instruments and device operation identifications, please see Table 4.5.2.

Note, during the initial setup and troubleshooting for GEM2-556, we reconfigured the instrument's transmission frequencies three times:

1. Once using the configuration file **/public$/scientists/Team_ICE/03-documentation/Transect/GEM2-556-C5.gem**
2. Once manually on the 50 Hz powerline frequency to approximate the original configuration.
3. A second time manually on the 60 Hz powerline frequency to achieve the original configuration.

We created two new sensor definitions, corresponding with configurations 1 and 2. Surveys made using configurations other than the original are noted below in Table 4.5.2.:

- **mcs.fs-polarstern.de/workspace/teams/ice/transects/01-ice-thickness/sensordef/gem2-556-mosaic-seaice-20200628.yaml**
- **mcs.fs-polarstern.de/workspace/teams/ice/transects/01-ice-thickness/sensordef/gem2-556-mosaic-seaice-20200702.yaml**

4.5.2.3 Complementary data

At least once a week, the transect survey was extended to the Lemon Drop and Root Beer Barrel albedo lines to monitor mass balance changes in conjunction with surface albedo changes. From the second half of July, the ARIEL instrument was incorporated in the instrument suite for four partial surveys along the transect route (13 July, 19 July, 21 July, and 23 July). On 8 July and 23 July, snow and surface characterization sampling was conducted in conjunction with the GEM-2 and Magnaprobe transect surveys. Additional GEM-2 and Magnaprobe measurements were made when conditions allowed, including:

1. along the road from Polarstern to MET City, then clockwise along Transect Loop from Polarstern to Droneville on 25 June.
2. Alli's Ridge point-measurement transects on 28 June and 9, 13, 21, and 28 July.
3. along the drill-hole survey between MetCity and Reunion Stakes on 14 and 26 July.
4. along the drill-hole survey between MetCity and Alli's Ridge on 19 July.
5. between the Seismic II site and Polarstern on 23 July.
6. along the path between the Sediment Trap site and Root Beer Barrel albedo line on 27 July.
7. along the drill-hole survey between the SIMBA (close to FYI coring) and the Drone Bone Stakes on 25 July.
8. point measurements along with ARIEL in the Log Area on 26 July.
9. point measurements at every station along the ROV albedo lines on 14 July and 21 July.

4.5.2.4 Challenges

Poor visibility and polar bear encounters prevented completion of the entire transect route on 16, 23, 24, and 27 July. Despite these incomplete surveys, the average number of transect surveys was 4.5 times per week. On two occasions (24 and 27 July), only the albedo lines were surveyed due to limited working hours.

The floe edge progressively eroded away over time due to melt and dynamics. As a consequence, small sections of the transect route also eroded away. Detours around these erosions were most notable on 26 and 26 July.

Over time, the transect route at Alli's Ridge became a multi-purpose route for coring and ridge work activities.

4.5.2.5 Miscellaneous

Before arriving to the MOSAiC floe, ice station work was carried out in a grid pattern survey using the GEM-2 556 and Magnaprobe-anja. These data were collected on 13 June.

Upon arrival to the fortress floe, initial surveys of snow and ice thicknesses were carried out on it and nearby floes to determine which floe provided the thickest ice and subsequent stability. These surveys were carried out on 17 June.

***Tab. 4.5.1**: An overview of instruments used on the Leg 4 transect.*

Instrument	Description	Device URN	Geophysical Parameter
GEM-2	Geophex GEM-2 Broadband Electromagnetic Induction Sensor	pack_ice:ice_ps:gem2-556	Total (sea ice + snow) thickness
GEM-2	Geophex GEM-2 Broadband Electromagnetic Induction Sensor	pack_ice:ice_ps:gem2-512	Total (sea ice + snow) thickness
Magnaprobe	GPS snow depth probe	pack_ice:ice_ps:magnaprobe-anja	Snow depth and melt pond depth
Magnaprobe	GPS snow depth probe	pack_ice:ice_ps:magnaprobe-kathrin	Snow depth and melt pond depth

***Tab. 4.5.2:** An overview of device operations of the sea-ice transect and related data.*

Date	Locations	GEM-2	Magnaprobe	Notes
June 13	Ice station	PS122/4_44-49	PS122/4_44-265	
June 17	Floe survey	PS122/4_44-225	PS122/4_44-266	
June 25	Instrument test, Polarstern to MET City along road	PS122/4_44-221	N/A	Configuration 1, sensor def **/gem2-556-mosaic-seaice-20200628.yaml**
	Instrument test, Polarstern to Droneville, clockwise around transect loop	PS122/4_44-222	N/A	Configuration 1, sensor def **/gem2-556-mosaic-seaice-20200628.yaml**
June 27	Transect Loop	PS122/4_44-223	PS122/4_44-267	Partial transect Configuration 1, sensor def **/gem2-556-mosaic-seaice-20200628.yaml**
June 28	Transect Loop	PS122/4_44-224	PS122/4_44-268	Partial transect Configuration 1, sensor def **/gem2-556-mosaic-seaice-20200628.yaml**

	Alli's Ridge	PS122/4_44-217	PS122/4_44-269	Middle, right, left transects at Alli's Ridge. Configuration 1, sensor def **/gem2-556-mosaic-seaice-20200628.yaml**
	Calibration	PS122/4_44-219	N/A	Configuration 1, sensor def **/gem2-556-mosaic-seaice-20200628.yaml**
June 29	Transect Loop	PS122/4_45-162	PS122/4_45-198	Configuration 1, sensor def **/gem2-556-mosaic-seaice-20200628.yaml**
June 30	Transect Loop	PS122/4_45-161	PS122/4_45-199	Both albedo lines, Configuration 1, sensor def **/gem2-556-mosaic-seaice-20200628.yaml**
July 2	Transect Loop	PS122/4_45-93	PS122/4_45-200	Configuration 2, sensor def **/gem2-556-mosaic-seaice-20200702.yaml**
	Calibration	PS122/4_45-92	N/A	Configuration 2, sensor def **/gem2-556-mosaic-seaice-20200702.yaml**
July 3	Transect Loop	PS122/4_45-160	PS122/4_45-201	Configuration 2, sensor def **/gem2-556-mosaic-seaice-20200702.yaml**
July 4	Transect Loop	PS122/4_45-159	PS122/4_45-202	Configuration 2, sensor def **/gem2-556-mosaic-seaice-20200702.yaml**
July 5	Transect Loop	PS122/4_45-158	PS122/4_45-203	Configuration 2, sensor def **/gem2-556-mosaic-seaice-20200702.yaml**
July 6	Transect Loop	PS122/4_46-68	PS122/4_46-234	Both albedo lines, Configuration 2, sensor def **/gem2-556-mosaic-seaice-20200702.yaml**
July 7	Transect Loop	PS122/4_46-69	PS122/4_46-235	Both albedo lines
July 8	Transect Loop	PS122/4_46-73	PS122/4_46-236	
July 9	Melt ponds	N/A	PS122/4_46-237	Melt pond by Root Beer Barrel albedo line
	Alli's Ridge	PS122/4_46-75	PS122/4_46-239	Ridge survey
July 10	Transect Loop	PS122/4_46-81	PS122/4_46-238	
	Calibration	PS122/4_46-82	N/A	
July 13	Transect Loop	PS122/4_47-6	PS122/4_47-220	ARIEL: PS122/4_47-4
July 13	Allis Ridge	PS122/4_47-10	PS122/4_47-242	Middle, right, left transects at Alli's Ridge.
July 14	Transect Loop	PS122/4_47-28	PS122/4_47-221	

	Met City Stakes	PS122/4_47-27	N/A	
	ROV Optics	PS122/4_47-29	N/A	
July 16	Transect Loop	PS122/4_47-74	PS122/4_47-225	Partial transect
	Met City Stakes	PS122/4_47-75	N/A	
July 17	Transect Loop	PS122/4_47-89	PS122/4_47-222	Both albedo lines
July 18	Melt ponds	N/A	PS122/4_47-223	Melt ponds aft of ship
July 19	Transect Loop	PS122/4_47-139	PS122/4_47-224	Both albedo lines and drill hole survey
	ARIEL transect	PS122/4_47-140	PS122/4_47-226	Partial transect, covering ~1/3 of route, ARIEL: PS122/4_47-147
July 20	Transect Loop	PS122/4_48-7	PS122/4_48-245	
July 21	Transect Loop	PS122/4_48-61 and PS122/4_48-180	PS122/4_48-246	Included ARIEL (PS122/4_48-36) for portion of transect and Lemon Drop albedo line
	Calibration	PS122/4_48-37		GEM-2 512
	Calibration	PS122/4_48-59		GEM-2 556
	ROV Optics	PS122/4_48-39		
	Alli's Ridge	PS122/4_48-38	PS122/4_48-275	Middle, right, left transects at Alli's Ridge.
July 23	Transect Loop	PS122/4_48-178	PS122/4_48-247	Partial transect, ARIEL: 122/4_48-185
July 24	Lemon Drop albedo line	PS122/4_48_274	PS122/4_48-248	
July 25	Transect Loop	PS122/4_48-176	PS122/4_48-249	
	Drill hole survey	PS122/4_48-175		
July 26	Transect Loop	PS122/4_48-174	PS122/4_48-250	
	ARIEL point comparison	PS122/4_48-171		
July 27	Root Beer Barrel albedo line	PS122/4_49-37	PS122/4_49-115	
	Lemon Drop albedo line	PS122/4_49-38	PS122/4_49-116	
July 28	Alli's Ridge	PS122/4_49-40	PS122/4_49-120	Middle, right transects at Alli's Ridge. Magnaprobe only for middle transect. Work interrupted due to fog.

4.5.3 Preliminary results

On a regular basis, we produced quicklooks of the total (ice+snow) thickness from the GEM-2 data to assess the instrument performance. Those have proved helpful in identifying major problems with the GEM-2 556 that led to the change in instruments. An example of such a quicklook of all available frequencies from 17 July is shown in Figure 4.5.1. The figure illustrates well the divide of ice types along the transect: the first half is dominated by rougher, second-year ice, and the second half consists predominately of first-year ice. The thickness measurements align well with the surface topography derived from the ALS laser displayed in Figure 4.5.2. During the course of approximately one month, we observed a decrease in mean thickness by ~1 m. While the mean thickness of approximately 2.5 m was fairly constant between end of June and 19 July, melting accelerated strongly between 19-26 July, yielding a loss of ~14 cm per day. In the Magnaprobe data, we observed a change in snow/surface scattering layer thickness from 9 ± 7 cm to 5 ± 2 cm between 29 June and 26 July (see Figure 4.5.3). Towards the end of the leg, the surface scattering layer thickness became more homogenous across the floe and ice types, as noted by the ~2 cm standard deviation in thickness. Average melt pond depths had a modest increase from 14 ± 10 cm to 18 ± 13 cm within the same period. However, their areal coverage doubled from 9% to 18% along the Leg 4 Transect Loop.

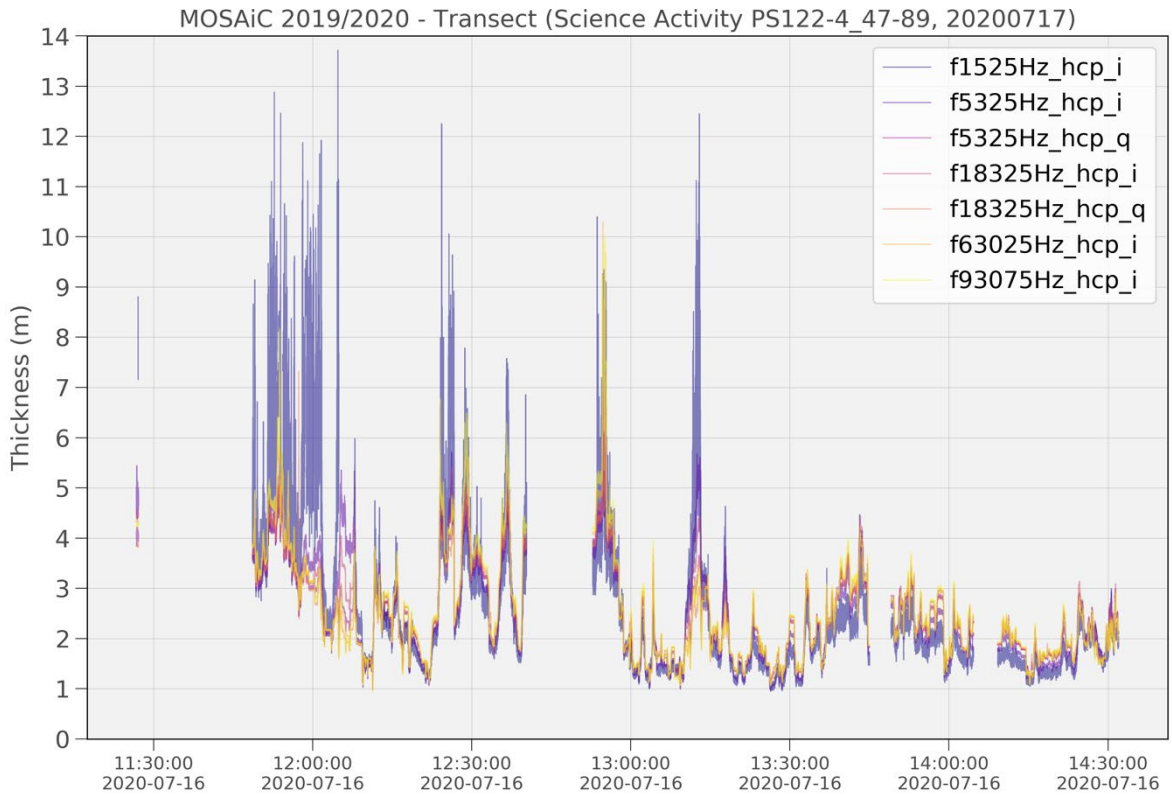

Fig. 4.5.1: *Quicklook from transect on 17 June. Thickness derived based on the different frequencies are plotted against time. The first half of the transect is characterized by rougher second-year ice, while the second half is dominated by thinner, first-year ice.*

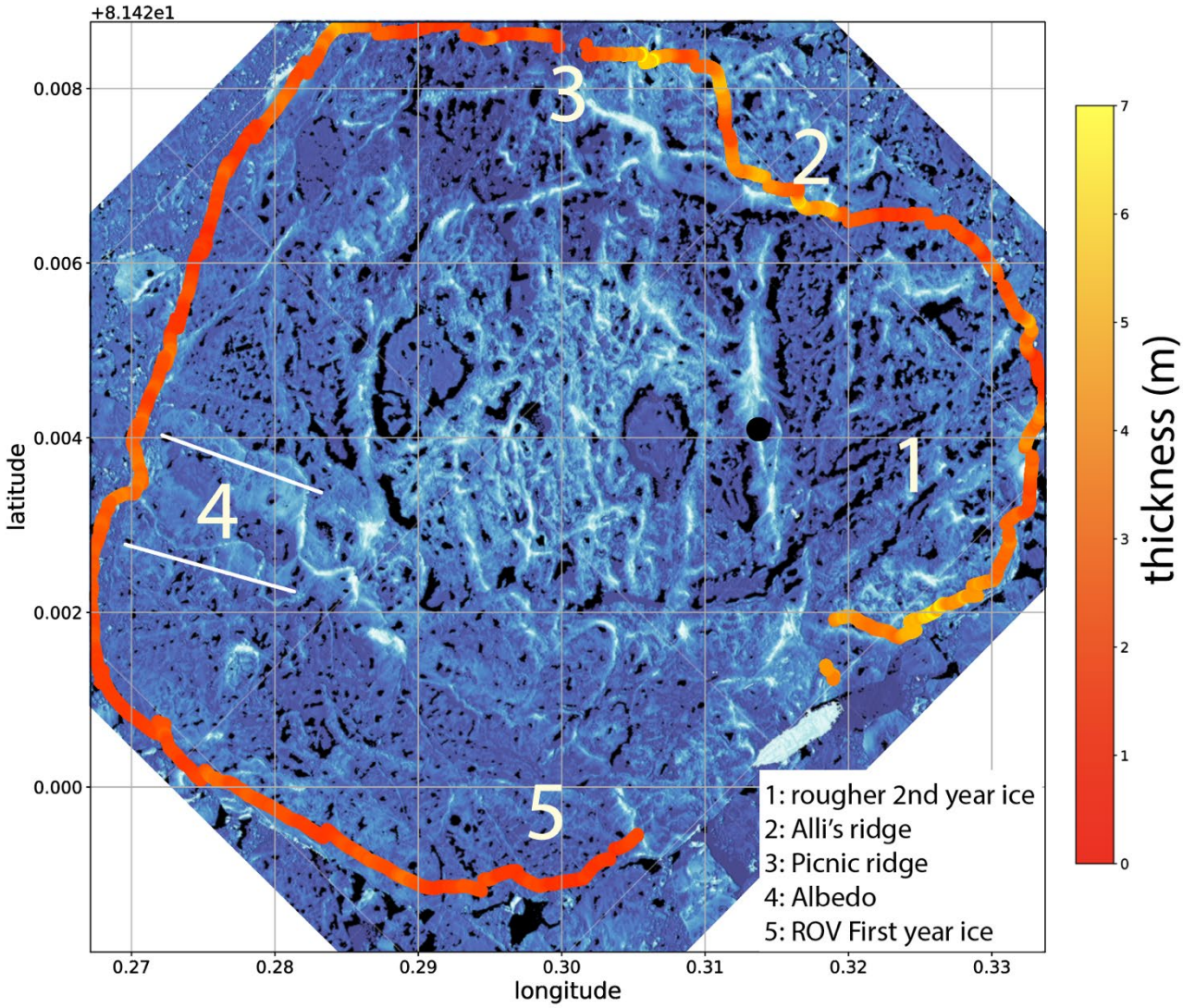

Fig. 4.5.2: *FloeMap from ALS survey on 22 July overlaid with the mean thickness from the GEM survey on 13 July. Different characteristics of the floe are marked with numbers. The GPS positions were drift corrected with the GPS information from the AIS transponder located at Met City (black dot).*

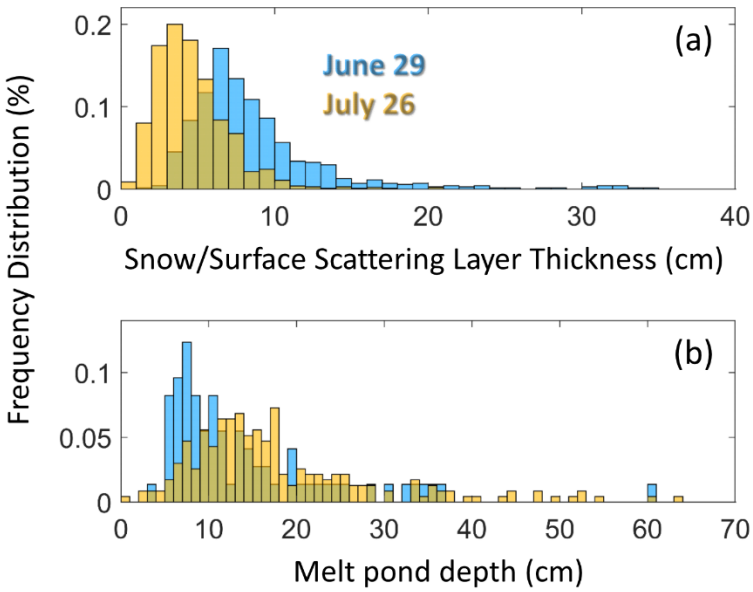

Fig. 4.5.3: *(a) Snow + surface scattering layer thickness, and (b) melt pond depth between 29 June and 26 July 2020 from the Magnaprobe data collected on Leg 4. Bin sizes are 1 cm.*

4.5.4 Data management

All data and their availability conform to the MOSAiC data policy (see Chapter 9 APPENDIX). All device operations were logged in the AWI sensorweb portal and all sensor raw data files are stored in platform section of MCS. Final geophysical parameters will be made available via the workspace section of MCS and archived in the PANGAEA data repository according the MOSAiC data policy. Metadata and device operation associations are also recorded in **/mcs.fs-polarstern.de/workspace/teams/ice/transects/mosaic-transect-actionlog.xlsx**

4.6 Sea ice and water properties based on ROV surveys

Ilkka Matero[1], Julia Regnery[1], Benjamin Lange[2], Evgenii Salganik[3], Giulia Castellani[1], Ian Raphael[4], Celia Gelfman[5], Katyanne Shoemaker[5], Sandra Tippenhauer[1]

Not on board: Christian Katlein[1], Marcel Nicolaus[1], Martin Schiller[1], Philipp Anhaus[1], Mats Granskog[2], Knut Vilhelm Høyland[3], Hauke Flores[1], Barbara Niehoff[1], Jutta Wollenburg[1]

[1] AWI
[2] NPI
[3] NTNU
[4] Dartmouth
[5] URI

4.6.1 Objectives

The research to be supported with the Remotely Operated Vehicle (ROV) as part of MOSAiC can be split into six separate parts with individual objectives. Evaluating the length scales of variability and temporal evolution of studied parameters through different seasons are common for all four. Beyond studies of the widespread level first- and second year ice, a focus of the ROV work will be on new ice, leads, and pressure ridges and their evolution through the seasons.

(1) The optics research aims to improve our understanding of the spatial and temporal variability of light transmittance through the snow-covered sea ice. Another aim is to quantify the contribution of snow and ice to light attenuation as distinct layers and as a function of depth, different ice types and stages of melt and freezing.

(2) Surveys using an upward-looking bathymetric multibeam-sonar and a high-precision altimeter are used to monitor the evolution of the ice bottom topography, which in combination with surface topography from terrestrial laser scans and aerial images, will allow for monitoring the evolution of co-located snow-air- and ice-ocean interfaces.

(3) Through lateral and vertical profiles, the ROV provides data on the spatio-temporal variability of a variety of physical (temperature, salinity) and bio-optical (fluorometry, UV and VIS absorbance spectroscopy) water properties.

(4) Towing nets under the sea ice will allow for evaluating the gypsum distribution and the evolution of the zooplankton community structure at different depths.

(5) Ice documentation (photography), as well as under-ice installations of sediment traps.

(6) Integration of an Underwater Hyperspectral Imager (UHI) to the ROV. Surveys using the UHI map the spectrum of light at high spatial resolution (centimeters) under both level and ridged ice in a gridded configuration. These data are planned to be used for mapping algae community density, spatial distribution and species composition, and in addition, to small-scale spatial analyses of optical properties of the ice in relation to surface features, melt ponds and under ice topography (e.g. block configurations of ridge keels).

4.6.2 Work at sea

There were 14 ROV dive days during PS122-4, with scientific data collected on 6 multibeam surveys, 4 UHI surveys, 6 depth profiles, 14 optics grid surveys and 13 optics transects co-located with surface albedo measurements. Several dive missions were done in collaboration with the ECO team, consisting of deployment and recovery of 8 sediment traps, 23 zooplankton trawls and 2 gypsum net trawls. The ROV team also spent half of one dive day gathering footage for documentation and outreach in collaboration with the MEDIA team.

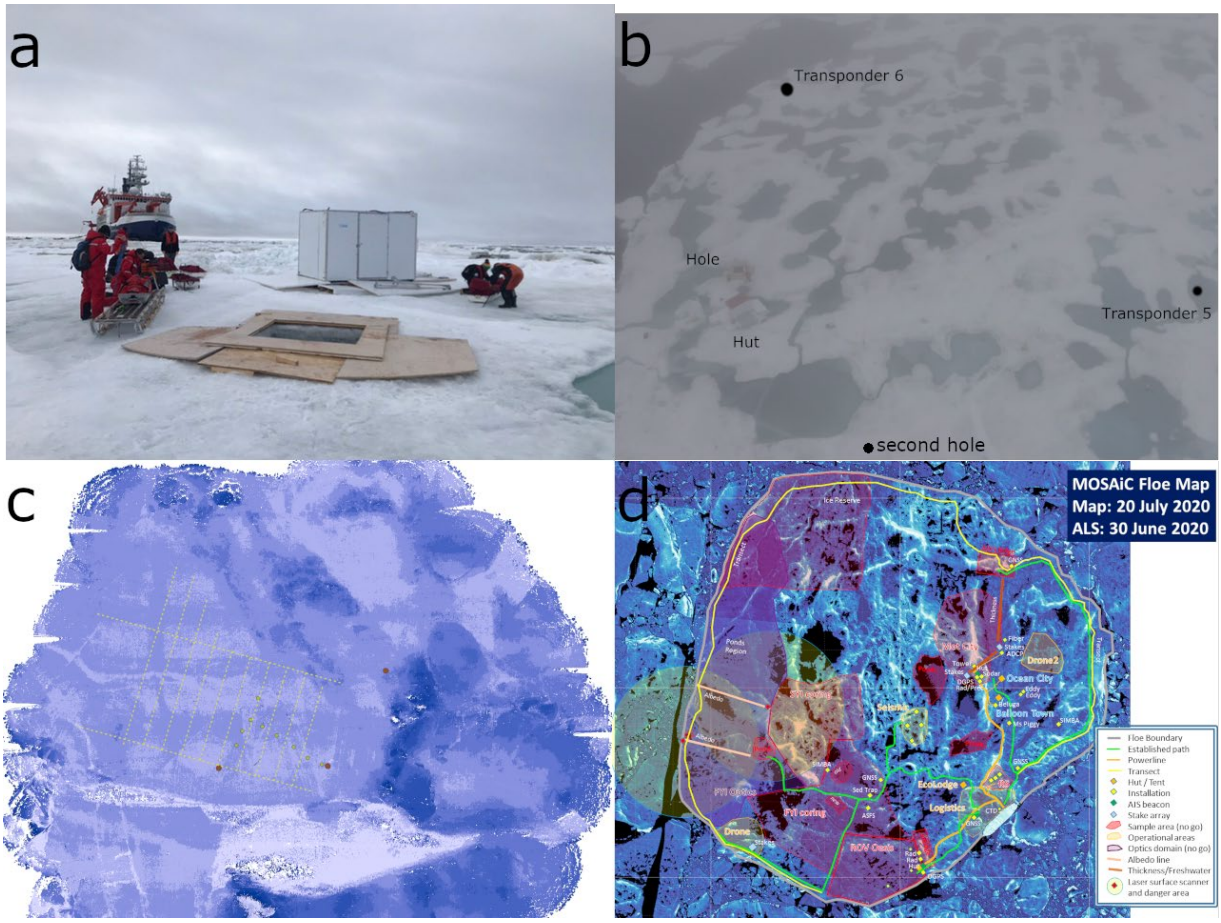

Fig 4.6.1: *(a) Hut, hole and floor at ROV site 4.5. Instead of building up the whole floor for the 'Space Station' tent, only the central 6 floor panels were setup around the hole. As the tent itself was not set up, this provided enough flooring for working with the BEAST and attaching the tripod. The ROV hut is shown in the background, and the white panels around the hut were installed for ablation shielding. (b) Aerial photo of the ROV site and dive area. The first dive hole and hut are shown annotated with 'Hole' and 'Hut' respectively. The second dive hole location is indicated with 'second hole', and the hut was relocated approximately 10 meters towards the nearby 'Jaridge' (HAVOC ridge observatory, see section 4.11) from the second hole location. Also included in the image are the prevalent foggy conditions observed on Leg 4. (c) A background map used for guidance during the optics grid dives. The yellow lines show the grid, with 10-m spacing between the near-vertical lines, and 50-m spacing between the horizontal lines. The yellow markers show the under-ice marker locations and the red larger markers show the transponder locations. The grid and markers are overlaid on a multibeam dive map from 24 June, with darker areas showing parts of the ice floe with larger drafts. (d) Floe map schematic overlaid onto an ALS topography map. The schematic shows the location of the ROV oasis in the lower part of the image, and the location of the bow of Polarstern approximately 240 m away from the hut. Panels a, b and c by Ilkka Matero, ALS topography map in panel d by Luisa von Albedyll, and the overlay map by Matt Shupe and Melinda Webster.*

Setup for the new ROV site (v. 4.0) started immediately after arriving back to the floe. First, a location for the ROV site was scouted on 19 June, followed by hole-making through 165 cm of ice on 20 June. Pulling a power cable and bringing a power hub to the site followed on 21 June. A weather window on 22 June allowed for sling loading the hut to the site via helicopter, and the rest of the infrastructure including three Long Baseline (LBL) transponders and 9 under-ice markers were installed on ice on 23 June. The under-ice markers were not installed in a similar regular grid pattern as for the previous legs of PS122 to avoid artificial drainage of the melt ponds in the FYI measurement area. The markers were instead set up following elevated features on the ice (Figure 4.6.1c). The LBL transponders were also installed on parts of the FYI ice where they were not expected to artificially drain melt ponds in the study area. For creating a stable base for the tripod and operations around the hole, four bottom and two top

panels of the Space Station floor were used (Figure. 4.6.1a). The hut was placed on an elevated platform made of 5 pallets to avoid potential flooding of the hut and surrounded by 4 ablation shields made of a wooden frame and white tarp-like material. The last dive at this location was done on 21 July, and the relocation of the site took place on 23 and 24 July.

The ROV site was relocated approximately 30 meters away from the first site due to concerns of stability of the FYI ice area where the hut was previously. The setup (v. 4.5) was otherwise similar to ROV site 4.0, and the setups shared the under-ice markers and transponder 5 location (Figure 4.6.1b). As part of the previous setup, transponder 6 was close to the ice edge, and was thus redeployed further in the FYI ice area as part of the site relocation. Transponder 3 was relocated to the new dive hole for the first dive at this location (on 26 July), and subsequently moved back to the previous dive hole, as the positioning with the new transponder locations did not work as well as hoped for. The new site was used for two dive days (26 and 28 July), before all the infrastructure was removed from the ice in anticipation of potential floe breakup. The hut was the last part of the ROV site to come back on board at around 2:30 PM on 30 July, less than 24 hours before the floe breakup.

The ROV (Figure 4.6.2) is a purpose-built measurement platform based on the M500 model (Ocean Modules) [1]. A set of two RAMSES-ACC-VIS (TriOs GmbH) spectroradiometers are used for the optics measurements, with one of the sensors mounted on the ROV and the other one set up for synchronous measurement of apparent light above the surface. A DT101 multibeam sonar (Imagenex) and a PA500 altimeter (Tritech) are used for studying the evolution of the under-ice topography. For a description of the tow nets (Figure 4.6.2b) see Section 6.2 about ROV net catches. The ROV platform also includes 3 video cameras, a still camera and a suite of sensors measuring the following parameters: radiance, conductivity, temperature, dissolved Oxygen concentration, pH, Nitrate, Chlorophyll-a, CDOM and backscatter. A full description of the measurement setup is available in *Katlein et al., 2017* [1].

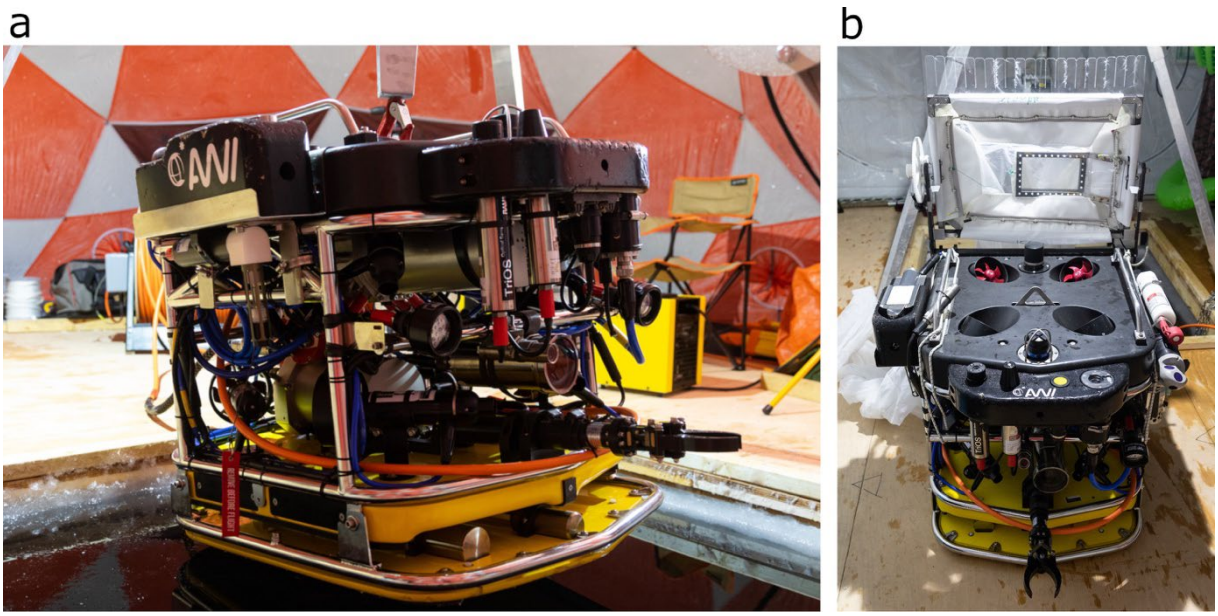

Fig 4.7.2: *The M500 ROV "Beast" (Ocean Modules) (a) over the ice hole of the first ROV site; (b) with the gypsum and zooplankton nets attached. Photos by M. Nicolaus.*

The ROV was operated with a team of 3 people. An additional person working as a polar bear guard completed the team and brought the total number of people involved in these operations to 4. During deployment and start of each dive, two team members were working on the ice and one person inside the hut. The scientists on the ice were responsible for inspecting the ROV and e.g. potential adjustments to cameras or mounting the nets, sediment traps or the UHI. The person inside the hut took care of setting up the software and verifying ROV controls and data/video streams working as intended. During the dives, one person took care of the

tether on the ice, and the two people in the hut were responsible for controlling the vehicle and scientific coordination of the dive. At the end of each dive, the ROV maneuvered back to the ice hole, tether wound back on its drum and both the ROV and the tether were brought to the hut. The ROV was stored in the hut to protect the equipment from polar bear visits. This is opposed to storing the ROV in water as was done on e.g. Leg 1, for which the motivation was to protect the equipment from large temperature fluctuations during periods with colder ambient temperatures than experienced on Leg 4.

The acoustic LBL positioning system provided accurate vehicle position estimates in the main survey grid, but acoustic shadowing of transponders due to nearby ridges resulted in limitations in the positioning accuracy (see Figure 4.6.1c for ice bottom topography and orientation). The positions of the under-ice markers and LBL transponders were recorded using handheld GPS devices, and these data were used for establishing the local grid. Having more than three LBL transponders available and installed would help for addressing the ridge shadowing on future legs and missions.

The ROV work was mostly carried out according to the plan set prior to the leg, with environmental conditions limiting the dive duration on two occasions. The environmental conditions in question were poor visibility due to fog and three polar bear visits to the site. The main equipment was not damaged as a result of the polar bear visits, but the power cable connecting the ROV site to the ship had to be inspected and maintained on three occasions.

***Tab. 4.6.1**: ROV operations registered in DSHIP. DSHIP_ID box contains the date (yyyymmdd) and device operation ID. Dive mission describes dive missions carried out on the dive.*

DSHIP_ID	**Dive mission**
20200624 **PS122/4_44_162**	Decide on optics grid location, testing LBL transponder coordinates, optics grid at 0.5 m under ice bottom, optics grid at 2 m under ice bottom, depth profile to 100 m, multibeam survey and video documentation of the nearby ridge for potential use for HAVOC ridge observatory
20200627 **PS122/4_44_191**	3 ROVnet tow horizons, sediment trap sling deployment and documentation of location, optics grid at 0.5 m from ice bottom, under-ice optics transect co-located with surface albedo transect, depth profile to 100 m
20200628 **PS122/4_44_206**	Optics grid at 2 m from ice bottom, under-ice optics transect co-located with surface albedo transect, 180 m radius multibeam survey
20200701 **PS122/4_45_61**	Optics grid at 2 m from ice bottom, under-ice optics transect co-located with surface albedo transect, 200+ m radius multibeam survey, mounting and testing UHI
20200703 **PS122/4_45_129**	Deployment of two sediment traps in series
20200704 **PS122/4_45_149**	2 ROVnet tow horizons, 2 x sediment trap recovery, optics grid at 2 m from ice bottom, optics grid at 1 m from ice bottom, under-ice optics transect co-located with surface albedo transect, depth profile to 100 m
20200707 **PS122/4_45_179**	Optics grid at 2 m from ice bottom, under-ice optics transect co-located with surface albedo transect, UHI transects under ‘Jaridge’ and under level ice between the other nearby ridge (‘Porridge’) and Marker 2
20200710 **PS122/4_46_172**	24h dive series, part 1, 3 ROVnet tow horizons, 3 x sediment trap deployment in series, under-ice optics transect co-located with surface albedo transect, UHI transects under Jaridge and under another nearby ridge (‘Porridge’), depth profile to 40 m
20200710 **PS122/4_46_174**	24h dive series, part 2, 3 ROVnet tow horizons, under-ice optics co-located with surface transect, depth profile to 40 m

20200710 **PS122/4_46_175**	24h dive series, part 3, 3 ROVnet tow horizons, under-ice optics co-located with surface transect, depth profile to 40 m
20200711 **PS122/4_46_176**	24h dive series, part 4, 3 ROVnet tow horizons, under-ice optics co-located with surface transect, depth profile to 40 m
20200711 **PS122/4_46_177**	24h dive series pt 5, 2 ROVnet tow horizons, 3 x sediment trap recovery, under-ice optics co-located with surface transect, optics grid dive at 1 m under ice, depth profile to 100 m
20200714 **PS122/4_47_31**	Multibeam survey with up to approx. 220 m tether radius, under-ice optics transect co-located with surface albedo transect, optics grid dive at 1 m under ice bottom, depth profile to 100 m
20200719 **PS122/4_47_135**	Sediment trap deployment x3, net tow 2 horizons, optics grid dive at 1 m below ice bottom, depth profile to 100 m
20200721 **PS122/4_48_4**	Multibeam survey omitting southern side due to drift ice and open water there, under-ice optics transect co-located with surface albedo transect, optics grid dive at 1 m under ice bottom, Sediment trap retrieval x 3, UHI ridge surveys
20200726 **PS122/4_48_213**	Under-ice optics co-located with surface transect, optics grid at 1 m under ice, UHI transects and grid survey, 2 ROVnet tow horizons
20200728 **PS122/4_49_105**	Multibeam survey omitting southern side due to open drift, under-ice optics co-located with surface transect, optics grid dive at 1 m under ice bottom

4.6.3 Preliminary results

Dives were done at a frequency of at least twice per week for the five weeks of operation at the site, and this allowed for regular monitoring of the changing conditions in under-ice optics, ice thickness, water column properties and under-ice biota. The ROV operations allowed for a multidisciplinary approach with the attached suite of sensors, as well as providing important support for the ECO team projects through weekly net trawl series and three sets of sediment trap deployments under the nearby Jaridge. Due to the large number of sensors on the BEAST, this report is limited to a general overview instead of a brief look at all available sensor data.

The visibility under ice was good initially, reflected by Secchi depth measurements between 13.5 – 15.5 m during the first two weeks. The visibility got worse through the weeks, reflected by the Secchi depth measurement of 8 m on 19 July. The visibility change was accompanied by a change in the hue of the water from clear and blueish colour towards a greener spectrum, interpreted as a result of increasing biological activity in the surface waters.

Larger fauna such as fish or seals were not observed during the dives, and the largest organisms seen were several jellyfish. Section 6.2 describing the ROVnet tows (Objective 4) will provide more insight into the biological activity observed in the water.

Another feature of interest was the significant accumulation of freshwater in the dive hole and just under the ice originating from snow and ice melt. This freshwater layer was observable with the camera recordings of the ROV as a sharp transition when diving through it downwards, and as blurred view when coming up into the dive hole as the thrusters mixed the saltier layer into the freshwater layer. The sharp transition was also recorded with the onboard CTD, and a salinity difference of approximately 25 PSU was measured between layers separated by a halocline of less than 5 centimetres. This freshwater layer was likely resulting in significant stress for the under-ice flora and fauna, as the ice bottom was surprisingly void of signs of life apart from abundant colonies of *Melosira Arctica*. We also observed platelet ice growing under the ice, existence of which was attributed to the presence of the distinct freshwater layer.

One significant challenge for the last two dives on 26 and 28 July was revisiting the grid and locations dived under precisely, as the post-relocation positioning did not prove to work accurately and parts of the FYI broke off during the previous days. This still allowed for gathering statistical data from the grid area, but direct comparisons between Multibeam data, for example, will be a challenge.

The next part describes addressing the objectives laid out in the start of this subsection. The optics research (Objective 1) was carried out through the grid dives at 3 depths under the ice bottom (0.5, 1 and 2 metres), through depth profiles and under-ice transects co-located with surface albedo measurements. Figure 4.6.3 shows an example of the data from two grid dives done at 1 meter below the ice bottom, and the distinct difference between the transmittance through the ice between two dates that are just 6 days apart. When we set up our measurement site, the surface was still mostly snow-covered, and pond formation was becoming more prevalent. From thereon, the surface evolved into individual discrete ponds and further progressed into an inter-connected pond network. These data hold promise for improving our understanding of the spatial variability and temporal evolution of transmission of shortwave radiation through first-year ice, spanning late melt onset to highly advanced state of melt including rotten ice and floe breakage.

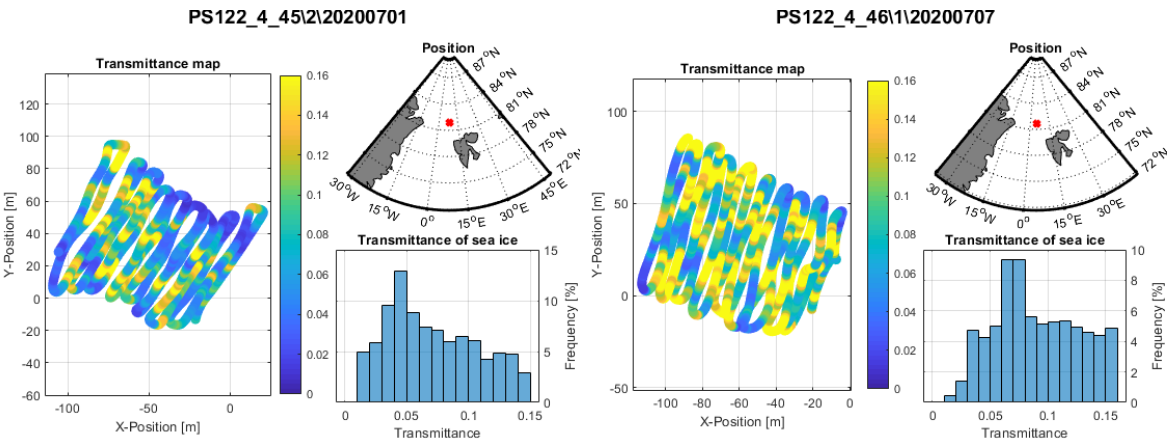

Fig. 4.6.3*: Transmittance map and histogram from the same part of the FYI ice area where the optics grid was set up. The dive pattern was altered for 20200707 and onwards for better positioning and to avoid ridges.*

Objective 2 was addressed through weekly Multibeam surveys. As indicated in the example difference map below (Figure 4.6.4), the draft of the ridges lost ice faster than the level FYI areas.

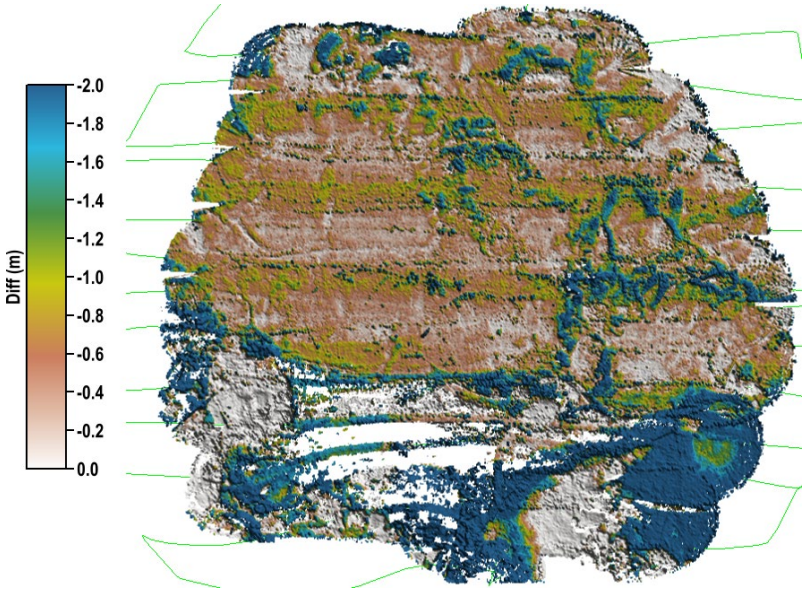

***Fig. 4.6.4**: Partially post-processed ice draft data showing the difference between 1 July and 24 June. The difference map is based on two multibeam surveys on the aforementioned dates. The diameter of the map is approximately 300 meters. The negative values indicate ice loss over the course of the week. Interestingly, the ridges are identifiable from the difference map based on ice loss in the range of meters, whereas the level FYI areas indicate a loss in the range of 10-20 cm.*

Objective 3 was addressed through regular depth profiles and lateral profiling particularly during the multibeam dives. The multibeam dives are done at a constant depth of 20 meters within the reach of the tether of up to 280 meters away from the dive hole. We were able to identify different water masses such as a freshwater layer under ice, the mixed layer and the halocline underneath. In addition to the physical parameters, distinct changes were measured in chlorophyll-a and PH between the different parts of the vertical water column. The top of the pycnocline was by chance just under 20 meters depth on one of the multibeam dives and, during this dive, we were able to observe indications of internal waves with a wavelength of tens of meters and signs of the water masses mixing in the CTD data.

Objective 5 was addressed during the dives whenever objects of interest were identified underwater, such as ridge keels and rafted ice pieces. Efforts were made to revisit the interesting features at least weekly. The rafted ice blocks shown in figure 4.6.5 were initially connected, separated and evolved into rotten ice over the weeks, and the other half broke off prior to the revisit on 14 July.

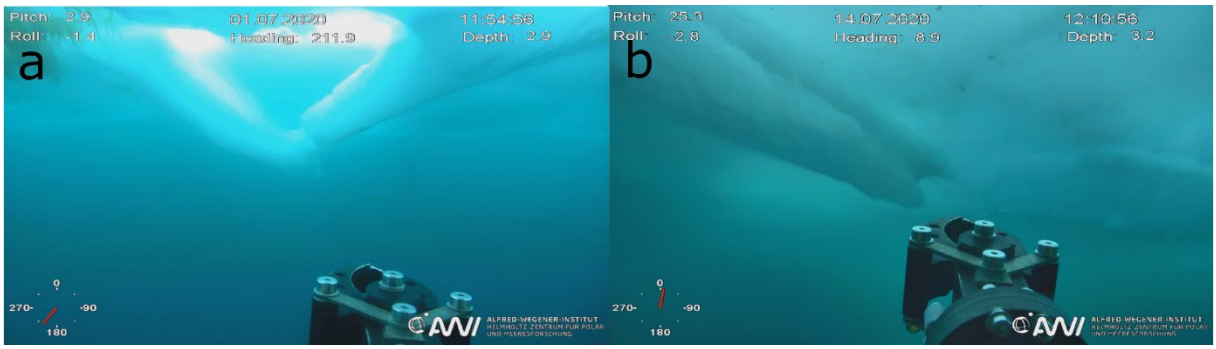

Fig. 4.6.5: Rafted ice in the dive grid, as observed on 1 and 14 July (a and b, respectively). The perspective between the frames is rotated by 180 degrees. The evolution of this feature was observed through documenting it with the HD video camera and high-resolution still photos from underneath.

The first installation of the Underwater Hyperspectral Imager (UHI) was done successfully (Objective 6), and the UHI was operated for a total of five dedicated dive missions. The post-processing protocol is being developed at the time of writing this. Below are two preliminary figures of the data.

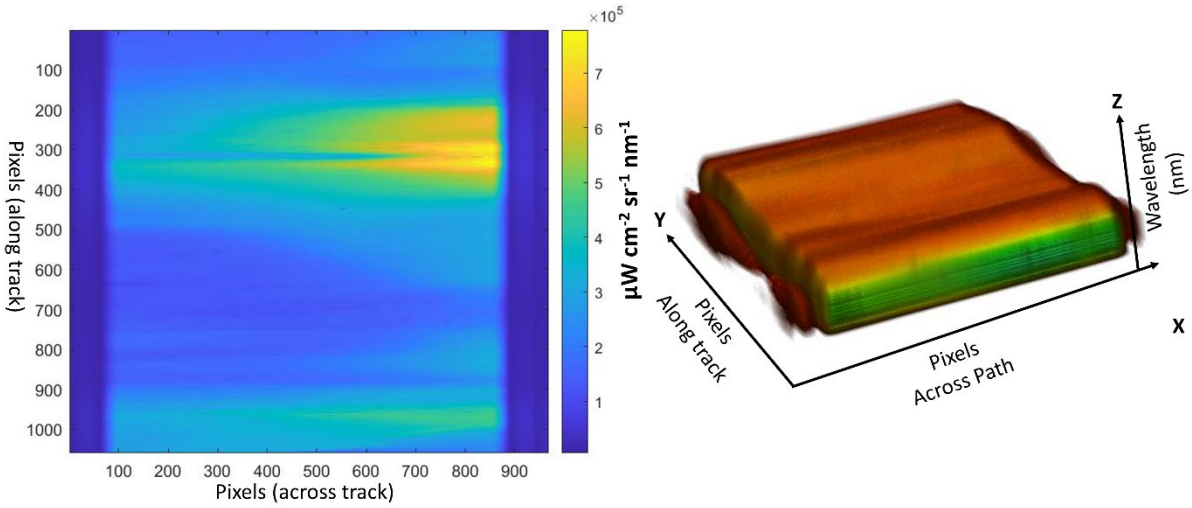

Fig. 4.6.6: *Preliminary survey data from the UHI showing a 2D/3D spatial representation of integrated radiance over a section of the survey (left) and the corresponding Image Cube (right) showing the 3D/4D representation including all spectral information over the survey section (NOTE: there is a different color scale and no color bar for the right image).*

4.6.4 Data management

All data and their availability conform to the MOSAiC data policy (see Chapter 9 APPENDIX). Data recorded on the dives on PS122-4 is stored in the Mosaic Central Storage in the “exdata” folder under the vehicle id “BEAST”. The dive data is stored in separate folders for each device operation (Appendix A). Data will be stored in the PANGAEA data repository: World Data Center PANGAEA Data Publisher for Earth & Environmental Science www.pangaea.de. All data are handled, documented, archived and published following the MOSAiC data policy. DOIs will be communicated to PANGAEA for later access via the future MOSAiC Data Portal.

References

Katlein, C., M. Schiller, H. J. Belter, V. Coppolaro, D. Wenslandt, and M. Nicolaus (2017), A New Remotely Operated Sensor Platform for Interdisciplinary Observations under Sea Ice, *Frontiers in Marine Science*, *4*(281), doi:10.3389/fmars.2017.00

4.7 Optics

Maddie Smith[1], Felix Linhardt[2], Amy Macfarlane[3], Ian Raphael[4], Melinda Webster[5], Julia Regnery[6], Ilkka Matero[6], Benjamin Lange[7], Marcel Nicolaus[6] (not onboard), Christian Katlein[6] (not onboard), Mario Hoppmann[6] (not onboard), Lovro Valcic[8] (not onboard), Don Perovich[4] (not onboard), Bonnie Light[1] (not onboard), Chris Polashenski[4,9] (not onboard), Mats Granskog[7] (not onboard), Dirk Notz[10] (not onboard)

[1] UW Seattle
[2] CAU
[3] SLF
[4] Dartmouth College
[5] UAF
[6] AWI
[7] NPI
[8] Bruncin
[9] USACE/CRREL
[10] U Hamburg

4.7.1 Objectives

The driving science question of the MOSAiC observational plan for optics is: how sunlight is partitioned by the sea-ice cover and the upper ocean over the course of the sunlit season? The specific science questions addressed are:

- What is the seasonal evolution of apparent optical properties (albedo, transmittance) for representative snow and ice covers (transect) and for representative ice types (study sites)?
- Is the Surface Heat Budget of the Arctic Ocean (SHEBA) albedo transect time series still representative of melting Arctic sea ice?
- How do optical properties of first-year ice (FYI) and multiyear ice (MYI) evolve under the same, large-scale forcing?
- What are the time-dependent apparent optical properties (AOPs) (e.g., albedo, transmittance) for a variety of observed ice types ("AOP library")?
- What are the time-dependent inherent optical properties (IOPs) (e.g., scattering properties) for a variety of observed ice types ("IOP library")?
- Over what spatial scales are ground measurements representative of the broader area (model grid cell and satellite footprint scales)?

The optics tasks presented in here have strong linkages to many interdisciplinary science questions within the MOSAiC framework:

- Sea ice mass balance: Surface and bottom ablation are strongly driven by the absorption of sunlight.
- Melt pond observations: pond depth and distribution are driven by solar heating, and subsequently govern the partitioning of heat.
- Snow metamorphism and surface scattering layer evolution: the changing physical and optical properties of the snow and ice surfaces due to incoming radiation.
- Ocean: mixed layer dynamics are impacted by the partitioning of sunlight by the ice cover.
- BGC: photosynthetic and photolysis processes.
- ECO: primary productivity, photophysiology.
- Airborne and Remote Sensing: hyperspectral, laser and radar altimetry, and scatterometer measurements are strongly tied to surface optical/physical conditions.

The specific questions above are investigated with the following tools:

- Surface albedo surveys (linear / grid survey; time series survey)

- Surface albedo study sites (both time series, and some 'destructive' measurements)
- Fixed radiation stations
- ROV transmittance surveys (grid; time series)
- Drones and helicopter measurements
- Sea ice cores for optical and texture characterization
- Profiles of optical properties (Light harp; Optical tunnels; IOP probe)
- Goniometer
- Hyperspectral camera

This chapter describes measurements made using these tools and presents preliminary results from the albedo surveys and study sites.

4.7.2 Work at sea

4.7.2.1 Surface albedo

Both spectral and broadband albedo measurements were collected regularly throughout Leg 4. Coincident measurements of spectral and broadband albedo were made whenever possible, with preference for spectral measurements when time constraints did not allow both.

Spectral albedo measurements were primarily made with an ASD FieldSpec3 spectroradiometer. The ASD measures radiant energy with a spectral range of 350-2500 nm. Albedos are calculated using the ration of incident (incoming) to reflected energy at each wavelength within this range. The unit is housed in a backpack with a fiber optic cable extending to the sensor. The sensor is mounted on the end of a 1-meter long arm in a gooseneck aimed at a spectralon cosine collector. This setup allows the observer to be very mobile while minimizing the footprint of the observer in the measurement (Fig. 4.7.1).

Broadband albedo measurements were performed with a Kipp and Zonen albedometer. It consists of two pyranometers recording the incoming radiation and the reflected radiation in the form of an electrical signal measured with a multimeter. This setup was used during Leg 3, and is the same one that used during the SHEBA experiment. Previously on SHEBA and Leg 3, the setup was used on a tripod. For Leg 4, the setup was used instead with a harness and arm to increase mobility and measurement speed (Fig. 4.7.1).

Fig 4.7.1: *Albedo transect along Lemon Drop Line on 24 July with the ASD (background) and Kipps (foreground).*

A total of three albedo survey lines were set up and regularly revisited. Two 200-m long transects on the primarily FYI area of the floe were setup on 19 June, shortly after arrival on the floe, and an ROV transect (total length 140 m) was established on 27 June. The 200-m transects were initially oriented West-East (start or 0 m at the West end) with measurements made to the South of the line. The ends of the lines were marked with flags, with white stakes marking every 20 m on all transects. Measurements were made every 5 m by pacing out the distance between subsequent stakes.

- The first line (Lemon Drop line, or LDL) was on primarily FYI, with some proto-ponds initially.
- The second line (Root Beer Barrel, or RBB) was to the North of LDL. It had thicker ice along the second half, with ridged and rafted ice evident.
- The ROV transect (Choco X-Roads) established within the ROV optics grid, extended 100 m to the SW from the hole, approximately along the line of navigational markers. Another 40 m line ran perpendicular, intersecting near the 50 m on the first line (extending 10 m to the North, and another 30 to the South). This area was comprised of relatively thin, primarily level, FYI.

The locations of these lines are shown on the map in Figure 4.7.2.

Key components of the optics program were collocated surface characterization and mass balance with albedo measurements. As much as possible, we took photos of the albedo footprint and measurements of the depth of the surface type (snow, surface scattering layer (SSL), or pond). Measurements were done in combination with additional surface characterizations whenever possible, particularly Near Infrared (NIR) camera images and microCT samples. Surface characterization transects typically targeted a few representative surface types along the lines, which were regularly revisited (see Section 4.2). GEM-2 and Magnaprobe surveys were done at least once a week to monitor the mass balance (snow, melt pond, and ice thickness) changes of the albedo lines (see section 4.5 – for details). In addition, six Lidar scan sets were completed over the Lemon Drop and Root Beer line areas (see section 4.4 for details).

Although the majority of the optics transects from the prior leg were unreachable or destroyed by dynamics, we were able to make two visits to the SYI line established on April 27 during Leg 3, near the radiation buoy 2020R14.

Additional opportunistic albedo measurements were made at locations of interest. For these locations, only spectral albedo (ASD) was measured. These opportunistic measurements included melt ponds (stern area of the *Polarstern*), mass balance stakes locations, and level ice with snow/SSL removal experiments (three experiments).

In addition to the measurement of melt pond albedos along the transects, ponds albedos were regularly observed as part of the melt pond observational program. These observations used an Ocean Optics spectrometer installed on a 1-m gimbaled arm. The details and results of these measurements can be found in the Pond section 4.12.

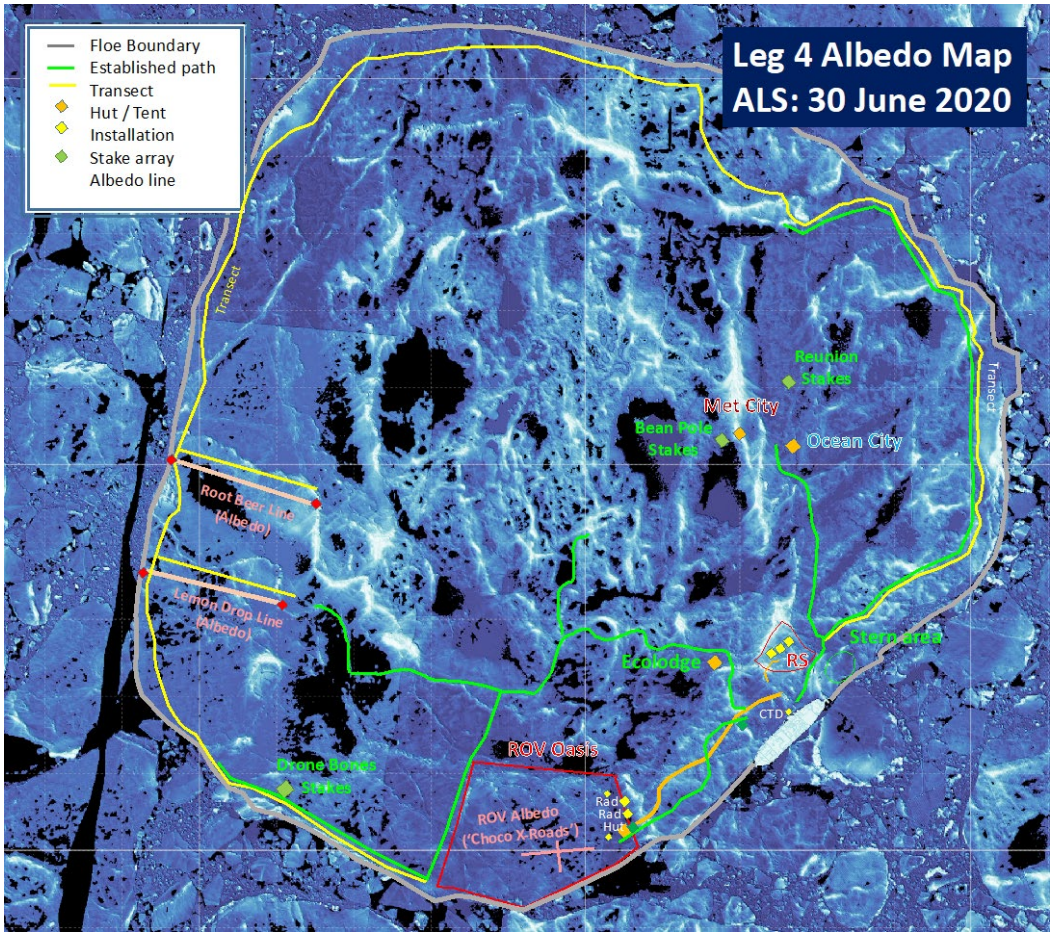

Fig. 4.7.2: *ALS Map showing locations where albedo measurements were made during Leg 4, including: Lemon Drop, Root Beer, and ROV albedo lines (in pink), stakes sites (green boxes), and Ecolodge and stern experiment areas (green labels).*

4.7.2.2 Fixed radiation stations

One radiation station (2020R15) was deployed on PS122.4. It was composed of three RAMSES radiometers which record the incoming, reflected, and transmitted irradiance. It was deployed on the 13 July at 14:08 UTC close to the ROV optics site near a ridged area (Jaridge) and some melt ponds (Fig. 4.7.3).

2020R15 had the following sensors attached: SAMIP5068, SAMIP50C5, SAMIP50C6. SAMIP50C6 was upward-looking on the surface while SAMIP5068 downward-looking. The distance to the surface of the SAMIP5068 was 83 cm on the deployment day. The third sensor, SAMIP50C5, was deployed one meter under the ice bottom. The ice thickness was 151 cm, the draft 140 cm, and the snow/surface scattering layer 1 cm. During the installation period, two data readings were completed as well as tilt corrections when needed. All parts of the radiation station were recovered on 29 July at 7:43 UTC. The distance to the surface from the downward-facing sensor was 94 cm.

Fig. 4.7.3: *AWI radiation buoy 2020R15*

Two AWI radiation stations that were deployed in or close to the old CO on Leg 3 were visited twice to download the data. These stations were 2020R14 and 2020R13. 2020R13 was destroyed by a ridge and only the two surface RAMSES were recovered. 2020R14 was close to the original Northern Loop transect (Fig. 4.7.4).

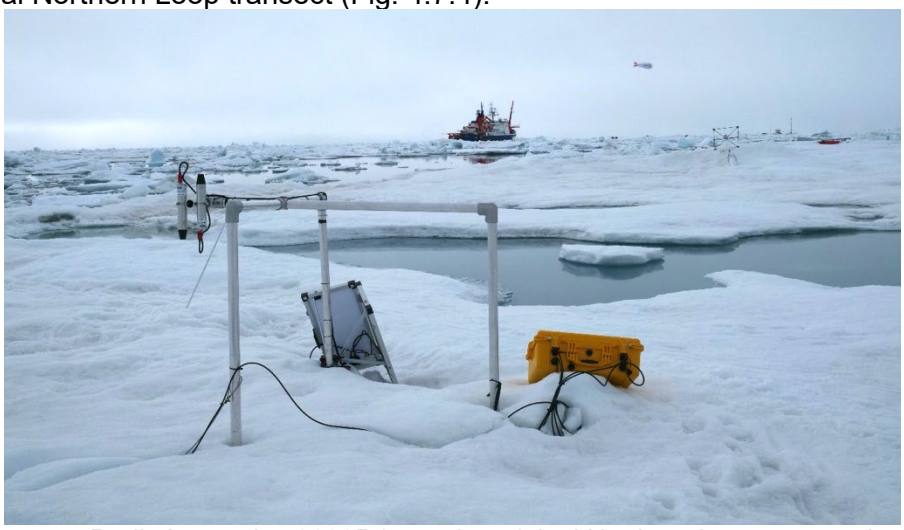

Fig. 4.7.4: *Radiation station 2020R14 on the original Northern Loop transect in July.*

4.7.2.3 ROV Optics

The ROV completed under-ice transmittance grids as part of its regular dive plan. In addition, transmittance transects along the ROV albedo transect ('Choco X-Roads') were done near-coincident with albedo measurements when possible. The optical measurements of the ROV are described in detail in the Section 4.6.

4.7.2.4 Aerial albedo measurements

Aerial measurements of albedo from UAVs and helicopter will be used to understand the scale-dependence of albedo measurements made on the ground.

There were two unmanned aerial vehicles (UAVs, or drones) used for albedo measurements during this leg. A copter equipped with paired pyranometers for broadband albedo measurements (from the University of Colorado) was flown regularly during Leg 4. This included one flight over both 200-m albedo lines (on 6 July) and over the ROV grid four times during the 24-hour sampling period (10-11 July). This platform was also equipped with a multispectral camera. A second copter equipped with an Ocean Optics spectrometer to make

spectral albedo measurements (from FMI) was flown on a test flight only during Leg 4. More details on these platforms can be found in Section 3.8.

Area-averaged albedo measurements were made using paired pyranometers installed on the helicopter on a limited number of flights. More details can be found in the helicopter section 4.3.

4.7.2.5 Optics and sea ice texture cores

'Optics cores' were taken weekly at both FYI and SYI coring sites. Five additional optics cores were taken during the leg: 3 coincident with L-Arm measurements, and 2 from ponds during destructive sampling of the RBB albedo line. Laboratory work following the completion of MOSAiC will analyze these cores for scattering and transmittance profiles. The work related to sea ice cores extracted for optical and texture studies are described in chapter 4.1 Ice Coring.

4.7.2.6 L-Arm measurements

Transmittance of light through sea ice was measured a number of times throughout the cruise using an articulated L-Arm setup by a member of the ECO team. The details of these measurements are described in Chapter 6. Three of these measurements were collocated with cores collected for optical analysis.

4.7.2.7 Light harp

An optical (light) harp was deployed on 15 January (during PS122.2) at the original SYI dark site / LM site. It has been recording and transmitting data directly via satellite since with no known interruptions. It is instrumented with upward- and downward-looking sensors spaced at 25-cm resolution to measure: vertical profiles of upwelling and downwelling radiation including low-light period/moonlight, four bands, with and without IR filter, and temperature.

4.7.2.8 Optical tunnels

A prototype for a new setup to obtain in situ transmittance profiles was tested. Two clear polycarbonate tunnels were installed in FYI near Reunion Stakes, with one in a melt pond and one in bare ice (Fig. 4.7.5). Measurements were made twice (8 and 19 July).

Figure 4.7.5: *Optical tunnels installed at the Reunion Stakes site near Met City and the ADCP hole. Tunnel 1 was under bare FYI (left), and Tunnel 2 was under a melt pond (right).*

4.7.2.9 IOP probe

An inherent optical properties (IOP) probe was used to measure the scattering profiles of ice at coring locations. Two full profiles were made at the FYI coring site, and one partial profile was made at the SYI coring site.

4.7.2.10 Goniometer

The goniometer was unable to be successfully operated on this leg.

4.7.2.11 Hyperspectral camera

The hyperspectral camera was installed at the Remote Sensing site for the duration of Leg 4, and is described in the Remote Sensing section 4.11.

4.7.3 Preliminary results

4.7.3.1 Surface albedo

In total albedo measurements were made at the survey lines:

- 14x on Lemon Drop Line (13 with broadband albedo, 5 with NIR transect)
- 12x on Root Beer Barrel Line (9 with broadband albedo, 1 with NIR/destructive sampling)
- 9x ROV (Choco X-Roads) (4 with broadband albedo, 3 with uCT)

In addition, we made opportunistic albedo measurements (ASD only):

- 5x in the Stern area (including 2x SSL removal experiments)
- 4x at Reunion Stakes (2 with NIR/uCT)
- 2x at Bean Pole Stakes
- 1x at Drone Bones Stakes
- 1x at FYI Coring site
- 2x at Ice Station on transit to the floe
- 5x at SSL removal pit at Ecolodge (all with NIR/uCT)

Note: totals include distinct days only, and do not include the high-frequency sampling during the 24-hour period.

These data characterize the evolution of the surface albedo of the MOSAiC Central Observatory during summer. From the three albedo lines, we can characterize the evolution of albedo on a wide range of sea ice and surface types. These data will be useful for comparing with the seasonal evolution observed during SHEBA and progressing climate model parameterizations.
Fig. 4.7.6 shows all broadband albedo measurements along the three albedo survey lines. While we generally observed a decrease in average albedos over the summer melt season, we can also see the differences between the thin ponded ice in the ROV area, where albedos were initially very low, and the SYI along the Root Beer line, where average albedos were higher. We see similar differences in the line-averaged spectral albedos (Fig. 4.7.7).

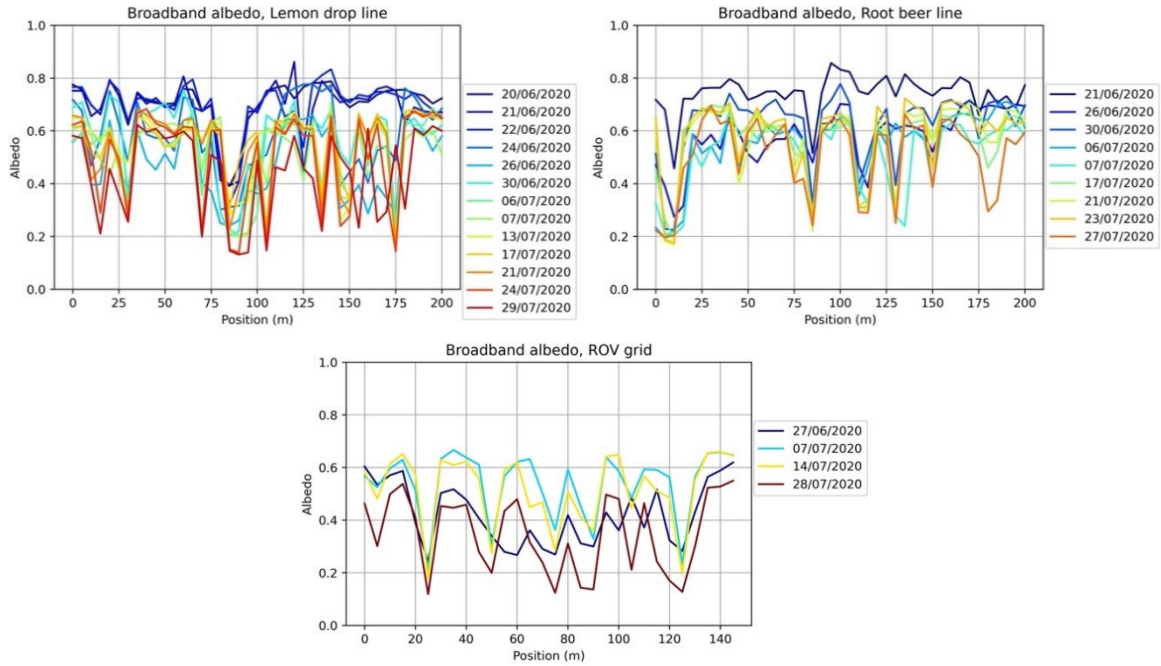

Fig. 4.7.6: *Broadband albedo measurements from all of Leg 4 on the three main albedo survey lines: Lemon Drop line (upper left), Root Beer Barrel line (upper right), and ROV Choco X-Roads (bottom). Lines are colored by day from early in the summer (blue) to late in the summer (red).*

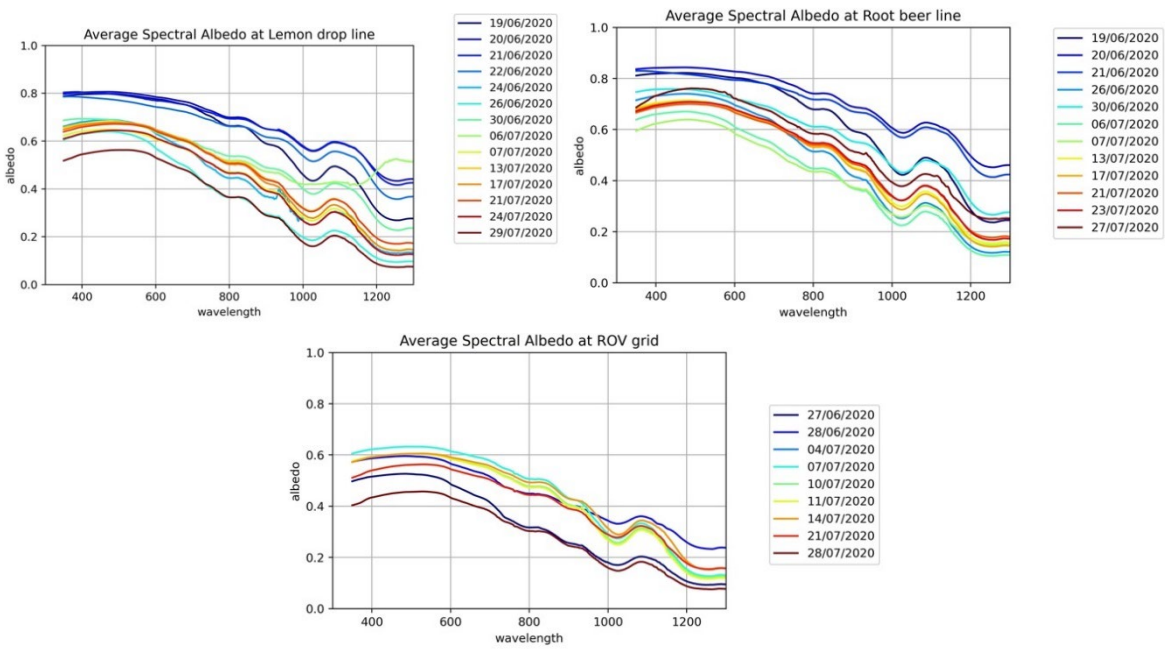

Fig. 4.7.7: *Line-averaged spectral albedo measurements from Leg 4 over the three main albedo survey lines: Lemon Drop line (upper left), Root Beer Barrel line (upper right), and ROV Choco X-Roads (bottom). Lines are colored by day from early in the summer (blue) to late in the summer (red).*

Collocated measurements, particularly surface characterization and mass balance transects, will be important in interpreting the temporal and spatial variability of albedo lines. For example, thickness drilling measurements along the Root Beer line on 17 and 19 July (Fig. 4.7.8) show thick, ridged and rafted ice, which likely contributed to higher albedos observed along parts of the line.

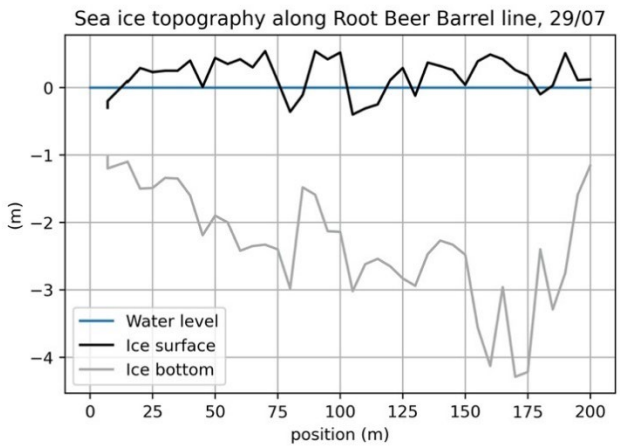

Fig. 4.7.8: *Sea ice topography of the Root Beer albedo line measured on 27 and 29 July. Ice surface (black line) below the water level (blue line) indicates ponded surface. Ice thickness is the difference between the ice surface and ice bottom (grey line).*

We identified 'library sites' along the albedo survey lines to capture the time evolution of key surface Arctic surface types throughout summer. These measurements can help us upscale our ground measurements to understand broad-scale changes in albedo across the Arctic. This is particularly important as we know that our floe does not represent the typical distribution of surface covers in the broader region. We use a number of points along our established albedo transects (measured every 5 m) as 'library sites' representing a variety of characteristic surface covers. These include:

- Melt ponds on thicker SYI (blue ponds) and thinner FYI (dark ponds)
- Bare SYI and FYI (evolution from snow-covered to 'surface scattering layer')
- Sediment-laden SYI
- Thin FYI

The high sediment load on our floe was a unique characteristic compared to other floes in the area and time series of albedo evolution from other field campaigns. An example of the evolution of spectral albedo at a library site with sediment is shown in Fig. 4.7.9, where the impact of the sediment is seen by the decrease in albedo at low wavelengths, and an increase in the wavelength of the peak albedo to slightly less than 600 nm

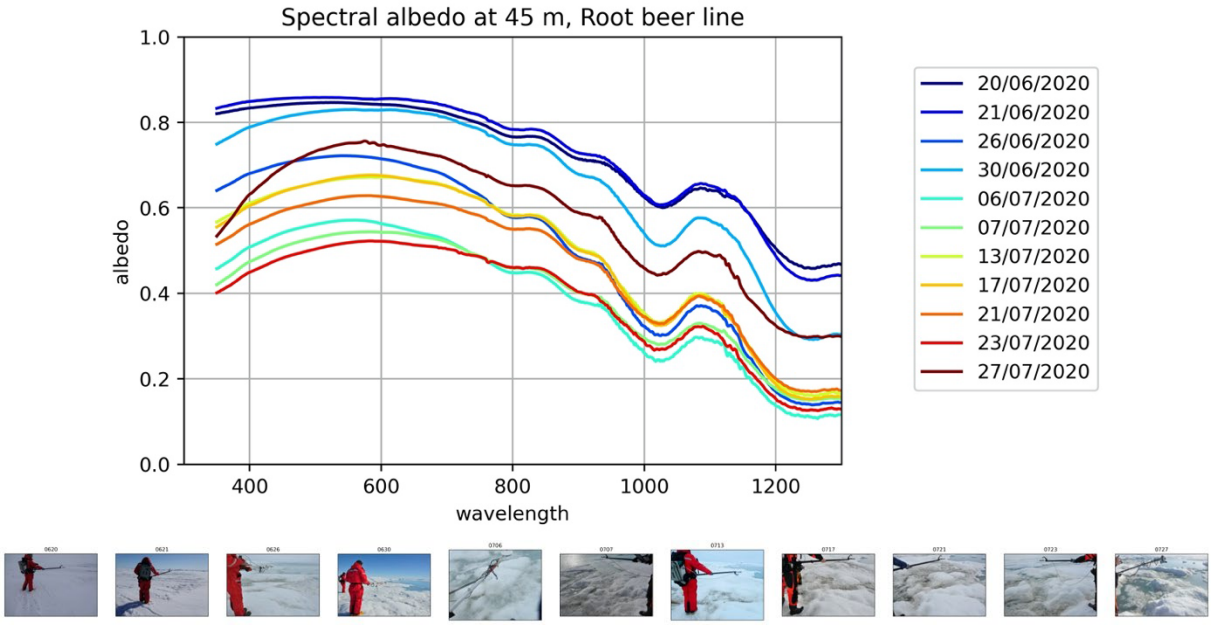

Fig. 4.7.9: *Evolution of spectral albedo at 45 m position on the Root beer line, where there was sediment-laden second-year ice. Series of photos from the site show the emergence of visible sediment on the surface. Lines are colored by day from early summer (blue) to late summer (red).*

The albedo line established on the SYI near radiation buoy 2020R14 during Leg 3 was visited twice during Leg 4. On 29 June, nearly all of the line remained, and we were able to measure both spectral and broadband albedo. On 15 July, only the last two points of the line (near the radiation station) were located and measured. Only broadband albedo was measured along this line during Leg 3. This is the only albedo line that was able to be measured during Leg 3 (prior to melt onset) and during melt on Leg 4. In the time series of broadband albedos in Fig. 4.7.10, we can see the impact of pond formation on previously snow-covered areas. Additionally, during the last visit on 15 July we observed the presence of sediment in the ice.

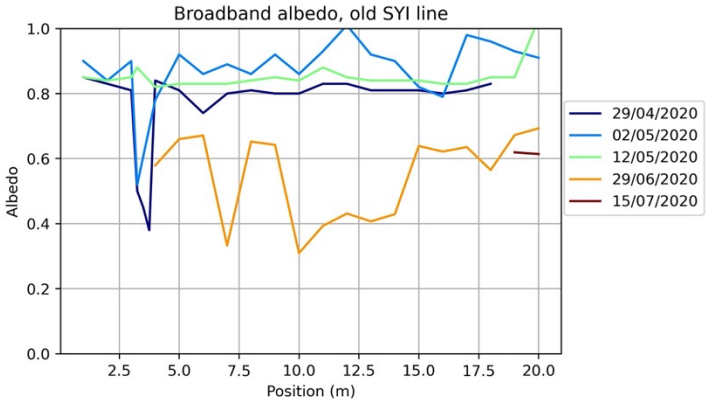

Figure 4.7.10: Broadband albedos measured along the SYI line established during Leg 3. Lines are colored by day from spring during Leg 3 (dark blue) to summer during Leg 4 (orange).

High-frequency sampling during a 24-hour sampling period on 10-11 July showed the effects of weather and short-term variability on surface albedo. During this period, we measured 17 locations (including bare and ponded ice) every 3 hours, and the full ROV transect every 6 hours. Although the weather was foggy and drizzly rather than the sun we had hoped for, we observed the evolution of the bare ice albedos with changing weather and solar input. Fig. 4.7.11 shows an example of the changes at a location with bare ice with a ~6-cm SSL ('bear fur'). The albedos initially increased slightly, possibly due to cooler temperatures, and then decreased on the morning of 11 July, likely due to rainfall. 850 nm and 950 nm are included in the time series of albedos as particular wavelengths, as these are the wavelengths observed by the NIR camera, which was used 3 times on site during the sampling period. There were negligible changes in pond albedos over the sampling period.

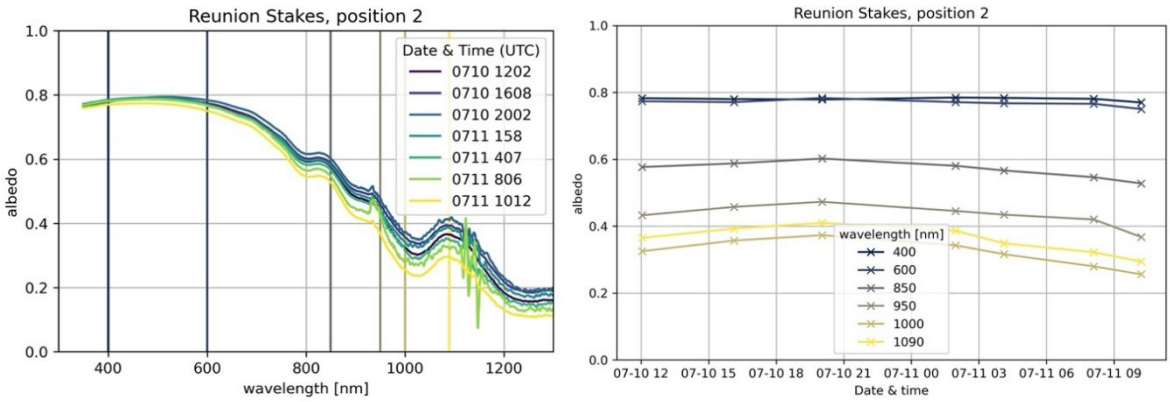

Fig. 4.7.11: *Example results from the 24-hour sampling period on 10-11 July. The location shown (position 2 at Reunion Stakes) was characterized by bare ice with 'bear fur' SSL. Spectral albedos (left) are colored by time, with measurements starting midday on 10 July in blue and midday on 11 July in yellow. Time series of albedos at specific wavelengths (demarcated by vertical lines) are shown on the right.*

A total of 3 snow/SSL removal experiments were completed. These experiments included regular spectral albedo measurements and coincident surface characterization with NIR and microCT, the latter of which are described in detail in the snow and surface characterization section 4.2. For each, side-by-side 3-m-by-3-m cleared and pristine areas were monitored over a period of time (until the relative surface changes were comparable). Two of these experiments were located in the stern area of the ship. One of these was in an area of lower freeboard and developed into an artificial pond, while the other was on a well-drained area and re-developed a ~5 cm SSL. The third experiment was next to the Ecolodge tent and also re-developed a SSL.

Observations along the ROV transect on 27 and 28 June provided a nice case study on the impact of a scant snowfall event on albedo. There was approximately 1 cm of fresh snow accumulation overnight on 27 June (Fig. 4.7.12). From comparing albedo transects in the ROV optics grid from 27 and 28 June, we can see the impact of snow on what had been a mostly bare (somewhat frozen) ice surface just hours prior (Fig 4.7.13).

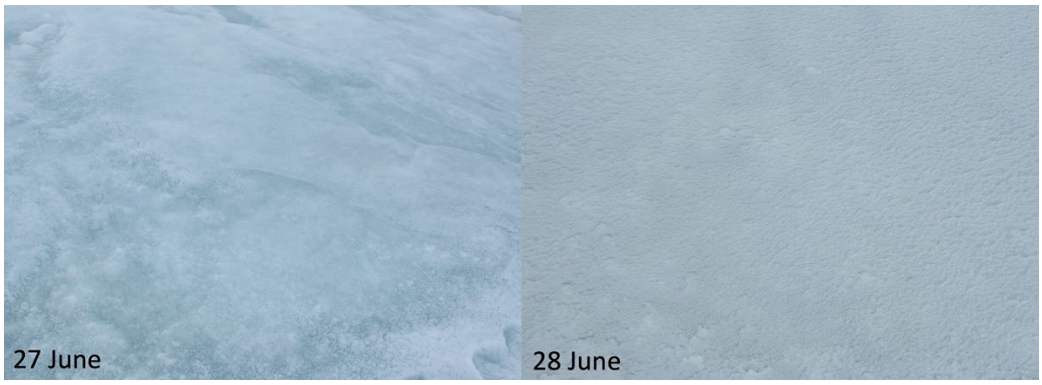

Fig. 4.7.12: *Photos of the surface near 40m on the ROV albedo line from 27 June (left) and 28 June (right). The surface is visibly wet and darker on the 27th. The surface was covered with a thin layer of fresh snow (~1 cm) on the 28th.*

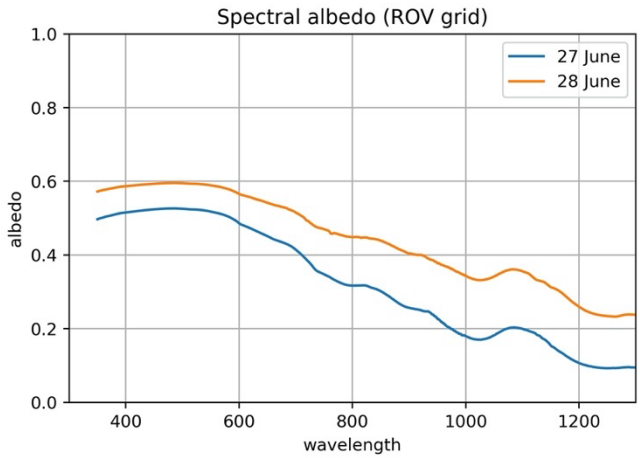

Fig. 4.7.13: *Line-averaged spectral albedo from the ROV albedo line on 27th June (blue) and 28th June (orange).*

4.7.4 Data management

All data and their availability conform to the MOSAiC data policy (see Chapter 9 APPENDIX). Albedo data (ASD and Kipps) is stored in the Mosaic Central Storage under mcs\platforms\pack_ice\ice_ps\dart_asd\exdata\PSS122-4_xx_xxx and mcs\platforms\pack_ice\ice_ps\dart_kipps\exdata\PSS122-4_xx_xxx. Corresponding pictures are stored in separate folders for each device operation. Each folder also includes an excel

spreadsheet with recorded metadata for a given set of observations, including who made the measurements, sky conditions, photo numbers, surface characterization measurements, and other notes.

Please refer to the excel spreadsheet for the appropriate photo credit information. If a photographer is not listed, refer to the cruise report and this chapter or the data set following the MOSAiC data policy (DSHIP and MSC).

Albedo and core optics data will be stored at the Arctic Data Centre following the agreement between ADC and the MOSAiC Project lead. DOIs will be communicated to PANGAEA for later access via the future MOSAiC Data Portal. The rest of the data will be stored at the PANGAEA data repository (World Data Center PANGAEA Data Publisher for Earth & Environmental Science www.pangaea.de.

All data are handled, documented, archived and published following the MOSAiC data policy.

Tab. 4.7.1: *Table of device names and URN numbers for optical instruments used during PS122.4.*

Instrument	**Device shortname**	**URN**	**# device operations**
Spectral surface albedo (ASD)	Dart_ASD	pack_ice:ice_ps:dart_asd	66
Broadband surface albedo (Kipps)	Dart_Kipps	pack_ice:ice_ps:dart_kipps	28
Transmittance L-Arm	Larm	pack_ice:ice_ps:larm	x
Light Harp	lightharp_1	**pack_ice:ice_ps**:lightharp_1	n/a
Optical tunnels (Spectral Evolution)	UW_SPECEVOL	pack_ice:ice_ps:uw_specevol	2
IOP Probe	IOP_Probe	light_optics:iop_probe	3
Hyperspectral camera	SPECIM_IQ_01	pack_ice:ice_ps:specim_iq_01	1

Tab. 4.7.2: *Table of DSHIP numbers for all albedo measurements during PS122.4. See sections 4.2 Surface Characterizations and 4.5 Transect for the DSHIP numbers of collocated measurements.*

Date	Time UTC	Location	ASD (Dart_ASD)	Kipps (Dart_Kipps)
13-Jun	14:26	Ice Station - stbd	PS122-4_44_39	x
14-Jun	11:20	Ice Station - port	PS122-4_44_56	x
19-Jun	11:56	Lemon Drop Line	PS122-4_44_106	x
19-Jun	14:12	Root Beer Line	PS122-4_44_107	x
20-Jun	12:11	Lemon Drop Line	PS122-4_44_108	PS122-4_44_110
20-Jun	13:31	Root Beer Line	PS122-4_44_109	x
21-Jun	12:08	Root Beer Line	PS122-4_44_149	PS122-4_44_150
21-Jun	13:50	Lemon Drop Line	PS122-4_44_151	PS122-4_44_261
22-Jun	10:34	Lemon Drop Line	PS122-4_44_138	PS122-4_44_137

24-Jun	7:56	Lemon Drop Line	PS122-4_44_158	PS122-4_44_159
26-Jun	12:18	Lemon Drop Line	PS122/4_44-178	PS122/4_44-180
26-Jun	13:27	Root Beer Line	PS122/4_44-181	PS122/4_44-179
27-Jun	11:54	ROV	PS122/4_44-207	PS122/4_44-210
28-Jun	13:20	ROV	PS122/4_44-211	x
29-Jun	9:50	Old SYI Line	PS122/4_45-21	PS122/4_45-22
30-Jun	12:17	Lemon Drop Line	PS122/4_45-23	PS122/4_45-24
30-Jun	13:38	Root Beer Line	PS122/4_45-25	PS122/4_45-26
4-Jul	11:38	ROV	PS122/4_45-135	x
5-Jul	12:50	Stern	PS122/4_45-136	x
6-Jul	11:53	Lemon Drop Line	PS122/4_46_6	PS122/4_46_7
6-Jul	14:20	Root Beer Line	PS122/4_46_8	PS122/4_46_9
7-Jul	9:26	ROV	PS122/4_46-23	PS122/4_46-24
7-Jul	11:58	Lemon Drop Line	PS122/4_46-25	PS122/4_46-26
7-Jul	12:57	Root Beer Line	PS122/4_46-27	PS122/4_46-28
10-Jul	10:35	Stern	PS122/4_46-113	x
10-Jul	11:04	ROV	PS122/4_46-114	x
10-Jul	12:02	Reunion Stakes	PS122/4_46-115	x
10-Jul	13:13	Stern	PS122/4_46-116	x
10-Jul	16:08	Reunion Stakes	PS122/4_46-117	x
10-Jul	16:40	Stern	PS122/4_46-118	x
10-Jul	17:25	ROV	PS122/4_46-119	x
10-Jul	19:15	Stern	PS122/4_46-120	x
10-Jul	20:02	Reunion Stakes	PS122/4_46-121	x
10-Jul	22:00	Reunion Stakes	PS122/4_46-122	x
10-Jul	22:18	Stern	PS122/4_46-123	x
10-Jul	23:14	ROV	PS122/4_46-125	x
11-Jul	1:22	Stern	PS122/4_46-126	x
11-Jul	1:58	Reunion Stakes	PS122/4_46-127	x
11-Jul	4:07	Reunion Stakes	PS122/4_46-128	x
11-Jul	4:27	Stern	PS122/4_46-129	x
11-Jul	5:07	ROV	PS122/4_46-130	x
11-Jul	7:20	Stern	PS122/4_46-131	x
11-Jul	8:06	Reunion Stakes	PS122/4_46-132	x
11-Jul	10:12	Reunion Stakes	PS122/4_46-133	x
11-Jul	10:31	Stern	PS122/4_46-134	x
11-Jul	10:58	ROV	PS122/4_46-136	x
13-Jul	12:05	Lemon Drop Line	PS122/4_47-42	PS122/4_47-44
13-Jul	14:04	Root Beer Line	PS122/4_47-45	PS122/4_47-46
14-Jul	10:00	ROV	PS122/4_47-47	PS122/4_47-48
15-Jul	10:10	Old SYI Line	PS122/4_47-49	PS122/4_47-50
16-Jul	12:50	Reunion Stakes	PS122/4_47-80	x
16-Jul	13:10	Bean Pole Stakes	PS122/4_47-81	x
16-Jul	14:26	Stern	PS122/4_47-82	x
17-Jul	12:15	Root Beer Line	PS122/4_47-123	PS122/4_47-124

17-Jul	13:14	Lemon Drop Line	PS122/4_47-125	PS122/4_47-126
20-Jul	11:45	Ecolodge SSL Experiment	PS122/4_48-6	
21-Jul	9:32	ROV	PS122/4_48-87	x
21-Jul	12:00	Root Beer Line	PS122/4_48-88	PS122/4_48-89
21-Jul	12:55	Lemon Drop Line	PS122/4_48-90	PS122/4_48-91
21-Jul	15:02	Ecolodge SSL Experiment	PS122/4_48-92	x
23-Jul	7:27	Ecolodge SSL Experiment	PS122/4_48-93	x
23-Jul	12:09	Root Beer Line	PS122/4_48-94	PS122/4_48-95
24-Jul	7:14	Ecolodge SSL Experiment	PS122/4_48-150	PS122-4_48-100
24-Jul	8:10	Lemon Drop Line	PS122/4_48-151	PS122/4_48-212
25-Jul	7:43	Drone Bone Stakes	PS122/4_48-152	x
25-Jul	8:29	Reunion Stakes	PS122/4_48-153	x
25-Jul	8:57	Bean Pole Stakes	PS122/4_48-154	x
27-Jul	7:36	Ecolodge SSL Experiment	PS122/4_49-50	x
27-Jul	8:50	FYI Coring Site	PS122/4_49-50	x
27-Jul	14:35	Root Beer Line	PS122/4_49-51	PS122/4_49-52
28-Jul	7:43	ROV	PS122/4_49-53	PS122/4_49-54
29-Jul	11:52	Lemon Drop Line	PS122/4_49-55	PS122/4_49-56

4.8 STAKES

Ian Raphael[1], Ilkka Matero[2], Madison Smith[3], Don Perovich[1] (not on board)

[1] Dartmouth College
[2] AWI
[3] University of Washington

4.8.1 Objectives

Point measurements of ice and snow mass balance (IMB) encompassing a full seasonal cycle from freeze-up to melt are rare. Likewise, despite high local variability of snow and ice cover, such observations are rarely collected in clusters (more than one observation point in a single location). The MOSAiC IMB observations are designed to address these challenges. In addition to interpreting thermodynamic processes, IMB measurements are also necessary for the interpretation of ice dynamics (Section 4.10), ROV measurements (Section 4.6), and others, including cross-disciplinary topics (e.g., false bottom formation, ocean-ice-atmosphere heat fluxes, etc.). Our primary goals on Leg 4 were to

- Characterize the transition from winter ice-growth into the summer melt season
- Quantify and separate basal and surface melt rates
- Observe variation in melt progression across different ice types, e.g. in refrozen lead, first-year ice (FYI), second-year ice (SYI)
- Observe variation in melt progression across different surface types, e.g. ponded ice, clean ice, sediment-laden ice
- Observe melt progression across different ice thicknesses and structures, e.g. level ice, undeformed ice, hummocks, ridges, and ice adjacent to the floe margin
- Link point mass balance observations with point surface optical measurements (Section 4.7), e.g. integrated and spectral albedo, in-ice spectral measurements
- Link point mass balance observations with distributed under-ice optical measurements, e.g. those made using the ROV, L-arm, and under-ice radiation stations
- Link point mass balance observations with local and zonal atmospheric observations, e.g. the MET City, TROPOS and AWI balloon, ASFS, and AWI mobile Flux sled observations (see Chapter 3)
- Link point mass balance observations with local and zonal oceanographic observations, e.g. ship based CTD casts, Ocean City MSS and ADCP measurements, distributed Upriser CTD measurements, and directed YSI and Castaway sampling (see Chapter 5, Lead Sampling, and section 4.13).

The devices used for point IMB observations on MOSAiC are grouped under the 'Stakes' task, and include:

- IMB buoys, including SIMBs, SIMBAs, IMBs
- Digital Thermistor Chains (DTC)
- Ablation stakes and hotwire thickness gauges

4.8.2 Work at sea

4.8.2.1 IMB buoys

Several IMBs were recovered at the end of Leg 4--information about these recoveries can be found in a separate document regarding the status and recovery of the distributed network.

4.8.2.2 DTC network

12 DTC units were found and visited during Leg 4, and no new units were deployed. Four DTC units were recovered from remote sites that were not planned to be revisited during MOSAiC. Eight of the remaining units were still presumed active at the time of the breakup of the fortress floe on 31 July.

Tab. 4.8.1 *List of DTC units that were read and/or recovered during Leg 4.*

MCS/DSHIP name	Unit name, map name	Deployment date (yyyy.mm.dd)	Deployment site (site origin)	Status / latest data read	Notes
DTC09_256	RS019	2020.01.28	ROV site at Fort Ridge T3 (Legs 1-3)	On ice / 2020.07.01	
DTC10_256	RS020	2020.01.28	ROV site at Fort Ridge T2 (Legs 1-3)	On ice / 2020.07.01	
DTC11_416	RS001	2019.11.05	Old remote sensing site (Legs 1-3)	Recovered / 2020.06.10	Recovered on 2020.07.22
DTC12_416	RS002	2019.11.05	Old remote sensing site (Legs 1-3)	Recovered / 2020.05.14	Recovered on 2020.07.14
DTC16_416	RS010	2019.11.07	Stress panels close to ship (Legs 1-4)	Recovered / 2020.04.27	Recovered on 2020.07.14 - Not connected between 2020.04.27 and 2020.05.08 due to moving ship; re-deployed on May 08 09:00 UTC. No data after redeployment
DTC20_416	RS008	2019.11.22	Northern Transect Loop (Legs 1-3)	On ice / 2020.07.15	stopped recording on 2020.02.27; detected 2020.05.15 (empty battery); continued from 2020.05.16 onwards
DTC21_416	RS011	2020.01.28	ROV site at Fort Ridge T1 (Legs 1-3)	On ice / 2020.07.01	Power connector broken during transport to deployment site, continued from 2020.02.04

MCS/DSHIP name	Unit name, map name	Deployment date (yyyy.mm.dd)	Deployment site (site origin)	Status / latest data read	Notes
DTC26_416	RS021	2020.02.05	Alli's Ridge (Legs 1-4)	On ice / 2020.07.26	Power connector broken during transport to deployment site, continued from 2020.02.07
DTC31_512	RS027	2019.11.22	Northern Transect Loop (Legs 1-3)	On ice / 2020.07.15	
DTC32_512	RS029	2019.11.22	Northern Transect Loop (Legs 1-3)	On ice / 2020.07.15	Battery cable ripped out 2020.04.17, spotted on 2020.04.22, active on 2020.04.24 10:00 UTC
DTC33_512	RS028	2019.11.22	Northern Transect Loop (Legs 1-3)	On ice / 2020.07.15	stopped recording on 2020.02.27; detected 2020.05.15 (empty battery); continued from 2020.05.16 onwards
DTC40_512	RS040	2020.05.06	David's Ridge (Legs 1-3)	Recovered / 2020.06.21	Recovered on 2020.07.01

4.8.2.3 Ablation Stakes and Hot Wires

The stakes sites are manual ice mass balance measurement sites. A 'stake' is actually a paired ablation stake and hotwire thickness gauge. The ablation stake gives the position of the ice and snow surfaces, while the thickness gauge indicates the position of the ice bottom. From these measurements, we can determine the total change in ice and snow thickness, and separate surface vs. basal melt/growth. At each site, we installed several stakes in grid patterns, measuring local spatial and temporal variability of ice thickness.

Virtually all of the stakes sites installed on previous legs were destroyed, either during Legs 1-3 or during the Leg 3/4 transfer, during which Polarstern was absent from ice camp. Ridge Ranch was the only site that was partially intact and operable upon our return to ice camp in June, though it was separated from our new CO floe, referred to as 'The Fortress.' We were able to visit Ridge Ranch to make measurements once, on 8 July. Due to the logistical

difficulties involved in accessing the site, we discontinued measurements at Ridge Ranch for the rest of Leg 4.

We established three new stakes sites on Leg 4: *Drone Bones*, *Reunion Stakes*, and *The Beanpole Stakes*, installed on 25 and 26 June and 7 July, respectively. We measured every site at least three times each week, and increased to bi-daily and finally daily measurements as melt rates increased. Descriptions of the sites follow below.

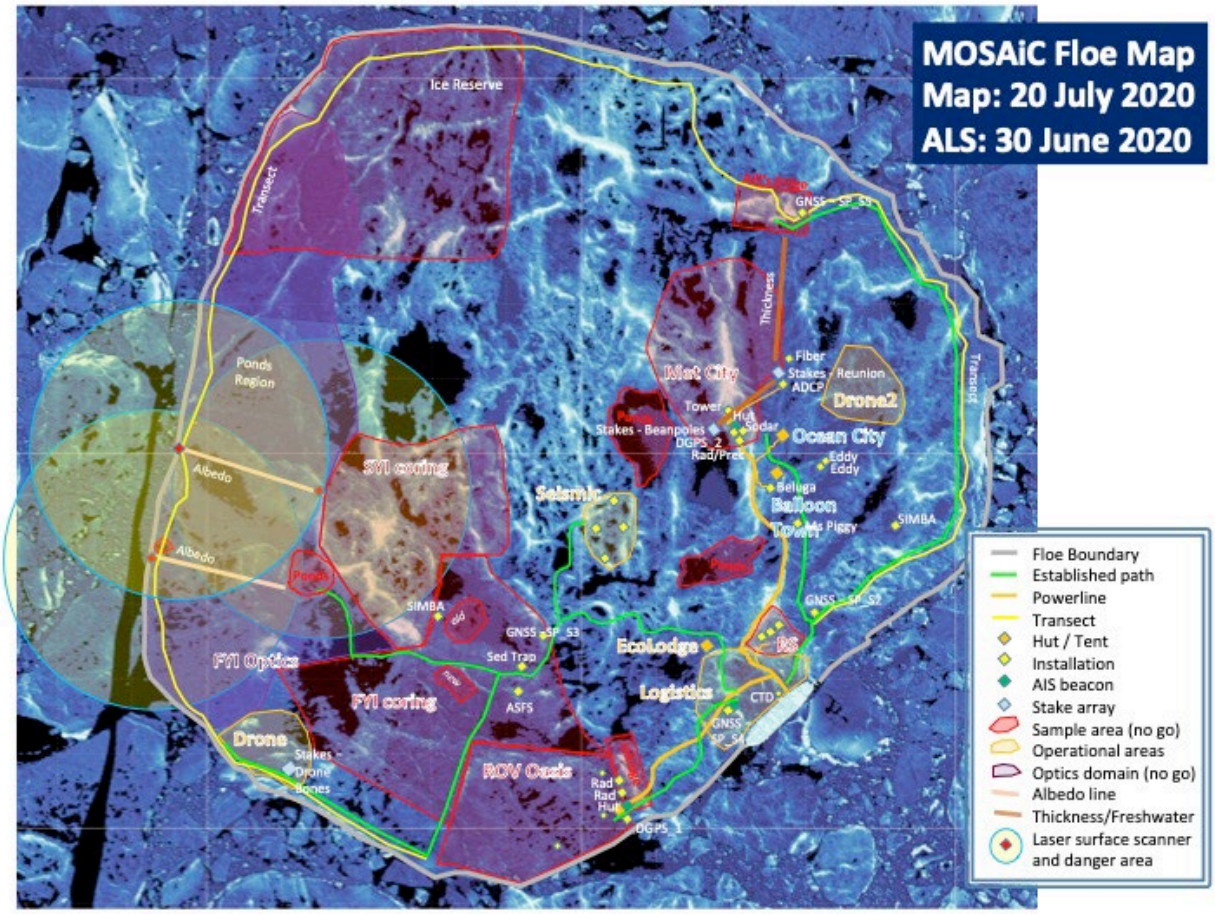

Fig. 4.8.1: *Floe map displaying the locations of all installations on the floe, including stakes sites. The stakes sites, from bottom left to top right, are: Drone Bones, The Beanpole Stakes, Reunion Stakes.*

Drone Bones

URN: *pack_ice:ice_ps:dart_stakes_clu_11*

We installed Drone Bones on Leg 4 on a mostly level FYI pan, adjacent to the floe edge where the presence of a lead was fairly consistent. It wais also bordered by a small ridge on one side, and a much larger ridge and rubble field at the floe edge. The plot was ~300m from the FYI Optics albedo sites -- Lemon Drop and Root Beer Barrel albedo lines. It was also on the edge of the TLS scanning field and directly next to the original drone site, which was eventually moved due to difficult access to this part of the floe.

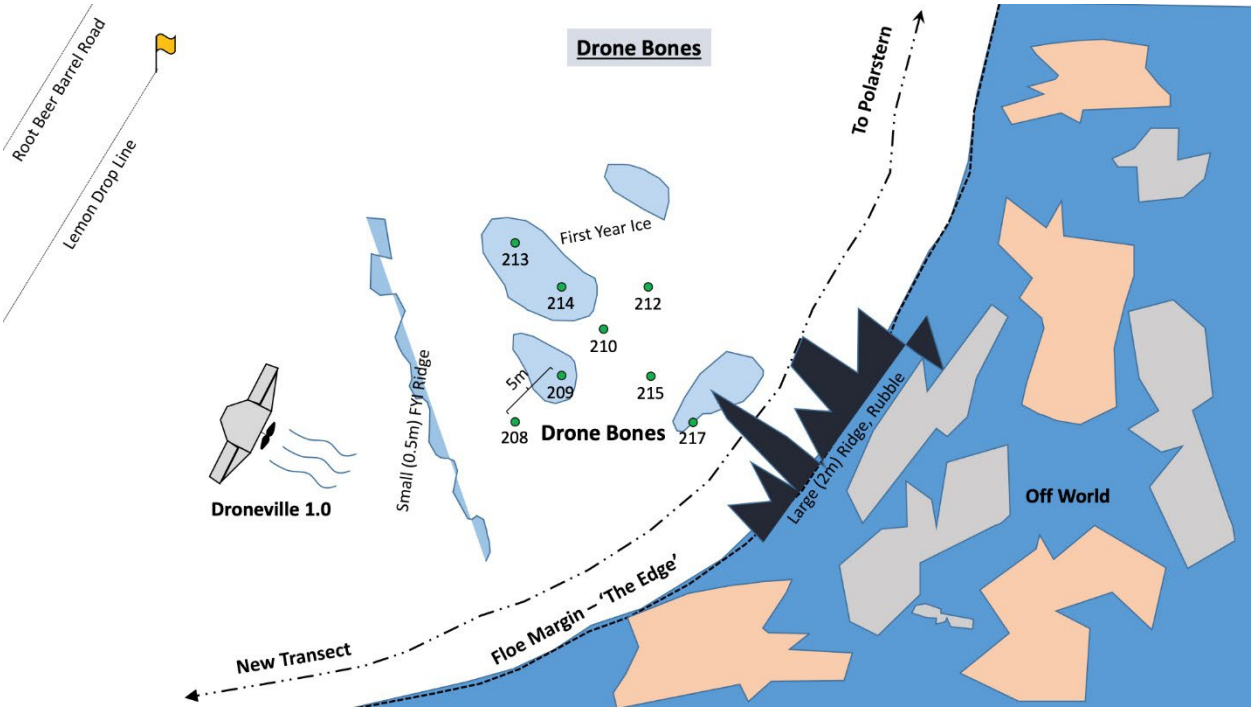

Fig. 4.8.2: *Diagram of Drone Bones and relevant features as of 23.07.2020. The ridge near the floe edge tapered off to level ice on either side. The scenery at the margin was constantly changing, with small adjacent floes converging, diverging, and shearing, slowly mechanically eroding the edge in addition to any lateral melt. Not to scale.*

Reunion Stakes

URN: *pack_ice:ice_ps:dart_stakes_clu_12*

We installed Reunion Stakes at the beginning of Leg 4 on a level pan of ice on a refrozen lead. This pan was formed during the same deformation that created Alli's Ridge in early January. The site was initially moderately ponded, with small, discrete melt ponds. During the melt season, it was surrounded by an extensive network of inter-connected, drained melt ponds that extended from the ship to Alli's Ridge and beyond to the floe edge. There was a notable freshwater lens in the area, that was first observed on 25 June and persisted until ~18 July. We also observed substantial false bottoms with thicknesses of 7-10 cm, which extended across the entire site and persisted until 20 July. The stakes were located next to MET City, Ocean City, Balloon Town, and the Fiber Tower.

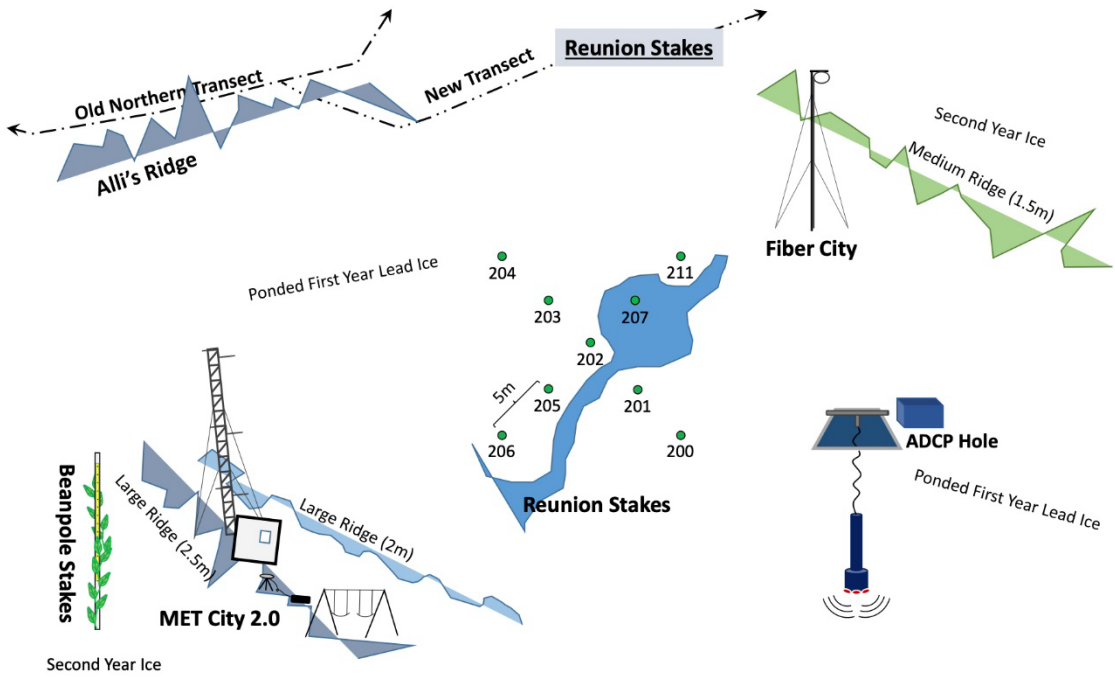

Fig. 4.8.3: *Diagram of Reunion Stakes and surrounding features as of 23.07.2020. The pond illustrated in the map was part of a much larger network of melt ponds that extended from top left to bottom right of the map. Not to scale.*

The Beanpole Stakes

URN: *pack_ice:ice_ps:dart_stakes_clu_13*

The Beanpole Stakes were installed on hummocky, sediment-laden SYI, directly next to the MET City ridge. There was a melt channel running through the plot, connecting two ~25-m diameter melt ponds. Ice thickness in the area was highly variable during installation; while most stakes had initial thicknesses of just over three meters, drill holes within 10 m of the plot found 2-5 m-thick ice.

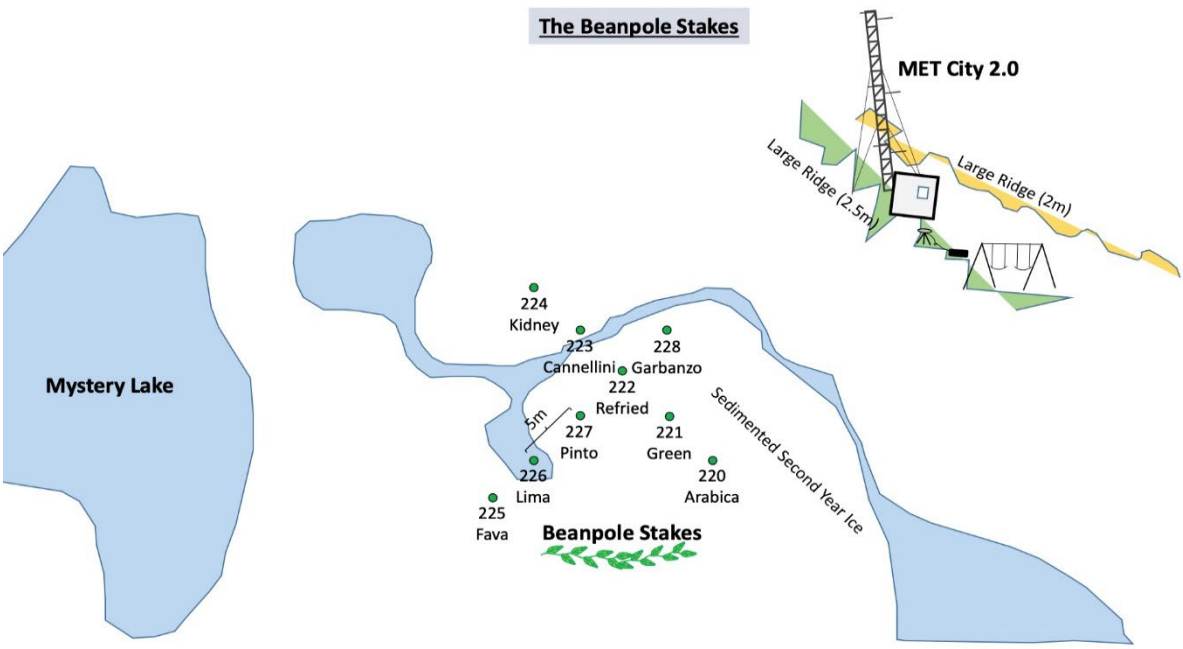

Fig. 4.8.4: *Diagram of the Beanpole Stakes and relevant features as of 23.07.2020. The ice between MET City and the stakes was heavily sediment-laden, increasing towards the bottom right of the map. There tended to be less sediment on the left side of the plot. Not to scale.*

Ridge Ranch

Ridge Ranch was installed during Leg 2 on level FYI. The site was adjacent to Fort Ridge (the ridge observatory). In addition to the hotwire gauges, the Ridge Ranch plot had measuring tape on the underside of the stakes, which was readable by the ROV.

On 18 March, the smaller secondary ridge on the Northern Transect Loop side of Ft. Ridge broke apart, and the subsequent dynamics destroyed Ft. Ridge and transported the Ridge Ranch site outside of the ROV's range. The stakes were unaffected by the dynamics. However, the site became adjacent to a large, frequently active lead for the remainder of Leg 3. In April, it was observed that some of the stakes closest to the lead exhibited either basal melt or reductions in their growth rates. Torsten Kanzow (cruise leader and Team Ocean), conducted fishing rod CTD's at the site, but found a stable mixed layer. Ridge Ranch was the only stakes site that was still fully operational on 16 May when *Polarstern* departed from the original Central Observatory.

4.8.2.4 False bottom & Freshwater Lens Characterization

We observed a freshwater lens in the ADCP hole adjacent to Reunion Stakes on 26 June during their installation. We noted that Reunion Stakes required ~10 times the normal voltage necessary to melt the hotwires free, presumably due to the much lower conductivity of the freshwater lens. Further, we felt a false bottom when measuring the stakes beginning on 8 July. In some cases, we were able to distinguish and measure the top and bottom of the false bottom, as well as the bottom of the sea ice, using the hotwire crossbar.

In order to more precisely measure the extent and properties of the freshwater lens and false bottoms, we conducted multiple thickness drilling transects, complemented by YSI and Castaway measurements, as well as collected ice cores. See section 4.13.

4.8.3 Preliminary (expected) results

Although all of the stakes sites experienced net negative mass balance over Leg 4, there were several periods of reduced melt, and even slight growth, in the average thickness for each site (Figure 4.8.5). Furthermore, there were dramatically different melt rates between individual stakes within the same site. Overall, all three stakes plots experienced ~75-90 cm of melt throughout the leg, with average melt rates of ~3cm/day over the entire period.

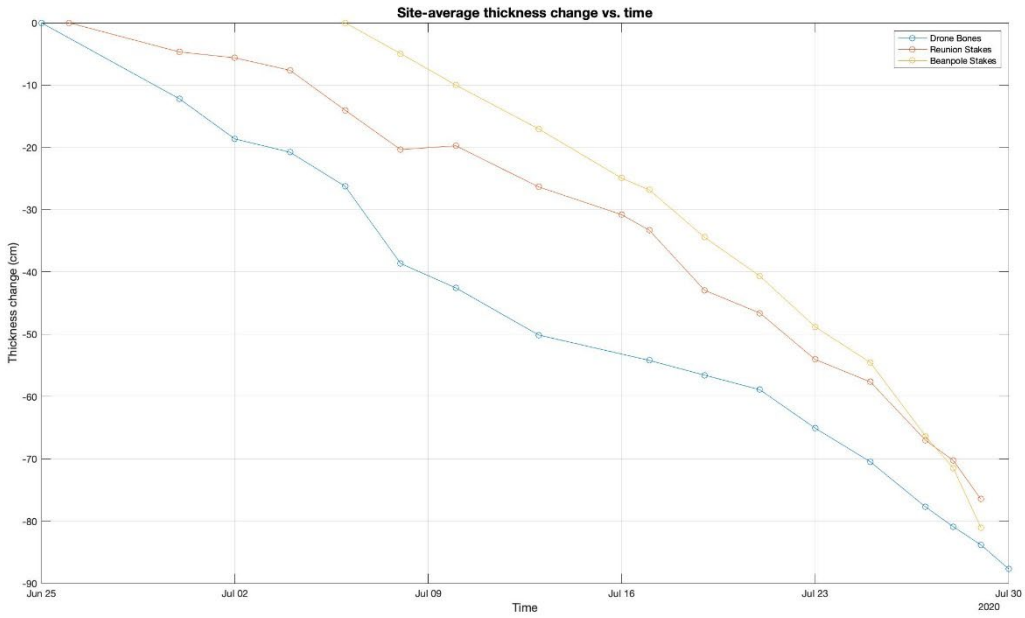

Fig. 4.8.5: *Site-averaged thickness change for all three plots throughout Leg 4. Note slight growth at Reunion Stakes from 8-10 July, as well as steeply increasing melt rates from 23 July.*

4.8.4 Data management

All data and their availability conform to the MOSAiC data policy (see Chapter 9 APPENDIX). All device operations were logged in the AWI sensorweb portal and all sensor raw data files are stored in the platforms section of MCS. Data will be stored at the PANGAEA data repository: World Data Center PANGAEA Data Publisher for Earth & Environmental Science www.pangaea.de. All data are handled, documented, archived and published following the MOSAiC data policy. DOIs will be communicated to PANGAEA for later access via the future MOSAiC Data Portal.

4.9 Ridge studies

Benjamin Lange[1], Evgenii Salganik[2], Ian A. Raphael[3], Jessie Gardner[4], Oliver Muller[5], Igor Sheikin[6], Ilkka Matero[7], Julia Regnery[7], Mats Granskog[1] (not on board), Knut Vilhelm Høyland[2] (not on board), Polona Itkin[4,8] (not on board)

[1]NPI
[2]NTNU
[3]Dartmouth
[4]UiT
[5]UiB
[6]AARI
[7]AWI
[8]CSU

4.9.1 Objectives

Pressure ridges are formed by the piling up of crushed ice blocks during sea ice convergence. Often the features shear during these events. While the ridge sail is the obvious surface part of the ridge, the submerged part – the ridge keel, is typically much larger and voluminous, and can make up 90% of the ridge volume. Both sails and keels are important surface roughness features that cause turbulence in the atmosphere and ocean. After the previous ridge observatories broke apart or were separated from the main floe, Leg 4 of MOSAiC established a new 'Ridge Observatory – Jaridge' and revisited Alli's ridge with the purpose of investigating the following research questions:

- Continue the time series of measurements of ridge consolidation and ice mass balance from Alli's Ridge: The body of a new pressure ridge is composed of ice blocks, with air and water pockets in between them, which are called voids. The water-filled voids will gradually freeze during the cold season, and the ridge will eventually consolidate. Winter and spring observations of consolidation have been conducted, and here we have continued this time series to observe changes in consolidation and ice mass balance from the onset to the advanced stages of melt.
- Infiltration and refreezing of fresher melt water within the voids and gaps of the unconsolidated regions of the ridges: during melt, the surface snow and ice create melt ponds, and this melt water can infiltrate cracks and voids within the sea ice. Within pressure ridges, it is hypothesized that the voids may be replaced by freshwater and, due to the higher freezing point of freshwater, the ice may refreeze, which has significant implications for ice mass balance.
- Ridge-associated ecosystems: Pressure ridges remain the least studied Arctic ice-associated ecosystem, with a basic lack of data for the winter season and limited studies from other seasons. Ridges are not represented in ecosystem models, as they neglect the complex structure of ridge habitats, which differs substantially from the level ice represented in models. It is expected that pressure ridges will become an increasingly important component of the new Arctic sea ice regime dominated by first-year ice, where the largest portion of the level ice melts completely in summer.

4.9.2 Work at sea

4.9.2.1 Sea Ice Ridge Observatories

We established a new Sea Ice Ridge Observatory ("Jaridge") on the bow side of the Polarstern during Leg 4. The ridge was located within the operational range of the new ROV site, which was established in the beginning of Leg 4. The ridge keel depth was up to 7.2 m according to ROV multi-beam measurements. Based on the surface sediment observations, the ridge was located between second-year ice (SYI) closer to the Polarstern and first-year ice (FYI), where

the main ROV transects were located in addition to the ROV albedo lines and FYI coring sites. The ridge was mainly built-up of young ice blocks ~20-40 cm thick, but also included thicker ice with sediment (likely SYI).

As the second component of the Ridge Work, we continued the time series of thickness transect work on Alli's Ridge that formed on the northern flank of the CO during the major deformation event in early January. The ridge's southern flank (closer to Polarstern) mainly consisted of blocks of young ice, while its northern flank (farther from Polarstern) included thicker SYI of the CO floe.

4.9.2.2 Buoy deployments and Recoveries

During MOSAiC Leg 4, we deployed/recovered the following buoys:

1. Deployed one ice mass balance buoy at Jaridge.
2. One ADCP was confirmed lost at Fort Ridge.
3. Recovered both AFZP (Acoustic Fish and Zooplankton Profiler) buoys (AKA: White Monster and Black Monsters), one upward- and one downward-looking, for studying the temporal variability in the occurrence of zooplankton, sea ice macrofauna and ice algal aggregates.

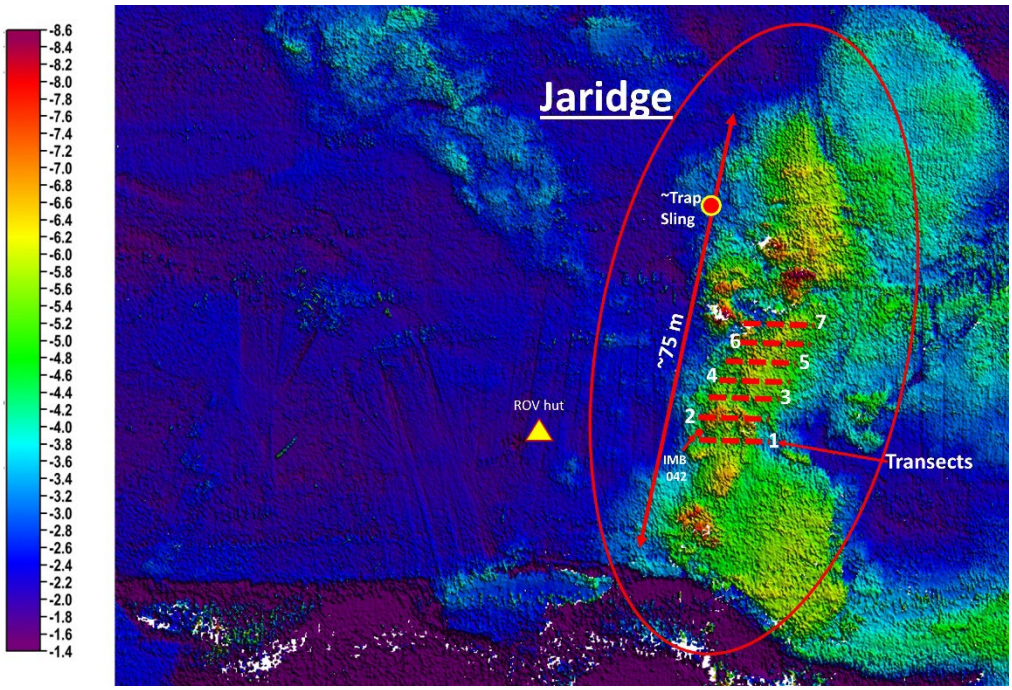

***Fig. 4.9.1**: Overview of Jaridge sampling locations with a multi-beam sonar survey showing ice draft around the ROV site as background. Jaridge is shown by the red ellipse. The thickness drilling surveys are represented by the dashed horizontal lines.*

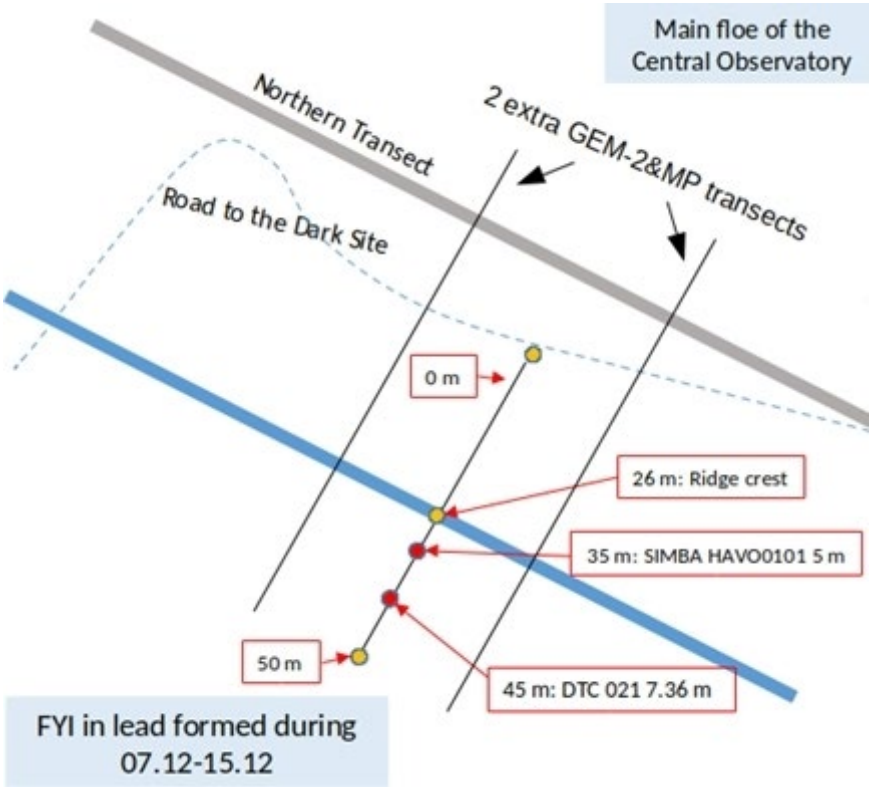

***Fig. 4.9.2**: Sketch of Alli's Ridge which formed in early January on the northern flank of the CO floe with details on locations of specific buoys. Distances are given along the established transect. This sketch was made during Leg 2; however, it was still representative of the Leg 4 site, and we revisited the same thickness transects for drill hole, GEM-2, and Magnaprobe measurements.*

Deployment of an IMB

We deployed one Bruncin IMB in Jaridge. It was deployed on 25 June 2020 at 82.02508 N 10.20166 E. Deployment event ID was PS122/4_43-68 2020M26. Initial ice thickness was 4.2 m, snow depth 0.60 m and freeboard 0.0 m. There were 20 cm of thermistor string in the air.

ADCP lost

A full day of recovery was attempted for the remaining ADCP/CTD deployment; however, after nearly the full day of augering and cutting, we discovered that a rafting event likely sheared off the bottom half of the ADCP pole and pulled the CTD chain with it. This meant that recovery was not possible.

Recovery of both AZFPs (White Monster and Black Monster)

AZFPPOPEdown (AKA: White Monster, event: PS122/4_43-152 AZFPPOPEdown) was recovered on 2 August 2020 at ~11:00 UTC and AZFPPOPEup (AKA: Black Monster, event: PS122/4_43-151 AZFPPOPEup) was recovered on 3 August 2020 at ~8:20 UTC. Both recoveries were made using the mummy chair from the ship. Below are pictures of the recovery process for both instruments. All data were completely recovered from both instruments, from deployment through to recovery.

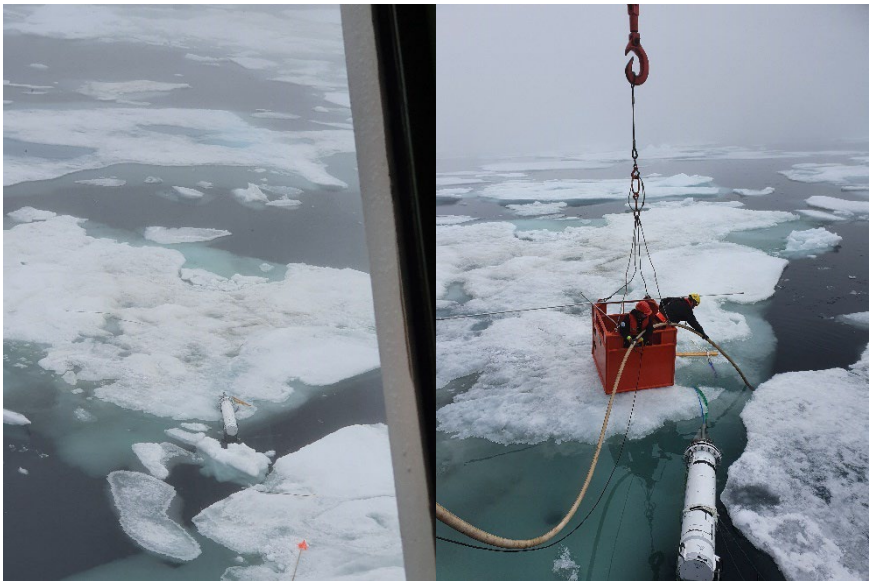

Fig. 4.9.3*: How the White Monster was found (left, credit: Ben Lange) and the ship-based recovery (right, credit: Ben Lange).*

Fig. 4.9.4*: How the Black Monster was found (left, credit: Ben Lange) and the ship-based recovery (right, credit: Ben Lange)*

4.9.2.3 Ridge transects

The ridge ice thickness and snow depth transects were done using a combination of a broadband electromagnetic induction sensors (Geophex GEM-2) and a Magnaprobe. The Magnaprobe snow depth measurements were taken along the surveyor's tape every meter. Where snow depths exceeded 120 cm, measurements were done using an avalanche probe. For ridge transects, GEM-2 was operated without the standard pulka used on the Transect Loop surveys. Measurements were discrete, collected every 1 meter along the surveyor's tape. The ski of the instrument was held as horizontal as possible. This was a two-person task, where the first person held the instrument, while the second person operated the field computer. The device recorded data for 5-10 seconds at every measurement point and then was logged off - a very similar fashion as the GEM-2 calibration measurements.

Ridge transects were done at three lines spaced ~10 m at Alli's Ridge. During Leg 4, we did five GEM/Magnaprobe surveys in addition to three thickness drilling surveys with a 2'' auger.

The GEM-Magnaprobe surveys were always conducted in the following order: center, right, left, when facing towards the ridge from the original Northern Transect Loop.

At Jaridge, we conducted a total of seven transects along different locations of the ridge. The first three transects were revisited once each. Please view the results section for an example of a thickness drilling transect at Jaridge.

4.9.2.4 Snow Transects

See Section 4.5.

4.9.2.5 Ridge Coring

We were able to have 5 full days of coring: four on Jaridge and one on Alli's Ridge. Alli's Ridge only included physics cores (temperature, salinity, dO18, and density). However, the four coring days at Jaridge included the full coring and void water gap sampling of physics cores and ECO cores. For additional details on ridge coring events, please also see Section 4.1. A summary of ridge cores is listed in Table 4.9.1.

***Tab. 4.9.1**: Overview of all ridge coring activities at Jaridge and Alli's Ridge. See also section 4.1 for ECO coring information.*

Date	Location	Event ID	Cores Taken
3. July	Jaridge	PS122/4_45-131 SI_corer_9cm	ECO, Temperature/Salinity/dO18 (one core)
10. July	Jaridge	PS122/4_46-178 SI_corer_9cm PS122/4_46-179 SI_corer_7cm	ECO, Temperature/Salinity/dO18 (one core), and Density (RHO)
18. July	Jaridge	PS122/4_47-199 SI_corer_9cm PS122/4_47-158 SI_corer_7cm	ECO, Temperature/Salinity/dO18 (one core), and Density (RHO)
24. July	Jaridge	PS122/4_48-229 SI_corer_9cm PS122/4_48-277 SI_corer_7cm	ECO, Temperature/Salinity/dO18 (one core), and Density (RHO) NOTE: Here, we had two coring locations. One at the peak of the ridge and one along the flank of the ridge (in the direction of the ROV hut).
15. July	Alli's Ridge	PS122/4_47-157 SI_corer_9cm PS122/4_47-158 SI_corer_7cm	Temperature/Salinity/dO18 (one core), and Density (RHO)

4.9.2.6 Borehole Jack

Borehole jack measurements were conducted at Jaridge on four separate occasions and on level ice adjacent to Jaridge. Tab 4.9.2 shows a a summary of measurements.

Tab 4.9.2: Overview of borehole jack measurements taken during Leg 4.

Date	Location	Event ID
2. July	Jaridge	PS122/4_45-204
5. July	Jaridge	PS122/4_45-205
14. July	FYI adjacent to Jaridge	PS122/4_47-243
19. July	Jaridge	PS122/4_47-244
28. July	Jaridge	PS122/4_49-117

4.9.3 Preliminary (expected) results

During the first coring and drilling events, we observed voids within Jaridge (Fig 4.9.5). However, later on, these voids were not observed and we have attributed this to the infiltration of melt water within the ridges and refreezing. This was also confirmed by visual inspection of cores where clear freshwater layers were observed. The displacement of saltwater from the ridge void spaces led to an increase in apparent thickness in the GEM surveys, visible between 28 June and 9 July (see Fig. 4.9.8). Salinity measurements also indicated freshwater layers within the ridge. Nevertheless, these are preliminary results and would need to be verified by further analyses, such as with the dO18 data. Here, we also show one example of profiles for temperature, salinity and density.

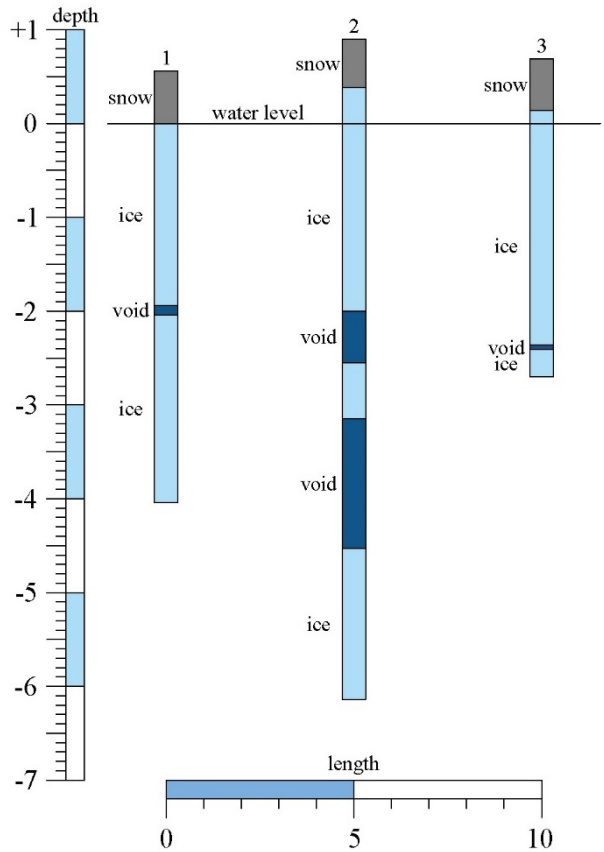

Fig. 4.9.5: *Snow and ice thickness profile of the Jaridge transect shown in Figure 2. Within the bottom ~1 m of ice, there were loose, unconsolidated small ice blocks, which could be felt with the ice thickness tape when pulling it up, but would not hold the tape tight. Drill hole '1' is the location of IMB042.*

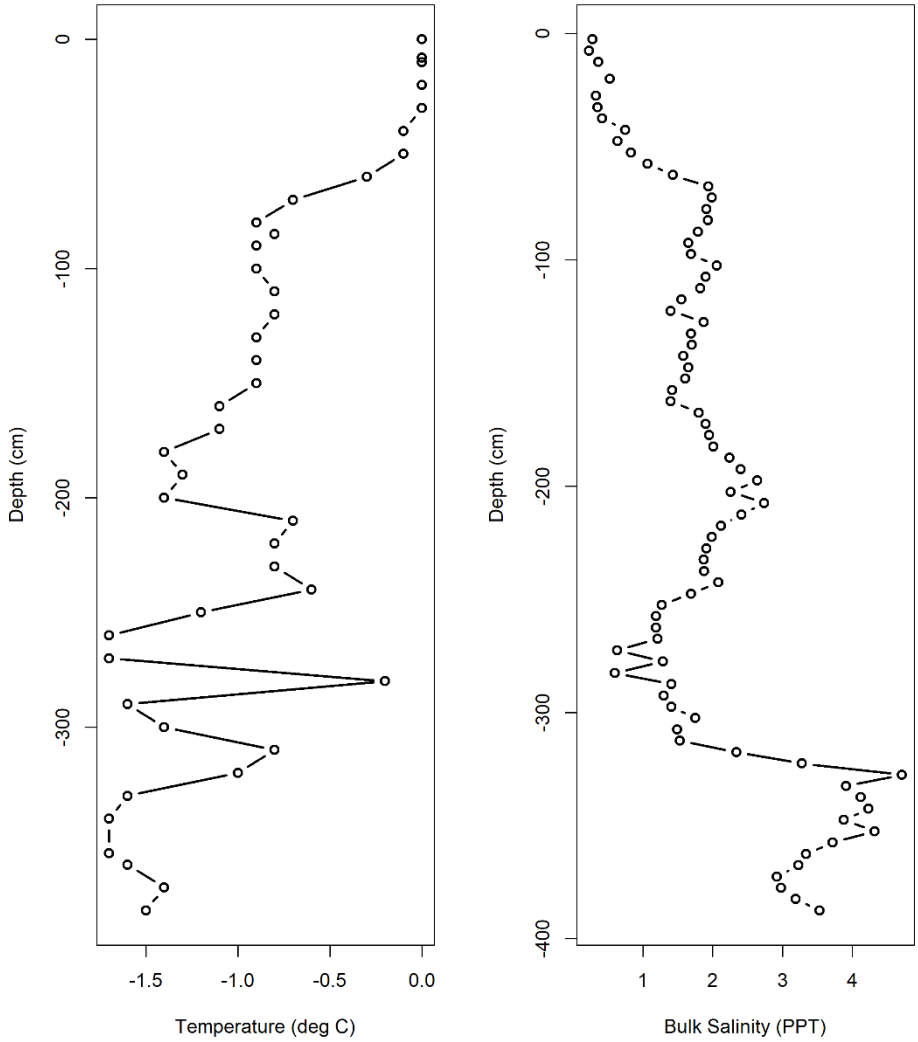

Fig. 4.9.6: *Temperature (left) and bulk salinity (right) profiles from Jaridge. The core was taken on 03 July 2020.*

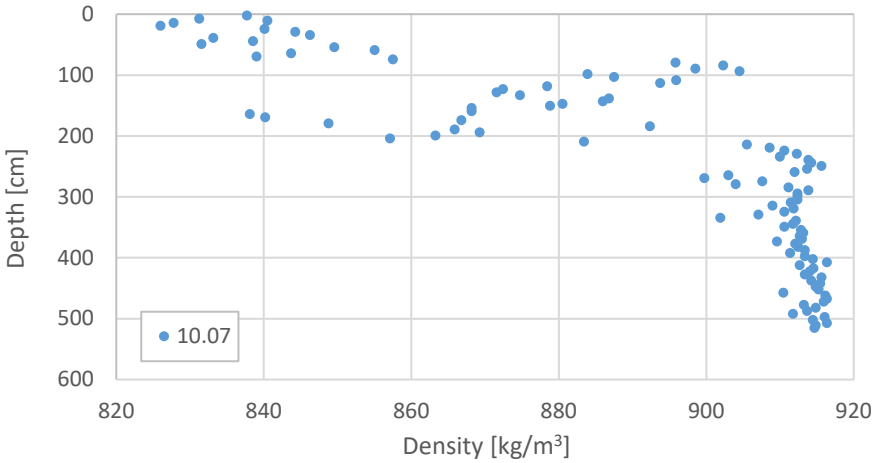

Fig. 4.9.7: *Density profile from Jaridge. The core was taken on 10 July 2020.*

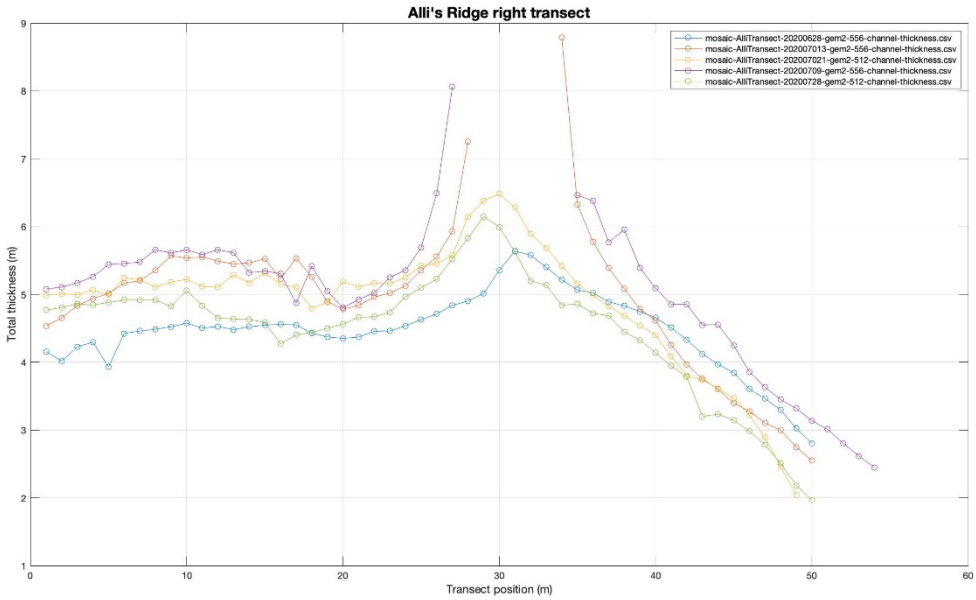

Fig. 4.9.8*: Time series of GEM-2 total thicknesses at Alli's Ridge from the 'right' transect.*

4.9.4 Data management

All data and their availability conform to the MOSAiC data policy (see Chapter 9 APPENDIX). All of the instruments have been added into the system of SENSOR.awi.de and all the data has been or will be added to the MCS. The data will be submitted according the data policy of MOSAiC. Data will be stored at the PANGAEA data repository: World Data Center PANGAEA Data Publisher for Earth & Environmental Science www.pangaea.de. DOIs will be communicated to PANGAEA for later access via the future MOSAiC Data Portal.

4.10 Ice dynamics

Ian Raphael[1], Igor Sheikin[2], Luisa von Albedyll[3], Chris Polashenski[1,10] (not on board), Jennifer Hutchings[7] (not on board), Jari Haapala[4] (not on board), Polona Itkin[5] (not on board), Andrea Haase[6] (not on board), Phil Hwang[8] (not on board), Nikolay Kolabutin[3] (not on board), Ruibo Lei[9] (not on board), Mikko Lensu[6] (not onboard), Annu Oikkonen[6] (not on board), Victor Smirnov[2] (not on board), David Clemens-Sewall[1] (not on board), Egor Shimanchuk[2] (not on board)

[1]Dartmouth
[2]AARI
[3]AWI
[4]FMI
[5]UiT/CSU
[6]HSVA
[7]Oregon SU
[8]UHud
[9]PRIC
[10]USACE/CRREL

4.10.1 Objectives

Ice dynamics are a major control for the properties and processes of Arctic sea ice. Dynamics significantly influence ice mass balance throughout the annual cycle. Winter divergence has a positive forcing on ice mass balance, since open leads during the winter increase heat flux from the ocean to the atmosphere and lead to new ice formation. The opposite is true during the melt season; the much lower albedo of open water increases energy input into the ice-ocean system, and therefore increases ice melt. Dynamics additionally change the physical and structural properties of sea ice, with implications for the strength and longevity of particular floes and regions, as well as shipping and logistical operations in and around sea ice. Ice dynamics also influence ecological, atmospheric, and oceanographic processes such as oceanic and atmospheric mixing/turbulence. By changing surface and basal ice roughness, ice dynamics provide sanctuaries for marine life, particularly in ridged areas. Further, the open water fraction within pack ice affects energy, gas, and particle fluxes between the ocean, ice, and atmosphere.

The overall objective of ice dynamics research at MOSAiC is to deepen the understanding of pack ice movement and deformation over a full annual cycle. In particular, we are examining spatial and temporal scales of motion and deformation, and how those vary regionally and seasonally. We also aim to establish a relationship between deformation scales and physical characteristics of pack ice, by linking dynamical observations with data from ice mass balance (IMB) buoys, ice cores, ice-mechanics experiments, and more.

4.10.2 Overview of measurement system

MOSAiC ice dynamics research is based on scaled measurements, from local measurements at the Central Observatory, to regional ice drift observations in the Distributed Network, and finally synoptic scale aerial and satellite products. For local scale observations, we established the MOSAiC Small scale Ice Dynamics Observing System (SIDOS) on the Central Observatory (CO). The system includes the following components:

- Laser strain observatory - LSO (Dartmouth College/CRREL)
- GNSS (Uhud) and DGPS stations (Dartmouth College/CRREL)
- Seismic stations (AARI)
- Stress gauges (Dartmouth College/CRREL, FMI)
- Stress panels (HSVA)
- Ice radar (FMI)

Legs 1, 2, and 3 saw the installation of seismic stations, stress gauges, stress panels, and GNSS/DGPS stations distributed across the CO floe on a scale of 0.25-5 km. Several stress sensors were lost/destroyed by ice dynamics throughout the campaign, and the LSO array was frequently rearranged for the same reason. The GNSS/DGPS array, as well as the seismic array, were adjusted as new stations were added or moved. The stress panels were recovered from the Logistics area at the end of Leg 3 and were not reinstalled. See Figures 4.6.1, 4.8.1, and 4.9.1 in the Legs 1, 2, and 3 cruise reports for the distribution and evolution of the SIDOS instrumentation array throughout previous legs.

4.10.3 Work at sea

When we arrived at the CO floe at the beginning of Leg 4, warm temperatures had already melted out the stress gauges and LSO array. The dynamics fieldwork was, therefore, a two-pronged effort: first, to reestablish the seismic and GNSS/DGPS arrays, and second, to recover as much instrumentation as possible.

At the beginning of the leg, we installed three seismic stations on a small baseline for testing, and then on a larger baseline across the CO floe for the duration of Leg 4. We initially installed three GNSS stations and two DGPS stations, followed by a fourth GNSS station later in the leg.

We recovered the LSO array from the old CO floe early in the leg, along with the DGPS and two GNSS stations that were deployed there on Leg 3. Additionally, we recovered four stress sensors and data loggers. Unfortunately, due to significant ice dynamics during the interim between Legs 3 and 4, it was difficult to locate, access, and recover the remaining stress sensors.

4.10.3.1 Laser Strain Observatory (LSO)

The LSO provides high-precision plastic and elastic ice strain data. The observatory is composed of an array of retro-reflectors fixed in the ice on metal posts, and an autonomous laser theodolite that tracks displacement of the reflectors with millimeter precision. This displacement measurement can be used to determine strain rate.

The LSO reflector array had already melted out by the time we returned to ice camp in June. The power cable was ripped out of the TM50 theodolite, presumably due to tripod melt and drift. According to the data record, the instrument stopped recording on 26 May. We recovered the TM50 and all 17 deployed reflectors on 21 June.

4.10.3.2 GNSS and DGPS stations

The GNSS and DGPS stations measure ice motion at high spatial and temporal precision (1 Hz and 0.5 Hz, cm precision), as well as provide a constant reference frame for floe-relative coordinate transformations.

Two GNSS stations and one DGPS station were deployed at the old CO floe at the end of Leg 3. Due to the infeasibility of regularly accessing the old CO floe for maintenance/data download, we decided to recover all of the stations from the floe and redeploy them on the new CO floe.

We initially installed three GNSS stations: one near the first-year ice (FYI) coring site (URN: *pack_ice:ice_ps:gnss_uoh_sp_s3*), one at the Leg 4 Transect Loop/MET City intersection (URN: *pack_ice:ice_ps:gnss_uoh_sp_s2*), and one at Alli's Ridge (URN: *pack_ice:ice_ps:gnss_uoh_sp_s5*). At the same time, we installed two DGPS stations, one at ROV (URN: *positioning_system:dc_dgps_1*), and one at MET City (URN: *positioning_system:dc_dgps_2*). We installed a final GNSS station in the Logistics area later in the leg (URN: *pack_ice:ice_ps:gnss_uoh_sp_s4*). See Fig. 4.10.2 for the distribution of the GNSS/DGPS array.

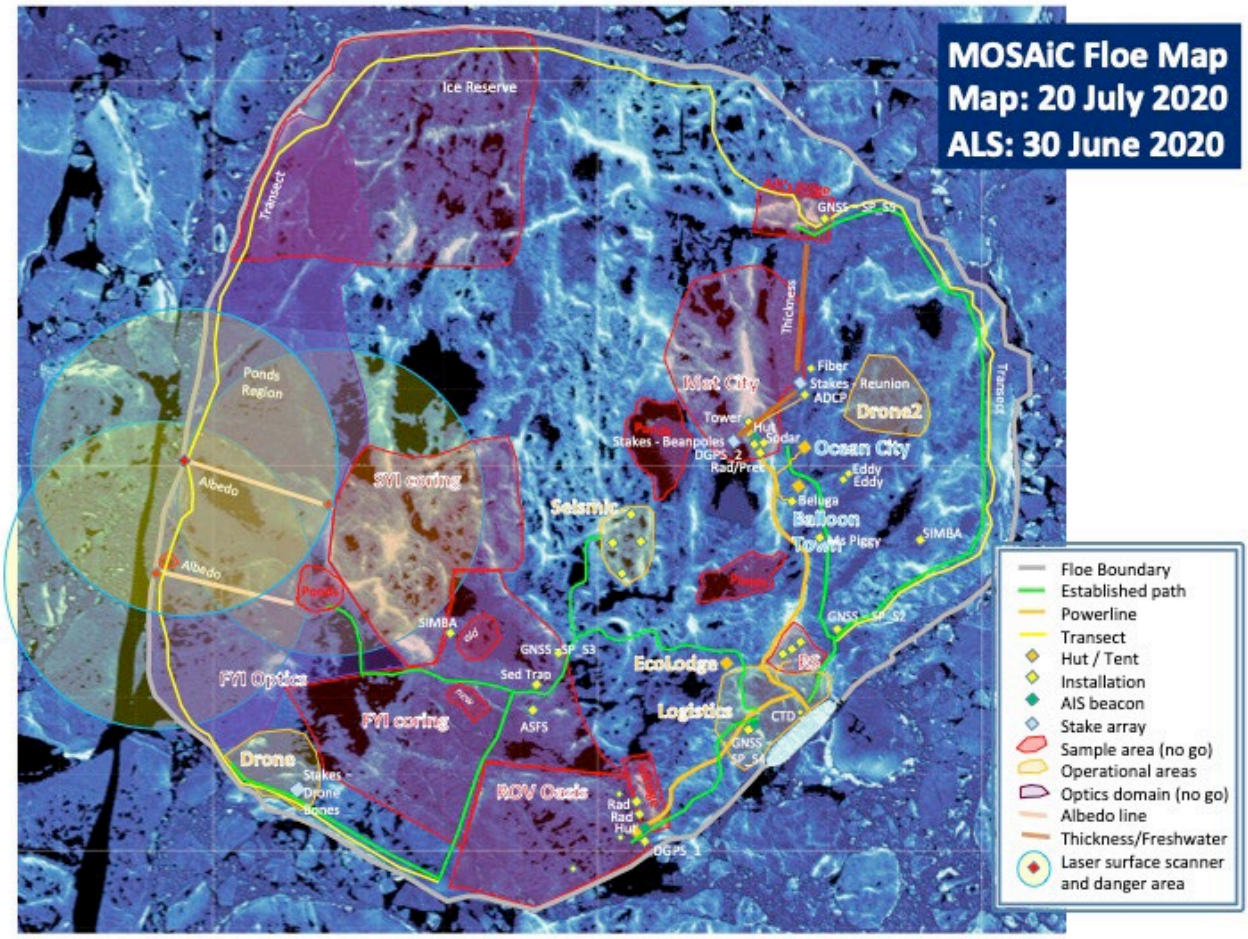

***Fig. 4.10.1**: Location of GNSS/INS stations, DGPS stations, and Seismic stations on 20 July.*

4.10.3.3 Seismic stations

Seismic stations obtain data on waves and fracturing in pack ice for a development of forecast methods for sea ice breaking.

Each of the three seismic stations (Alfa, Beta, Gamma) includes seismometer CME 4311, tiltmeter ИН-Д3-360, autonomous recorder "Baykal-8" for logging signals, GPS-antenna, antenna for signal transmission to the base and battery for powering station. Measurements were recorded to the "Baykal-8" data logger with 100 Hz frequency. Data of the seismic stations were also transmitted by the wireless connection to a laptop deployed onboard the *Polarstern* for real-time visual monitoring of seismic observations.

Three seismic stations were deployed on the main floe at 19-20 June 2020 and worked until 27 July, with the various configurations listed in Table 4.10.1.

Tab. 4.10.1: *Configurations of the seismic measurements.*

Name	Description	Dates
Configuration A point #7	All three stations were established on one platform in the red tent at the Logistics-area (fig. Seismic-01) for testing and calibration.	Start: 2020-06-19 Finish: 2020-06-25
Configuration B points #0, #1, #2	Three stations were established in a small triangle with a size about of 50 m in central area of the main floe (fig. Seismic-02).	Start: 2020-06-25 Finish: 2020-07-13
Configuration C points #0, #2, #5	According to the original plan, three stations had to be installed on the three various floes (main floe, old floe and SYI floe). However, an installation of GAMMA station at the old floe shows that this configuration is impossible for actual safety and weather conditions. Therefore, during one week ALFA and BETTA stations work in small triangle at the main floe and GAMMA station at the old floe. The position of the old floe during this configuration is presented in the Logistics-file of PS1221-4_43-135 as well as in the data base for snow buoy 300234066087170.	Start: 2020-06-25 Finish: 2020-07-13
Configuration D points #0, #3, #4	Three stations were established in a big triangle with a size about of 500 m in central area of the main floe (fig. Seismic-02).	Start: 2020-07-22 Finish: 2020-07-27

Note that the stations worked for some time in the transit configurations, when one station changed position and the remaining two were on standby.

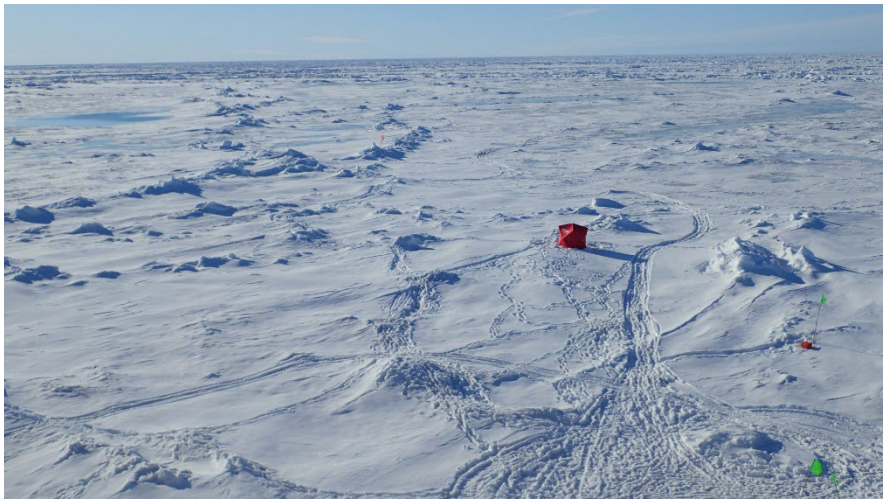

Figure 4.10.2: *Red tent with an inside platform for testing and calibration of equipment.*

Seismometers and tiltmeters were deployed on measurement platforms that provided a hard mechanical contact with the ice floe. Fig. 4.10.5 presents two types of platforms. The wooden table and box were refrozen in an ice hole (about of 0.5 m below the surface) at the end of April. At the start of July, the box reached the ice surface because of extensive surface ice melt. One second measurement platform was a wood pallet established in a shallow ice hole covered by snow and ice crystals.

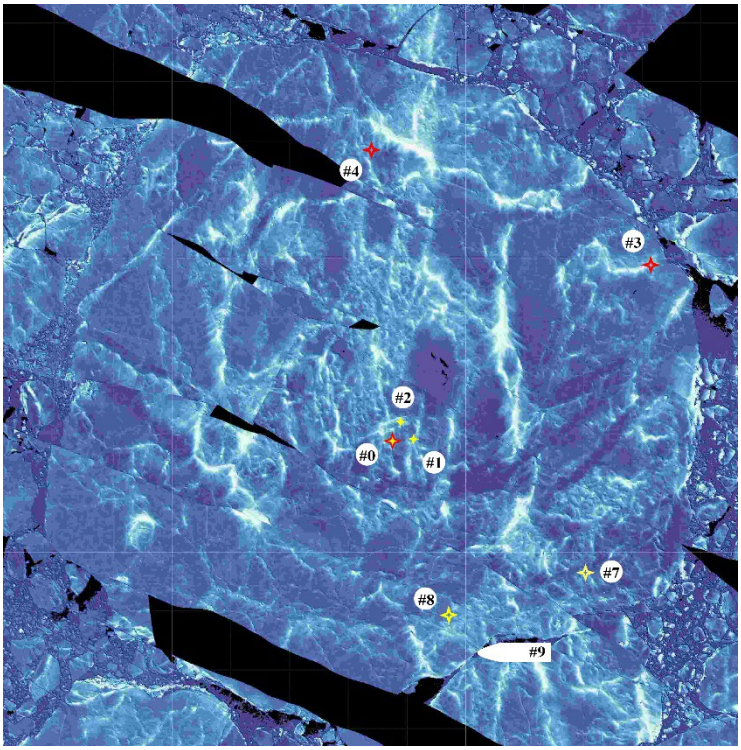

Figure 4.10.3: *Position of measurement points at the various configurations. Small triangle (#0, #1, #2), big triangle (#0, #3, #4), test and calibration (#7, #8, #9).*

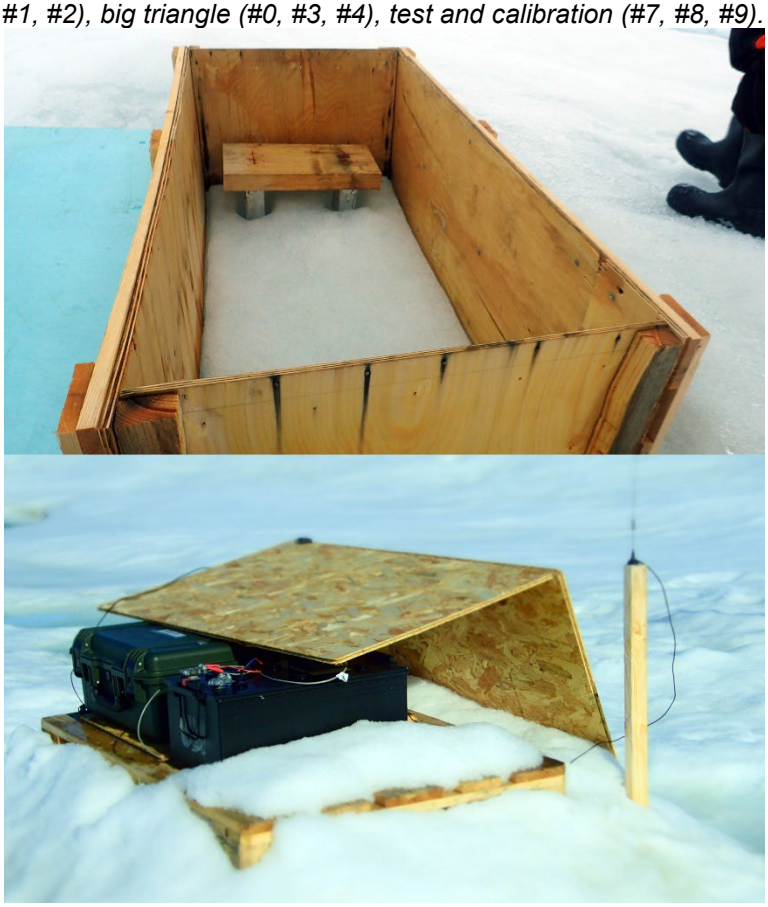

Figure 4.10.4. *The measurement platforms for the refrozen wood table with the box (top) and wooden pallet (bottom).*

The database includes one hour-long files in the SEED format. This is the standard format for the Global Seismic Network. All stations used GPS synchronization, and the Log file consist of GPS data as well as actual system parameters. The tables below present the data pattern in accordance with the actual configurations.

Table 4.10.2: *MOSAiC-2 (Leg-4). Seismics. ALFA station time sheet, positions and actions.*

data/time	0	1	2	3	4	5	6	7	8	9	10	11	12	13	14	15	16	17	18	19	20	21	22	23	remarks
17.06.2020																				9	9	9			onboard test
18.06.2020																									
19.06.2020																									
20.06.2020										7	7	7	7	7	7	7	7	7	7	7	7	7	7	7	calibration (red tent)
21.06.2020	7	7	7	7	7	7	7	7	7	7	7	7	7	7	7	7	7	7	7	7	7	7	7	7	
22.06.2020	7	7	7	7	7	7	7	7	7	7	7	7	7	7	7	7	7	7	7	7	7	7	7	7	
23.06.2020	7	7	7	7	7	7	7	7	7	7	7	7	7	7	7	7	7	7	7	7	7	7	7	7	
24.06.2020	7	7	7	7	7	7	7	7	7	7	7	7	7	7	7	7	7	7	7	7	7	7	7	7	
25.06.2020	7	7	7	7	7	7	7	7	7	7				2	2	2	2	2	2	2	2	2	2	2	small triangle point 2
26.06.2020	2	2	2	2	2	2	2	2	2	2	2	2	2	2	2	2	2	2	2	2	2	2	2	2	
27.06.2020	2	2	2	2	2	2	2	2	2	2	2	2	2	2	2										repair SME connector
28.06.2020																									
29.06.2020								8	8	8	8	8	8	8											LOG area test
30.06.2020							2	2	2	2	2	2	2	2	2	2	2	2	2	2	2	2	2	2	small triangle point 2
01.07.2020	2	2	2	2	2	2	2	2	2	2	2	2	2	2	2	2	2	2	2	2	2	2	2	2	
02.07.2020	2	2	2	2	2	2	2	2	2	2	2	2	2	2	2	2	2	2	2	2	2	2	2	2	
03.07.2020	2	2	2	2	2	2	2	2	2	2	2	2	2	2	2	2	2	2	2	2	2	2	2	2	
04.07.2020	2	2	2	2	2	2	2	2																	repair SME connector
05.07.2020													2	2	2	2	2	2	2	2	2	2	2	2	small triangle point 2
06.07.2020	2	2	2	2	2	2	2	2	2	2	2	2	2	2	2	2	2	2	2	2	2	2	2	2	
07.07.2020	2	2	2	2	2	2	2	2	2	2	2	2	2	2	2	2	2	2	2	2	2	2	2	2	
08.07.2020	2	2	2	2	2	2	2	2	2	2	2	2	2	2	2	2	2	2	2	2	2	2	2	2	
09.07.2020	2	2	2	2	2	2	2	2	2	2	2	2	2	2	2	2	2	2	2	2	2	2	2	2	
10.07.2020	2	2	2	2	2	2	2	2	2	2	2	2	2	2	2	2	2	2	2	2	2	2	2	2	
11.07.2020	2	2	2	2	2	2	2	2	2	2	2	2	2	2	2	2	2	2	2	2	2	2	2	2	
12.07.2020	2	2	2	2	2	2	2	2	2	2	2	2	2	2	2	2	2	2	2	2	2	2	2	2	
13.07.2020	2	2	2	2	2	2	2	2	2	2	2	2	2	2	2	2	2	2	2	2	2	2	2	2	
14.07.2020	2	2	2	2	2	2	2	2	2	2	2	2	2	2	2	2	2	2	2	2	2	2	2	2	batery exchange
15.07.2020	2	2	2	2	2	2	2	2	2	2	2	2	2	2	2	2	2	2	2	2	2	2	2	2	
16.07.2020	2	2	2	2	2	2	2	2	2	2	2	2	2	2	2	2	2	2	2	2	2	2	2	2	
17.07.2020	2	2	2	2	2	2	2	2	2	2	2	2	2	2	2	2	2	2	2	2	2	2	2	2	
18.07.2020	2	2	2	2	2	2	2	2	2	2	2	2	2	2	2	2	2	2	2	2	2	2	2	2	
19.07.2020	2	2	2	2	2	2	2	2	2	2	2	2	2	2		3	3	3	3	3	3	3	3	3	big triangle point 3
20.07.2020	3	3	3	3	3	3	3	3	3	3	3	3	3	3	3	3	3	3	3	3	3	3	3	3	
21.07.2020	3	3	3	3	3	3	3	3	3	3	3	3	3	3	3	3	3	3	3	3	3	3	3	3	
22.07.2020	3	3	3	3	3	3	3	3	3	3	3	3	3	3	3	3	3	3	3	3	3	3	3	3	
23.07.2020	3	3	3	3	3				3	3	3	3	3	3	3	3	3	3	3	3	3	3	3	3	batery exchange
24.07.2020	3	3	3	3	3	3	3	3	3	3	3	3	3	3	3	3	3	3	3	3	3	3	3	3	
25.07.2020	3	3	3	3	3	3	3	3	3	3	3	3	3	3	3	3	3	3	3	3	3	3	3	3	
26.07.2020	3	3	3	3	3	3	3	3	3	3	3	3	3	3	3	3	3	3	3	3	3	3	3	3	
27.07.2020	3	3	3	3	3	3	3	3	3	3	3	3	3	3											

Legend

test and calibration — small triangle — big triangle

1,2….9 - instalation point number — covered by LOG-file

Table 4.10.3: *MOSAiC-2 (Leg-4). BETTA station time sheet, positions and actions.*

data/time	0	1	2	3	4	5	6	7	8	9	10	11	12	13	14	15	16	17	18	19	20	21	22	23	remarks
17.06.2020														9											onboard test
18.06.2020																									
19.06.2020															7	7	7	7	7	7	7	7	7	7	calibration (red tent)
20.06.2020	7	7	7	7	7	7	7	7	7	7	7	7	7	7	7	7	7	7	7	7	7	7	7	7	
21.06.2020	7	7	7	7	7	7	7	7	7	7	7	7	7	7	7	7	7	7	7	7	7	7	7	7	
22.06.2020	7	7	7	7	7	7	7	7	7	7	7	7	7	7	7	7	7	7	7	7	7	7	7	7	
23.06.2020	7	7	7	7	7	7	7	7	7	7	7	7	7	7	7	7	7	7	7	7	7	7	7	7	
24.06.2020	7	7	7	7	7	7	7	7	7	7	7	7		0	0	0	0	0	0	0	0	0	0	0	small triangle point 0
25.06.2020	0	0	0	0	0	0	0	0	0	0	0	0	0	0	0	0	0	0	0	0	0	0	0	0	
26.06.2020	0	0	0	0	0	0	0	0	0	0	0	0	0	0	0	0	0	0	0	0	0	0	0	0	
27.06.2020	0	0	0	0	0	0	0	0	0	0	0	0	0	0	0	0	0	0	0	0	0	0	0	0	batery exchange
28.06.2020	0	0	0	0	0	0	0	0	0	0	0	0	0	0	0	0	0	0	0	0	0	0	0	0	
29.06.2020	0	0	0	0	0	0	0	0	0	0	0	0	0	0	0	0	0	0	0	0	0	0	0	0	
30.06.2020	0	0	0	0	0	0	0	0	0	0	0	0	0	0	0	0	0	0	0	0	0	0	0	0	
01.07.2020	0	0	0	0	0	0	0	0	0	0	0	0	0	0	0	0	0	0	0	0	0	0	0	0	
02.07.2020	0	0	0	0	0	0	0	0	0	0	0	0	0	0	0	0	0	0	0	0	0	0	0	0	
03.07.2020	0	0	0	0	0	0	0	0	0	0	0	0	0	0	0	0	0	0	0	0	0	0	0	0	
04.07.2020	0	0	0	0	0	0	0	0	0	0	0	0	0	0	0	0	0	0	0	0	0	0	0	0	
05.07.2020	0	0	0	0	0	0	0	0	0	0	0	0	0	0	0	0	0	0	0	0	0	0	0	0	
06.07.2020	0	0	0	0	0	0	0	0	0	0	0	0	0	0	0	0	0	0	0	0	0	0	0	0	
07.07.2020	0	0	0	0	0	0	0	0	0	0	0	0	0	0	0	0	0	0	0	0	0	0	0	0	
08.07.2020	0	0	0	0	0	0	0	0	0	0	0	0	0	0	0	0	0	0	0	0	0	0	0	0	
09.07.2020	0	0	0	0	0	0	0	0	0	0	0	0	0	0	0	0	0	0	0	0	0	0	0	0	
10.07.2020	0	0	0	0	0	0	0	0	0	0	0	0	0	0											
11.07.2020													0	0	0	0	0	0	0	0	0	0	0	0	batery exchange
12.07.2020	0	0	0	0	0	0	0	0	0	0	0	0	0	0	0	0	0	0	0	0	0	0	0	0	
13.07.2020	0	0	0	0	0	0	0	0	0	0	0	0	0	0	0	0	0	0	0	0	0	0	0	0	
14.07.2020	0	0	0	0	0	0	0	0	0	0	0	0	0	0	0	0	0	0	0	0	0	0	0	0	
15.07.2020	0	0	0	0	0	0	0	0	0	0	0	0	0	0	0	0	0	0	0	0	0	0	0	0	
16.07.2020	0	0	0	0	0	0	0	0	0	0	0	0	0	0	0	0	0	0	0	0	0	0	0	0	
17.07.2020	0	0	0	0	0	0	0	0	0	0	0	0	0	0	0	0	0	0	0	0	0	0	0	0	
18.07.2020	0	0	0	0	0	0	0	0	0	0	0	0	0	0	0	0	0	0	0	0	0	0	0	0	batery exchange
19.07.2020	0	0	0	0	0	0	0	0	0	0	0	0	0	0	0	0	0	0	0	0	0	0	0	0	big triangle point 0
20.07.2020	0	0	0	0	0	0	0	0	0	0	0	0	0	0	0	0	0	0	0	0	0	0	0	0	
21.07.2020	0	0	0	0	0	0	0	0	0	0	0	0	0	0	0	0	0	0	0	0	0	0	0	0	
22.07.2020	0	0	0	0	0	0	0	0	0	0	0	0	0	0	0	0	0	0	0	0	0	0	0	0	
23.07.2020	0	0	0	0	0	0	0	0	0	0	0	0	0	0	0	0	0	0	0	0	0	0			
24.07.2020								0	0	0	0	0	0	0	0	0	0	0	0	0	0	0	0	0	batery exchange
25.07.2020	0	0	0	0	0	0	0	0	0	0	0	0	0	0	0	0	0	0	0	0	0	0	0	0	
26.07.2020	0	0	0	0	0	0	0	0	0	0	0	0	0	0	0	0	0	0	0	0	0	0	0	0	
27.07.2020	0	0	0																						

Legend

test and calibration — small triangle — big triangle

1,2….9 - instalation point number — covered by LOG-file

Table 4.10.4: *MOSAiC-2 (Leg-4). GAMMA station time sheet, positions and actions.*

data/time	0	1	2	3	4	5	6	7	8	9	10	11	12	13	14	15	16	17	18	19	20	21	22	23	remarks
17.06.2020															9										onboard test
18.06.2020																									
19.06.2020															7	7	7	7	7	7	7	7	7	7	calibration (red tent)
20.06.2020	7	7	7	7	7	7	7	7	7	7	7	7	7	7	7	7	7	7	7	7	7	7	7	7	
21.06.2020	7	7	7	7	7	7	7	7	7	7	7	7	7	7	7	7	7	7	7	7	7	7	7	7	
22.06.2020	7	7	7	7	7	7	7	7	7	7	7	7	7	7	7	7	7	7	7	7	7	7	7	7	
23.06.2020	7	7	7	7	7	7	7	7	7	7	7	7	7	7	7	7	7	7	7	7	7	7	7	7	
24.06.2020	7	7	7	7	7	7	7	7	7	7	7	7	7	7	7	7	7	7	7	7	7	7	7	7	
25.06.2020	7	7	7	7	7	7	7	7	7	7			1	1	1	1	1	1	1	1	1	1	1	1	small triangle point 1
26.06.2020	1	1	1	1	1	1	1	1	1	1	1	1	1	1	1	1	1	1	1	1	1	1	1	1	
27.06.2020	1	1	1	1	1	1	1	1	1	1	1	1	1	1	1	1	1	1	1	1	1	1	1	1	
28.06.2020	1	1	1	1	1	1	1	1	1	1	1	1	1	1	1	1	1	1	1	1	1	1	1	1	
29.06.2020	1	1	1	1	1	1	1	1	1	1	1	1	1	1	1	1	1	1	1	1	1	1	1	1	
30.06.2020	1	1	1	1	1	1	1	1	1	1	1	1	1	1	1	1	1	1	1	1	1	1	1	1	
01.07.2020	1	1	1	1	1	1	1	1		1	1	1	1	1	1	1	1	1	1	1	1	1	1	1	batery exchange
02.07.2020	1	1	1	1	1	1	1	1	1	1	1	1	1	1	1	1	1	1	1	1	1	1	1	1	
03.07.2020	1	1	1	1	1	1	1	1	1	1	1	1	1	1	1	1	1	1	1	1	1	1	1	1	
04.07.2020	1	1	1	1	1	1	1	1	1	1	1	1	1	1	1	1	1	1	1	1	1	1	1	1	
05.07.2020	1	1	1	1	1	1	1	1	1	1	1	1	1	1	1	1	1	1	1	1	1	1	1	1	
06.07.2020	1	1	1	1	1	1	1	1	1	1	1	1	1	1	1	1	1	1	1	1	1	1	1	1	
07.07.2020	1	1	1	1	1	1	1	1	1						1	1	1	1	1	1	1	1	1	1	batery exchange
08.07.2020	1	1	1	1	1	1	1	1	1	1	1	1	1	1	1	1	1	1	1	1	1	1	1	1	
09.07.2020	1	1	1	1	1	1	1	1	1	1	1	1	1	1	1	1	1	1	1	1	1	1	1	1	
10.07.2020	1	1	1	1	1	1	1	1	1	1	1	1	1	1											
11.07.2020													1	1	1	1	1	1	1	1	1	1	1	1	batery exchange
12.07.2020	1	1	1	1	1	1	1	1	1	1	1	1	1	1	1	1	1	1	1	1	1	1	1	1	
13.07.2020	1	1	1	1	1	1	1	1	1	1	1														
14.07.2020													5	5	5	5	5	5	5	5	5	5	5	5	old floe point 5
15.07.2020	5	5	5	5	5	5	5	5	5	5	5	5	5	5	5	5	5	5	5	5	5	5	5	5	
16.07.2020	5	5	5	5	5	5	5	5	5	5	5	5	5	5	5	5	5	5	5	5	5	5	5	5	
17.07.2020	5	5	5	5	5	5	5	5	5	5	5	5	5	5	5	5	5	5	5	5	5	5	5	5	
18.07.2020	5	5	5	5	5	5	5	5	5	5	5	5	5	5	5	5	5	5	5	5	5	5	5	5	
19.07.2020	5	5	5	5	5	5	5	5	5	5	5	5	5	5	5	5	5	5	5	5	5	5	5	5	
20.07.2020	5	5	5	5	5	5	5	5	5	5	5	5	5	5	5	5	5	5	5	5	5	5	5	5	
21.07.2020	5	5	5	5	5	5	5																		
22.07.2020																4	4	4	4	4	4	4	4	4	big triangle point 4
23.07.2020	4	4	4	4	4	4	4	4	4	4	4	4	4	4	4	4	4	4	4	4	4	4	4	4	
24.07.2020	4	4	4	4	4	4	4	4	4	4	4	4	4	4	4	4	4	4	4	4	4	4	4	4	
25.07.2020	4	4	4	4	4	4	4	4							4	4	4	4	4	4	4	4	4	4	batery exchange
26.07.2020	4	4	4	4	4	4	4	4	4	4	4	4	4	4	4	4	4	4	4	4	4	4	4	4	
27.07.2020	4	4	4	4	4	4	4	4	4	4	4	4	4	4	4										

Legend

test and calibration | small triangle | big triangle | old floe

1,2….9 - instalation point number | covered by LOG-file

4.10.3.4 Stress gauges

Stress sensors measure local horizontal ice stress by detecting the change in frequency of three internal, actively-vibrating wires. Using a network of stress sensors, DGPS/GNSS stations, and the LSO, we can approximate the stress field and responding strains within the local floe. The sensors were installed primarily within and around the CO, though some were installed as far as 2.5 km from *Polarstern* (for detailed locations see Figure 4.8.1 in the Leg 2 cruise report).

Eight Dartmouth College/CRREL Geokon vibrating-wire stress gauges were installed during Leg 1. These sensors recorded stress every minute. In addition, five identical sensors from FMI were installed which recorded stress every 10 minutes. One DC/CRREL sensor was destroyed in mid-November, leaving twelve intact sensors. All gauges from Leg 1 were installed in remnant/second-year ice.

During Leg 2, three more DC/CRREL sensors were deployed in the CO (one in remnant ice on the Northern Transect Loop, and two in FYI in the ROV observatory), making fifteen operational sensors at the end of Leg 2. They required infrequent battery exchange and data download, but otherwise operated unattended. All gauges were deployed on level pans of ice with diameters of at least 100 m.

During Leg 3, we lost one FMI sensor (FMI003) to ridging in Rocket Trap lead on approximately 17 March. By 22 March, the first time we could access the area, the data logger had been crushed and submerged below the water. We managed to recover the sensor from the rubble, but the data logger and data were lost.

The DC/CRREL sensors transmit data to the ship via radio link every 12 hours, although occasionally the radio links would not communicate for a number of days before resuming. At the end of Leg 3, 5 DC/CRREL sensors were still working. Two more (1950 and 1954) stopped communicating on 14 May when the ship relocated further from them and are presumed to still have been operating. One sensor, 1949, continued transmitting until 15 May, after the 12-13 May deformation event, but given its proximity to a ridge, it was likely destroyed shortly thereafter. Sensor 1959 was destroyed in the 12-13 May deformation event. Sensor 1987 was destroyed by Rocket Trap lead on 15 March. The five working DC/CRREL stress sensors transmitted their last data of Leg 3 early in the morning of 17 May, as *Polarstern* departed from the CO. See the Leg 3 cruise report for figure and further information.

Upon returning to the floe at the beginning of Leg 4, two sensors reestablished communication with the base station aboard *Polarstern*, and intermittently transmitted data before permanently losing connection several days later. Four sensors were recovered during Leg 4, including FMI002, FMI004, CRVW1958, and the ‘Old Lady’ stress buoy.

4.10.3.5 Stress panels

Originally, the stress and temperature sensors deployed in the ship hull in void 92 were combined with a set-up of stress panels in the ice next to the ship. They had been taken out during Leg 3 and were not re-deployed. However, the stress and temperature sensors in the ship hull in void 92 were operating through Leg 4. During most of Leg 4, the ship did not experience ice pressure and was using the thrusters to actively push itself against the floe. One noteworthy exception took place in the early morning of 12 July when ice pressure built up at the aft of *Polarstern* and pushed the ship 150 m forwards towards ROV Oasis. Data were downloaded from void 92 on 4 August and backed-up on the MCS under PS122/4_43-150.

4.10.3.6 Ice radar

The ice radar is used to analyze the local ice dynamics at high temporal and spatial scales in the vicinity of the ship. Raw analogical ship radar data are digitalized to capture the echoes from nearby sea-ice features. This provides a full scan of an area covering 20 x 20 kilometers with 8.3 meters horizontal resolution every 2 seconds. During Leg 4, the ship-radar was a valuable tool for monitoring the constant motion of the surrounding floes, especially as fog was

persistent and hindered visibility. For more details on the properties of the ship-radar system, see previous MOSAiC cruise reports.

Ice radar images have been collected on MOSAiC since 25 October 2019. However, acquisition was stopped when entering the 12-nm zone of Svalbard and was re-started on 9 June. The DShip entry of Leg 4 is PS122/4_43-18, but after consultation of the data team, saving raw data was continued under DShip entry PS122/2_14-115.

Leg 4 was clustered in three phases, which should be considered independent of each other when analyzing the ice radar data. From 9-17 June, *Polarstern* was travelling to the MOSAiC floe. From 18 June to 31 July, *Polarstern* was stationary at the floe, with one major repositioning on 12 July. From 31 July onwards, *Polarstern* was travelling again to pick up installations in the distributed network. On several days, the ship was stationary for hours while doing instrument recovery operations.

During Leg 4, little deformation was observed on the MOSAiC floe itself, but surrounding floes were very mobile and observed to shear, diverge and converge. Notes on the dynamics are summarized in the preliminary results section 4.10.3 (preliminary results).

There have been data gaps in the collection of the ice radar system of 50 minutes on the following days: 18, 19, 21, 23, 29 June and 7, 13, 15, 20, 24 July. Unfortunately, the gaps were discovered during post-processing, which includes creating 1-minute long averaged snapshots every 10-minutes and the creation of daily animations.

4.10.3.7 Sea ice strength/mechanics measurements

The aim of ice strength measurements is to determine the local strength of different ice types and their seasonal variations. Measurements of vertical and horizontal ice strength were carried out on earlier legs according to a methodology developed in the Ice Physics Laboratory of the AARI (patent №2348018) and described in “Methodic manual for studying physical-mechanical characteristics of ice formations as initial data for calculation of ice loading on shores, bottom and sea constructions” (SPb, AARI, 2011, p. 179).

For these measurements, a 50 meter x 50 meter area named ‘seismics’ was reserved. The site contains level second-year ice and is located next to the ROV site, next to the seismic station in the logistic area. Local ice strength measurements were conducted with an automatic hydro complex “ЛГК 131-01” borehole probe-indenter “ЛГЦ095.055.0050.002.”

These measurements were not conducted on Leg 4, though similar borehole jack indenter measurements were conducted as part of the Ridge work (link to Ridge work).

4.10.3.8 Uniaxial compressive strength measurements

Uniaxial compressive strength measurements were not conducted on Leg 4.

4.10.4 Preliminary results

Leg 4 was characterized by calm conditions of the MOSAiC floe, while the drift speed was high. The relative motion of ice floes with respect to the floe conditions was observed on a daily base. On a near-daily basis, displacements of ice floes of several 100 meters took place in a distance of ~3-7 km from the *Polarstern*. During 23 adn 26 June, the ice close to *Polarstern*

experienced deformation, mainly divergence that created open water on both sides of the ship. Between 28 and 29 June, surrounding smaller floes rotated relative to our floe, while shearing dominated the area from 9 to 12 o'clock from the *Polarstern* in a distance of ~2-4 km. This motion led to erosion of the floe edge, with the greatest erosion occurring in the northwest corner of our floe, opening to form leads where ridges were located before. The effects of this motion are well documented in the near-daily measurements along the Leg 4 Transect Loop (see chapter 4.5). A convergence and shear event on 8 July resulted in rafting and ridging of a few meters of ice along the southern floe edge close to ROV Oasis. On 10 July at 22:40, a hotspot of motion occurred on *Polarstern's* starboard side at three kilometers' distance. The floes close to the western edge of the MOSAiC floe moved several kilometers to the northeast. The shearing motion continued throughout 11 July and increased in intensity in the early morning of 12 July. As a result, ice pressure built up at the aft of *Polarstern* and pushed the ship 150 m forwards towards ROV Oasis. Since mid-July, ice concentration occasionally reduced to 70-80%, and the floe was often in free drift, only loosely in contact with the surrounding ice floes. This led to strong relative motion between the single floes, often including rotation. Between 24-26 July, the MOSAiC floe itself started to spin, doing almost two full 360-degree loops. In the early morning of 30 July, the first substantial cracks in the floe were observed, mainly located between the ship and the former Met City area, which widened in the late evening. Repeatedly, neighboring floes were shearing along the edge of our floe, eroding them and potentially leading to internal pressure. Approximately at 1 UTC on 31 July, the drift speed of the floe increased again, and the cracks within the floe widened and became disintegration points of the floe.

4.10.5 Data management

All data and their availability conform to the MOSAiC data policy (see Chapter 9 APPENDIX). All device operations were logged in the AWI sensorweb portal and all sensor raw data files are stored in platform section of MCS. Data will be stored at the PANGAEA data repository: World Data Center PANGAEA Data Publisher for Earth & Environmental Science www.pangaea.de. All data are handled, documented, archived and published following the MOSAiC data policy. DOIs will be communicated to PANGAEA for later access via the future MOSAiC Data Portal.

4.10.6 References

Oikkonen A, Haapala J, Lensu M, Karvonen J, Itkin P (2017), Small-scale sea ice deformation during N-ICE2015: From compact pack ice to marginal ice zone, J. Geophys. Res. Oceans, 122, 5105–5120, doi:10.1002/2016JC012387.

4.11 REMOTE SENSING PROGRAM

Mallik Mahmud[1], Aikaterini Tavri[2], Luisa von Albedyll[3], Felix Linhardt[4], Evgenii Salganik[5], Gunnar Spreen[6] (not on board), Estel Cardellach[7] (not on board), T. Casal[8] (not on board), Oguz Demir[9] (not on board), Claude R. Duguay[10] (not on board), Friederike Fohlmeister[11] (not on board), Carolina Gabarró[7] (not on board), Stefan Hendrick[3] (not on board), Joel Johnson[9] (not on board), Ruibo Lei[12] (not on board), Steen Savstrup Kristensen[13] (not on board), Randy K. Scharien[2] (not on board), Mike Schwank[14] (not on board), Maximilian Semmling[15] (not on board), Julienne Stroeve[16,17] (not on board), Wei Wan[18] (not on board), John Yackel[1] (not on board)

[1]UCalgary
[2]UVictoria
[3]AWI
[4]CAU Kiel
[5]NTNU
[6]UNI-Bremen
[7]ES.ICM-CSIC
[8]ESA
[9]EDU.OSU
[10]UWaterloo
[11]DLR
[12]PRIC
[13]DTU
[14]WSL
[15]GFZ
[16]UCL
[17]UManitoba
[18]PU

4.11.1 Objectives

The goal of the remote sensing program during MOSAiC is to evaluate current and future satellite missions with high-resolution, ground-based remote sensing measurements. Although plot scale measurements during MOSAiC will not fully cover the footprint of many satellite observations, they will enable investigations of the temporal evolution of signals caused by environmental changes such as snow accumulation and metamorphism, temperature changes, ice growth and melt, desalination, ice crust formation and wind-packing of snow, etc. Details on objectives can be found in the MOSAiC science plan and in previous cruise reports.

4.11.2 Work on ice

4.11.2.1 At a glance

Leg-4 was a fresh start for the remote sensing program since no instrument or infrastructure was left on the floe at the end of Leg-3. The major task for the Leg-4 remote sensing team was to find and establish a new site for the remote sensing program. In addition, a substantial amount of time was spent on repairing and troubleshooting broken instruments from previous legs. Setting up and maintaining the main site was challenging given the melting conditions at the floe. Our first remote sensing measurements were recorded on 26 June and lasted until 30 July 2020, a day before the floe broke up. During our stay on the floe, we acquired time series and discrete measurements from numerous instruments including radars, radiometers, GNSS, cameras, and spectrometers. These measurements were accompanied by regular snow pits and ice core measurements. In addition to calibrating active microwave radar and passive microwave radiometer, we also performed destructive experiments at the site towards the end of the measurement cycle.

4.11.2.2 New remote sensing city

Determining the location of the new Remote Sensing City was exceptionally challenging. Based on our search criteria (e.g., stability, quick infrastructure development, etc.), we had to limit ourselves to second-year ice. Our goal was to find a stable location at close proximity to the ship so that power and network connections could be established in the earliest phase of the new infrastructure development on the floe. After scouting the floe areas with ICE Team

Lead Melinda Webster, finally, we found a suitable location for the new Remote Sensing City, which was approximately 100 m away from the ship. This site was surrounded by small ridges, which offered a gentle slope to the center of the scanning area. We had thicker snow on the site, perhaps deeper than any previous sites during MOSAiC. The first snow sampling at the site recorded 70 cm of an isothermal snowpack. Meltwater at the snow-ice interface was also found. The evolution of the remote sensing site can be seen from Figures 4.11.1 - 4.11.3.

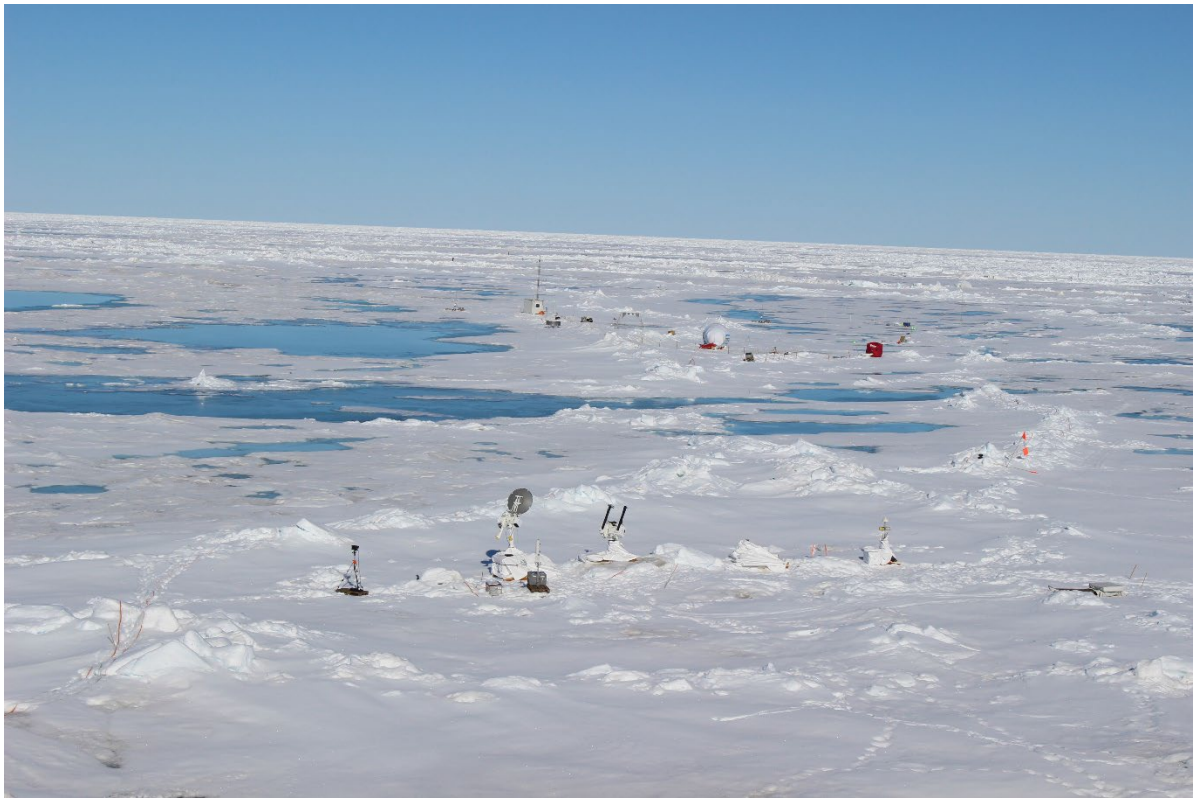

Fig. 4.11.1: *Remote Sensing City on the MOSAiC (fortress) floe during Leg-4. The picture was taken during the early operational phase on 1 July 2020. Photo: Aikaterini Tavri.*

Fig. 4.11.2: *Operational Remote Sensing City on 14 July 2020. Photo: On-site camera.*

Fig. 4.11.3: *Remote Sensing City surrounded by melt ponds on 29 July 2020, two days prior to floe break-up. Airborne photo: Jonathan Hamilton.*

4.11.2.3 Infrastructure development at the site

The remote sensing (RS) hut had been used previously as an installation on site for easy access to power and LAN connection for all instruments. Unlike previous legs, we did not use the RS Hut given the space limitations on-site, rapid surface melt, and the need for quick instrument recovery if the floe became unstable. As Team ATMOS lost their hut during last leg, they required a hut for their installations on site. After consulting with the remote sensing lead scientist (Gunnar Spreen) on land, we offered our hut to the Met City. This generosity came with minor costs to our infrastructure. Having several instruments on site, we came up with a viable solution for power supply based on the instrument requirements. In addition, the installation had to be waterproof and safe for cable connectivity. After consulting with the Log and LAN teams, we modified a zarges box as the safe power hub for the remote sensing site. Having the power hub set-up was crucial for instrument operations; thus, we were able to collect continuous datasets after the installation of the power supply.

Another important installation for remote control of the instruments on site was the LAN hub. LAN service is critical for off-site operations and data download. For this, we required a waterproof case big enough to accommodate RadioLAN installations. Due to very limited availability, we were happy to receive a spare box offered by Matthew Shupe (co-cruise leader), which remains available for use until the end of Leg-5. After successfully testing the new RadioLAN system (MOXA), we connected all remote sensing instruments to the RadioLAN system on 5 July 2020. The system stayed on site until the last day of operation (30 July 2020) (Figure 4.11.4).

Fig. 4.11.4: *Lightweight power hub (zarges box), RadioLAN hub (grey box) and FloeNavi station (orange pelicase) installation at Remote Sensing City. Photo: Antonia Immerz.*

4.11.2.4 Status of instruments

On ice, the Remote Sensing City was comprised of a variety of instruments including active microwave radars, passive microwave radiometers, different types of cameras (i.e. visible, infrared, and hyperspectral) and GNSS-R. Additionally, spectrometers were also installed for radiation measurements (Figure 4.11.5). On Polarstern, we had one passive microwave radiometer and three GNSS instruments. A list of operational instruments during Leg-4 can be found in Table 4.11.1.

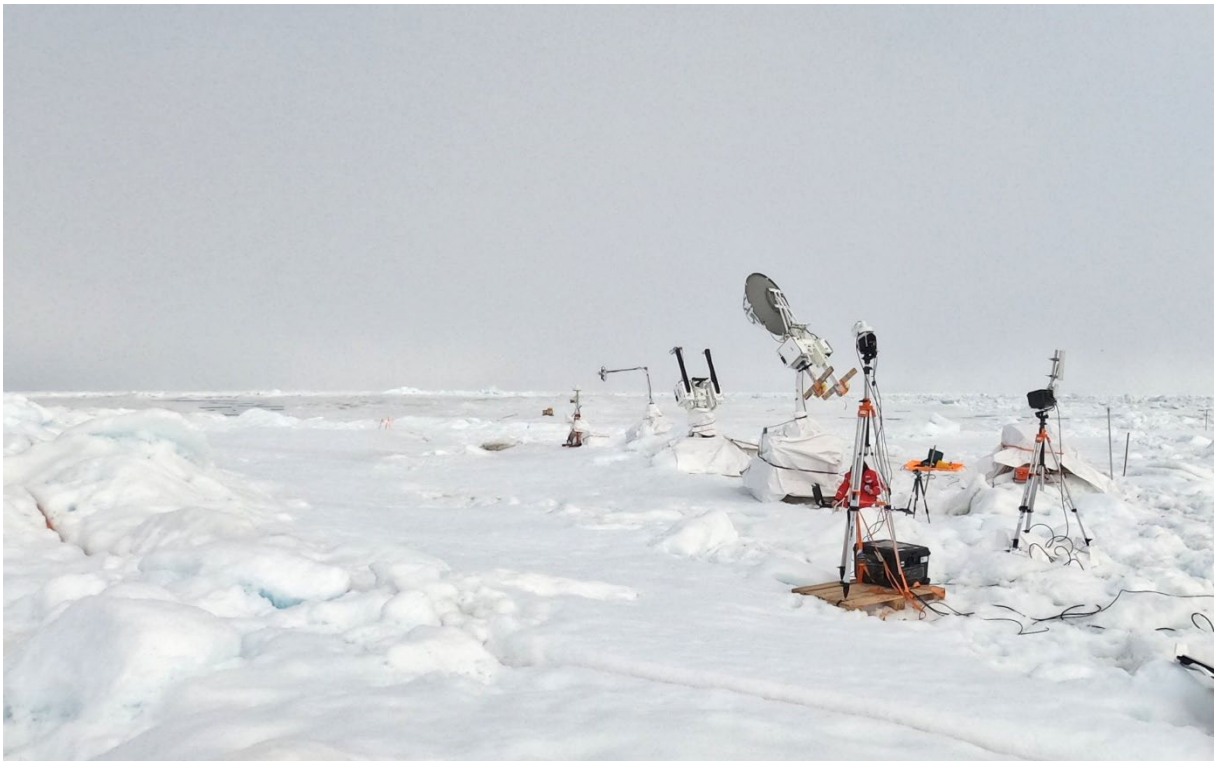

Fig. 4.11.5: *Layout of instruments at the Remote Sensing City on 15 July 2020. Photo: Mallik Mahmud.*

Tab. 4.11.1: *List of operational remote sensing instruments during Leg-4.*

Instrument	**Details**	**PI**	**Institution**	**Leg-4 personnel**
On the ice				
L-band Scatterometer	Fully-polarimetric radar (1.26 GHz)	R. Scharien	U. Victoria	M. Mahmud
KuKa radar	Fully-polarimetric wideband FMCW radar (Ku-band: 12-18 GHz; Ka-Band: 30-40 GHz)	J. Stroeve	U. Manitoba	M. Mahmud
HUTRAD	6.85, 10.65, 18.70 GHz radiometers	J. Lemmetyinen/ T. Casal	FMI/ESA	M. Mahmud
Infrared Camera	Surface temperature	G. Spreen	U Bremen	M. Mahmud
Visible Camera	Visual overview of RS site	G. Spreen	U Bremen	M. Mahmud
HyperSpectral Camera	Specism IQ	G. Spreen	U. Bremen	F. Linhardt
GNSS-R	Reflected GNSS signals from snow/ice	E. Cardellach/ T. Casal	ICE-CSIC/ ESA	A. Tavri
ARIEL	1.27 GHz radiometer (L-band)	C.Gabarro	ICE-CSIC	L. Albedyll

On *Polarstern*				
GNSS-R & atmosphere	reflected GNSS signals from snow/ice and GNSS for atmospheric water vapor	M. Semmling	GFZ	A. Tavri
GNSS Ionosphere	Ionospheric scintillations for GNSS measurements	F. Fohlmeister	DLR	A. Tavri
EMIRAD2	1.4 GHz (L-band)	S.Savstrup Kristensen/ T. Casal	DTU/ESA	A. Tavri

Active microwave radars

Since arriving onboard Polarstern, one of the time-consuming tasks for the RS team was repairing and troubleshooting instruments. We started our leg with several broken instruments including KuKa radar, L-scat, X-scat, and noisy data for C-scat. The repairing operations were performed during the *Polarstern* transit to the MOSAiC floe and in-parallel to remote sensing operations on site afterwards.

We started the repair activities with the KuKa radar, which was not functional since Leg-2. The main malfunctions were associated with the computer board and radar control board, as well as the GPS card. All these parts were broken for both Ka and Ku radars after an unexpected power outage during Leg-2. After replacing the broken parts, the instrument was brought back to life. However, the HH polarization data were noisy during testing. After careful examination, we discovered many broken wires inside the Ka radar box, which could have been the source of the broken radar signals. We proceeded by replacing and repairing several cable connections. Finally and thankfully, we received the expected radar spectrum from both polarizations. The instrument was operational with incidence angle range 0 (nadir looking) to 65 degree (3-degree step), and azimuth angle range from -45 to 45 degree (Figure 4.11.6). Unfortunately, KuKa radar was not operational during transect work due to the missing transect mount and melting ice surface conditions (most notably deep melt ponds).

Fig. 4.11.6: *KuKa radar operations on ice. The KuKa radar is positioned at 65-degree incidence angle. Photo: Aikaterini Tavri.*

After the successful repair of the KuKa radar, we diverted our effort to the C-scat, which was unstable in receiving radar signals. Thanks to the engineers on board, we resolved the issue. The instrument was operational during our pre-deployment testing on board. However, we could not get it running on site. The main challenges with this instrument were associated with the radar connectivity and positioner wiring. After repairing and replacing several wires, the problems were mitigated. However, the data were still noisy due to problems associated with the radar control board oscillator. In addition, the position configuration was lost during previous operational legs, complicating the system operability. After spending several weeks configuring and resolving each problem, and despite several efforts, the system was not operational during Leg-4.

In parallel to the C-scat repair, we worked on L-scat. During Leg-3, the instrument tipped over on ice during a storm. In addition to many other broken parts, the main issue was that the radar was not moving at the correct elevation angle range. Therefore, it could not perform automated sky calibration, and, as a result, it could not record any data. Although getting a working space at the wet lab for a big instrument like L-scat was not easy for us, we managed to adjust to the space limitation. After thorough inspection and assessment, we found that the motor inside the positioner was broken from its core. Since we did not have any spare part, the only solution was to make a new one for the instrument. Coordinating with the ship technician, we managed to replicate the functional part of the motor. The process was quite intensive, and it took several days for us to replicate the broken parts; however, the efforts were worthwhile. L-scat was operational during our Leg with an incidence angle range from 15 to 65 degrees (3-degree step) and azimuth range from -45 to 30 degrees. Occasionally, the instrument was moved along-track by 1 m (as suggested by PI) to achieve independent measurements. The L-scat was also calibrated during Leg-4 (Figure 4.11.7). The calibration procedure and relevant data were documented.

Fig. 4.11.7: *L-scat calibration with corner reflector. Photo: Mallik Mahmud.*

X-scat was broken since Leg-2. We replaced the motherboard and hard-drive of the radar CPU unit. Although the computer started, we could not establish communication with the radar unit. After spending a couple of weeks troubleshooting, we decided to divert our effort towards the deployment of operational instruments.

Passive microwave radiometers

Due to unexpected interferences found in the data during Leg-2, a new sensor of the L-Band (1.4 GHz) passive microwave radiometer ARIEL was shipped with Leg-4. During two preliminary test-runs in proximity to the ship, no interferences in the new sensor were observed, and the regular measurement program was started. All measurements are documented in Table 4.11.2. The measurement program consisted of walking the transects (see also chapter transects) in combination with GEM-2 (ice thickness) and Magnaprobe (snow/pond depth) measurements, point measurements of characteristic ice types, and simultaneous measurements at the Remote Sensing site. On 26 July, measurements next to the GNSS-R were performed and on 23 and 26 July, snow work was done simultaneously with the measurements. Unfortunately, parts of the construction of the sledge were missing, and we improvised a new bracket out of bamboo stakes which holds ARIEL in approximately 40° at 1.50 m from the ground (Figure 4.11.8). To avoid interferences with metal parts, we used ropes and tape to construct the new bracket. ARIEL joined four transects, but the uneven terrain with hummocks and melt ponds introduced substantial movement of the instrument. During the transects, occasional stops documented the brightness temperature of different ice types, e.g. sediment-rich ice, ridges, and melt ponds. In addition, two long-term (several hours) measurements at the remote sensing site were conducted, as well as two series of point measurements in the logistics area.

Tab. 4.11.2: *An overview of device operations of ARIEL measurements*

Date	Survey Type	ARIEL	GEM-2	Magnaprobe
July 13	Transect Loop	PS122/4_47-4	PS122/4_47-6	PS122/4_47-220
July 18	Remote Sensing Site	PS122/4_47-148	N/A	N/A
July 19	Transect Loop	PS122/4_47-147	PS122/4_47-140	PS122/4_47-226
July 21	Transect Loop	PS122/4_48-36	PS122/4_48-61 PS122/4_48-180	PS122/4_48-246
July 23	Point measurements Log area	122/4_48-184	N/A	N/A
July 23	Transect	122/4_48-185	PS122/4-48_178	PS122/4_48-247 Snow-work: PS122/4_48-86
July 26	Remote Sensing site	122/4_48-194	N/A	N/A Snow-work: PS122/4_48-177
July 26	Point measurements Log area	122/4_48-194	PS122_48-171	N/A

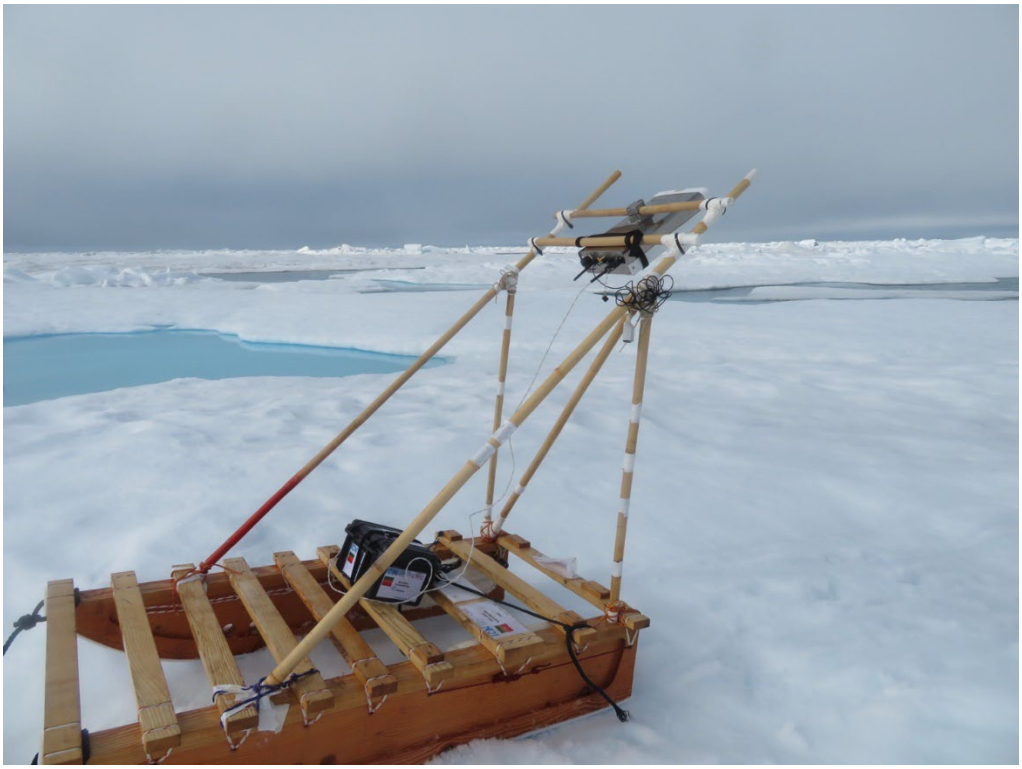

Fig. 4.11.8: *Set-up for ARIEL used on Leg 4 facing the surface scattering layer during the transect on July 23. The instrument is fixed on a bamboo stick at a 150-cm height at an approximately 40° angle. Photo: Luisa von Albedyll.*

HUTRAD – a 3-channel passive microwave radiometer (6.85, 10.65, 18.70 GHz) was deployed during the later part of Leg-4 (Figure 4.11.9). In addition to logistical challenges, space constraint, polar bear activity and severe melting at the site delayed the deployment process. After deployment, the instrument was operational at 50-degree incidence angle corresponding

to existing and upcoming satellite missions. The instrument was also calibrated during Leg-4 (Figure 4.11.10). Calibration documentation can be found in MCS data folder. Other passive microwave radiometers (e.g., SSMI and ELBARA) were not deployed as suggested by respective PIs on land because of the fast melting conditions.

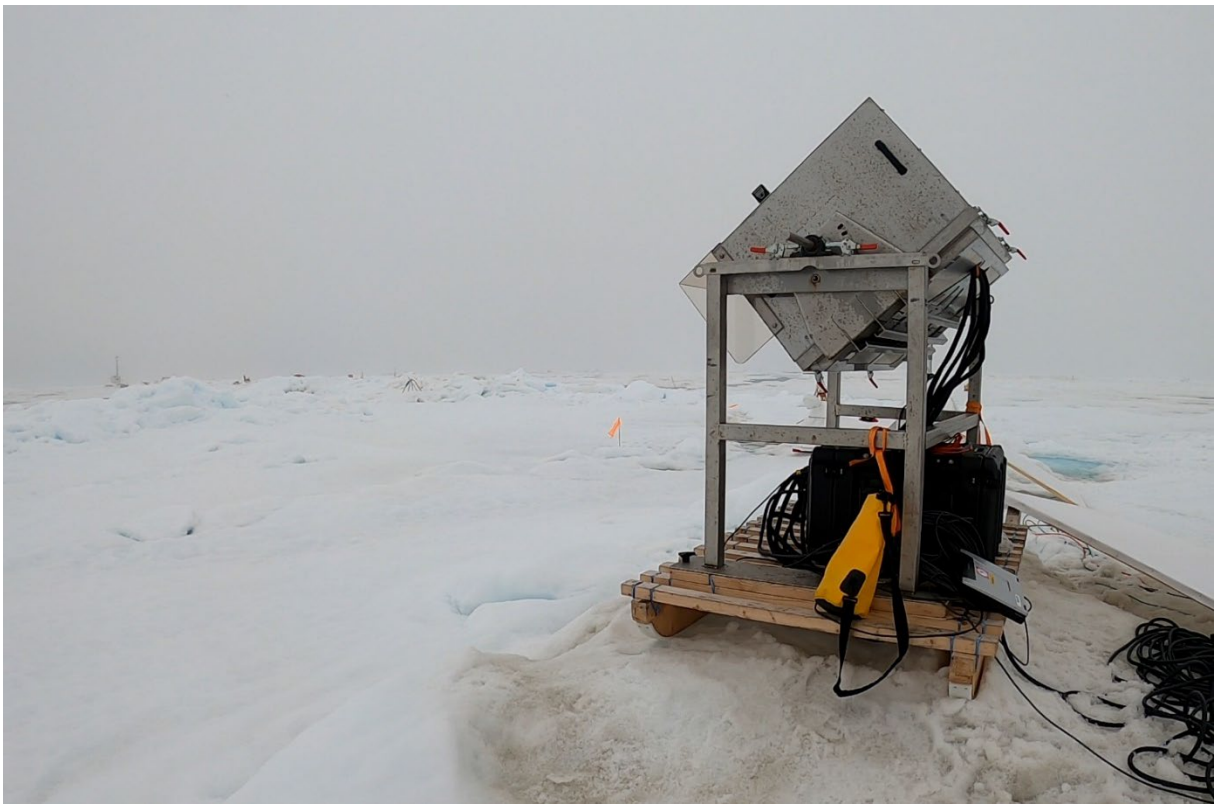

Fig. 4.11.9: *HUTRAD deployment at the remote sensing site. The instrument was positioned at a 50-degree incidence angle. Photo: Mallik Mahmud.*

Fig. 4.11.10: *HUTRAD calibration at the Remote Sensing site on 07.29.2020. Photo: Aikaterini Tavri.*

Fig. 4.11.11: *Passive microwave radiometer EMIRAD2 onboard Polarstern during sky calibration. Photo: Aikaterini Tavri.*

The EMIRAD-2 microwave radiometer was continuously operational onboard *Polarstern* from the previous Legs (Figure 4.11.11). Sky calibration in 150° was operated every 2 days. Data quality reports were frequently generated and communicated to the PIs. Detailed information on the calibration days and photos, and instrument operation can be found in the data archive.

<u>Camera</u>

We had a late start with infrared and visible cameras on site due to the missing power box onboard, which was a critical component for setup. The camera power box was the lost victim of cargo shuffling during the rotation of Leg-3 and Leg-4. After contacting the PI on land and Leg-3 responsible personnel, we located the box at an unexpected location, and the cameras were deployed immediately afterward. Both the cameras were running continuously until the end of the floe. The visible camera and the IR camera were acquiring data in time-lapse mode every 3 minutes and 10 minutes, respectively. We also installed the Hyperspectral camera on the site earlier than other cameras since it ran on battery power. In the starting phase, some issues with the internal white reference prevented acquisitions, leading to fully white or black images and no usable spectra. After troubleshooting, the camera delivered one image per 30 minutes, with occasional breaks, when the camera software ran into errors. The acquisition setting used was the 15-degree downwards angle, keeping the horizon in view (Figure 4.11.12). A challenge was the unstable position of the camera, as the tripod had to be mounted on a pallet and melting conditions led to unstable angles. With the horizon in the acquisition frame, this problem can be mitigated in post-processing. Similar problems were found with the white reference, as the small tripod experienced preferential melt around the tripod legs, slowly tipping the white reference from its level position. Regular site maintenance included re-alignment of the white reference.

Fig. 4.11.12: *Preview image from hyperspectral camera's RGB-viewfinder across the remote sensing site. The white square marks the approximate extent of the hyperspectral acquisition. The small tripod carries a white reference plate. On the right edge of the frame L-scat and KuKa radar are visible.*

GNSS

GNSS-R on ice was one of the few instruments that were deployed at the early stage of the set-up phase since it was light-weight and could be operational on battery-power. Since June 28, GNSS-R was acquiring continuous data both at linear and circular polarizations (Figure 4.11.13). However, instability in battery charger caused interruption in continuous measurements on several occasions. The instrument was repositioned (no more than 3-meter from the initial position) due to a melt formation around the instrument. Detailed information on the system operations were recorded and archived. Additionally, other installations onboard *Polarstern* such as the GNSS_JAVADd3, the GNSS receivers gors and tiny and the GNSSntLab, were operational throughout Leg 4 providing continuous measurements from previous Legs.

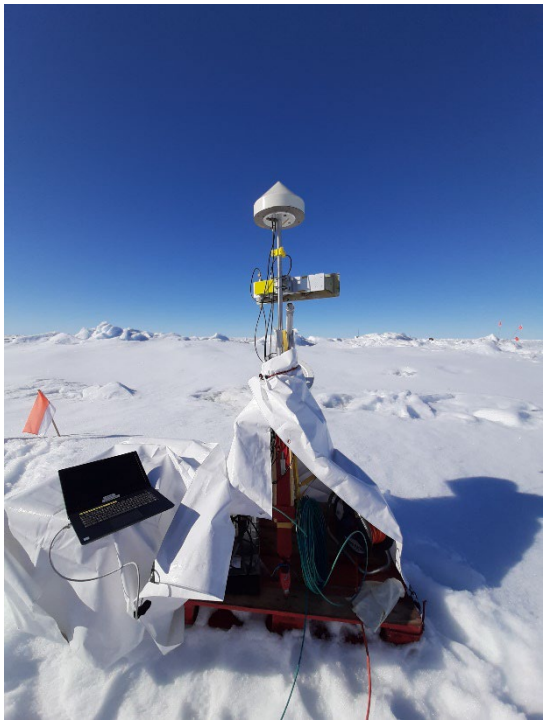

Fig. 4.11.13: *GNSS-R configuration on site. Ablation shields were placed around the instrument and the receiver box to delay lateral melt. Photo: Aikaterini Tavri.*

Operations of remote sensing instruments are summarized in Table 4.11.3. Specifications of these instruments can be found in SensorWeb and previous cruise reports.

Tab. 4.11.3: *Details on operations of remote sensing instruments*

Instrument	Recording start	Recording end	Data type	SensorWeb Device name	DSHIP event ID
L-band scatterometer	06.26.20	29.07.20	Continuous	scat-l	PS122-4_43-72
KuKa radar	06.25.20	07.19.20	Continuous	kuka radar	PS122-4_43-73
HUTRAD	07.22.20	07.29.20	Continuous	hutrad	PS122-4_43-130
Infrared camera	07.10.20	07.30.20	Continuous	ir_variocam_01	PS122-4_43-101
Visible camera	07.10.20	07.30.20	Continuous	vis_infralan_01	PS122-4_43-80
Hyperspectral camera	07.02.20	07.29.20	Continuous	specim_iq_01	PS122-4_43-78
GNSS-R	06.28.20	07.29.20	Continuous	gnss-r_icefloe	PS122-4_43-71
GNSS-R & Atmosphere	since Leg 1	ongoing	Continuous	GNSS-receiver-GORS, GNSS-receiver-TINY	PS122-1_1-30
GNSS Ionosphere	since Leg 1	ongoing	Continuous	GNSS_JAVADd3GNSS_NTlab_FE	PS122-1_1-30
EMIRAD2	06.09.20	08.12.20	Continuous	emirad2	PS122-4_43-38
ARIEL	07.13.20	07.26.20	Discrete	balamis_rad	see Table 2

4.11.1.1 Ancillary datasets acquired at the remote sensing site

<u>RAMSES radiation station</u>

Three RAMSES spectrometers were installed during the 24-hour sampling experiment, where radiance, irradiance and scalar irradiance were measured in the UV/VIS spectrum ranges (Figure 4.11.14). During the experiment, data were recorded at every minute, which was adjusted to a 10 min measurement span afterward. The system was operational during 10-29 July 2020 adjacent to other remote sensing instruments to provide continuous measurements on albedo and surface reflectance (SensorWeb Devices: cau_ramses_1, cau_ramses_2, cau_ramses_3; DShip event PS122-4_46-197).

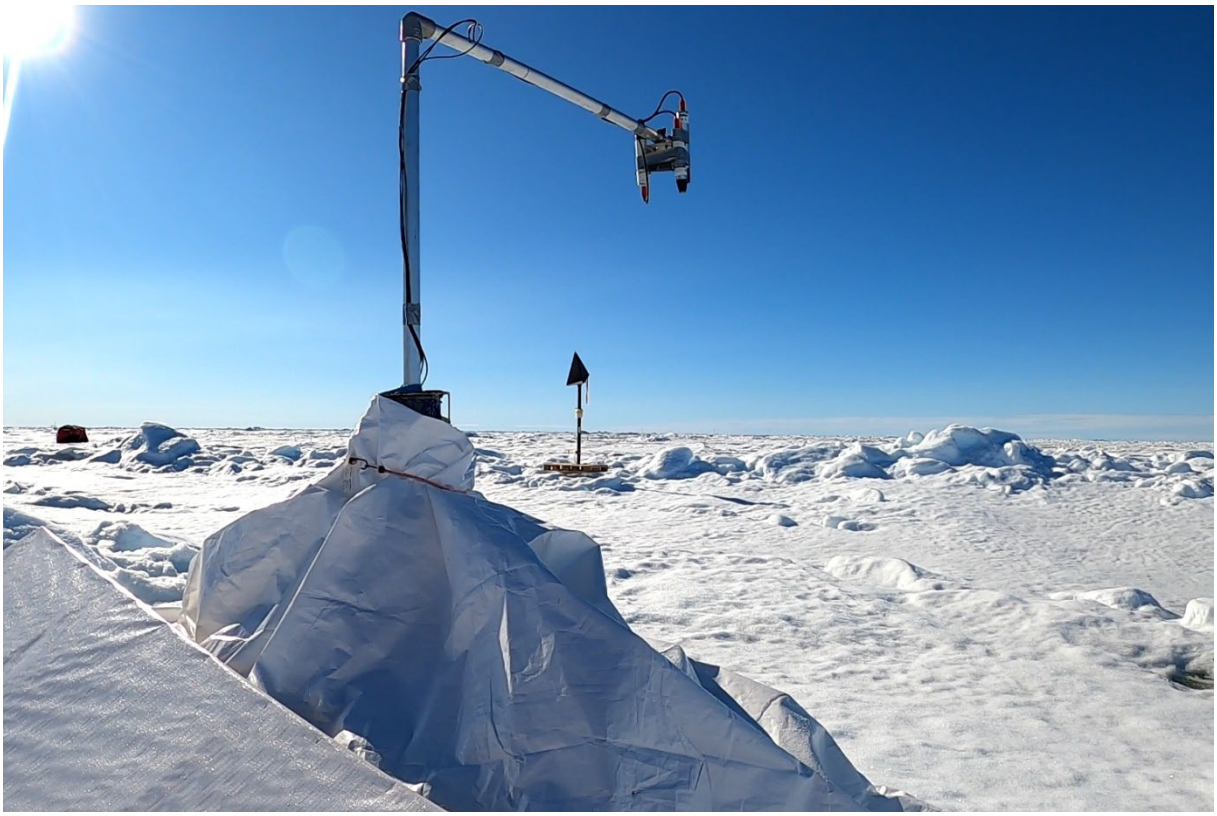

Fig. 4.11.14: *RAMSES radiation station configuration. Photo: Mallik Mahmud.*

Snow pits

Since the establishment of the Remote Sensing City, snow sampling was started adjacent to the instruments to capture dynamic snow conditions at the site (Figure 4.11.15). Snow depth, density, grain size, dielectrics, snow volume structure, surface characterization, sample for CT scan, and NIR photos were acquired on a regular basis. For details on snow measurement, see sub-chapter on snow. Main interest for snow sampling at the Remote sensing site was associated with snow dielectrics and density measurements for retrieving snow wetness.

Ice cores

Temperature, salinity, and density profiles from multiple cores in three locations at the remote sensing site were collected (Figure 4.11.15). These ice core datasets are vital to characterize ice structure and brine channel distribution, which are critical to interpret remote sensing measurements.

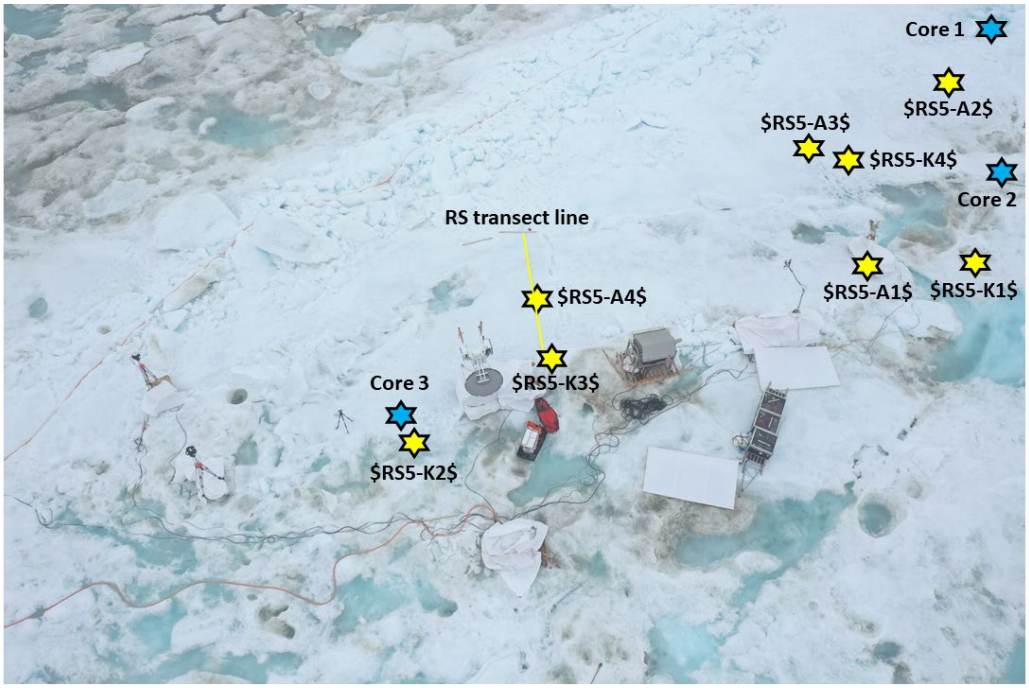

Fig. 4.11.15: *Aerial photo indicating the snow pit (yellow marker) and coring (blue marker) locations at the Remote Sensing City. Snow pit ID corresponds to the Dship action log, and core ID corresponds to Table 4.11.4. Background photo: Jonathan Hamilton.*

Tab. 4.11.4: *Details on coring events at the remote sensing site*

Core ID	DShip Event	Timestamp	Comment
1	PS122/4_45-163 si_corer_9cm	06.29.20	Temperature ice core (5 cm sections) at RS site
2	PS122-4_46-100 si_corer_7cm	07.11.20	Temperature and Salinity ice core (5 cm sections) at RS site
3	PS122/4_49-103 si_corer_7cm	07.27.20	Temperature, Salinity and Density ice core 5 cm sections) at RS site

4.11.2.5 Experiments

<u>24-hr sampling</u>

During UTC 10:00 on 10 July to UTC 10:00 on 11 July 2020, the remote sensing team joined the 24-hour sampling marathon at the MOSAiC floe. We acquired remote sensing measurements at high temporal resolution (e.g., every 30 min) for 24 continuous hours from the L-scat and KuKa radar to capture the diurnal variability in snow-covered sea-ice surface and volume. In addition to active microwave radar instruments, the albedo and reflectance of the snow surface were measured every minute from the radiation station on site. All cameras (visible, IR and hyperspectral) and GNSS-R were operational in continuous mode. ‘B’ type snow pit measurements along with near-infrared (NIR) photographs, and surface characterization samples were also acquired at 6-hour intervals to capture the variability at the snow surface and volume. One ice core was also collected during the 24-hour sampling period for ice temperature, density and salinity measurements at the Remote Sensing City.

<u>Destructive measurements</u>

Towards the end of Leg-4 (on 29 July 2020), we performed several destructive experiments at the remote sensing site. The first one was the penetration depth experiment (Figure

4.11.16). The goal of the experiment was to understand the penetration depth of microwave energy at lower frequency (e.g., L-band; 1.27 GHz). For the penetration depth experiment, we put a 50 cm × 50 cm metal plate (3 mm in thickness) under the snow cover at the radar scanning area. We systematically positioned the metal plate at 6 different locations to measure at different incidence angles. The results from the experiment will offer insight into the radar penetration capability during melt season at L-band frequency at different viewing angles.

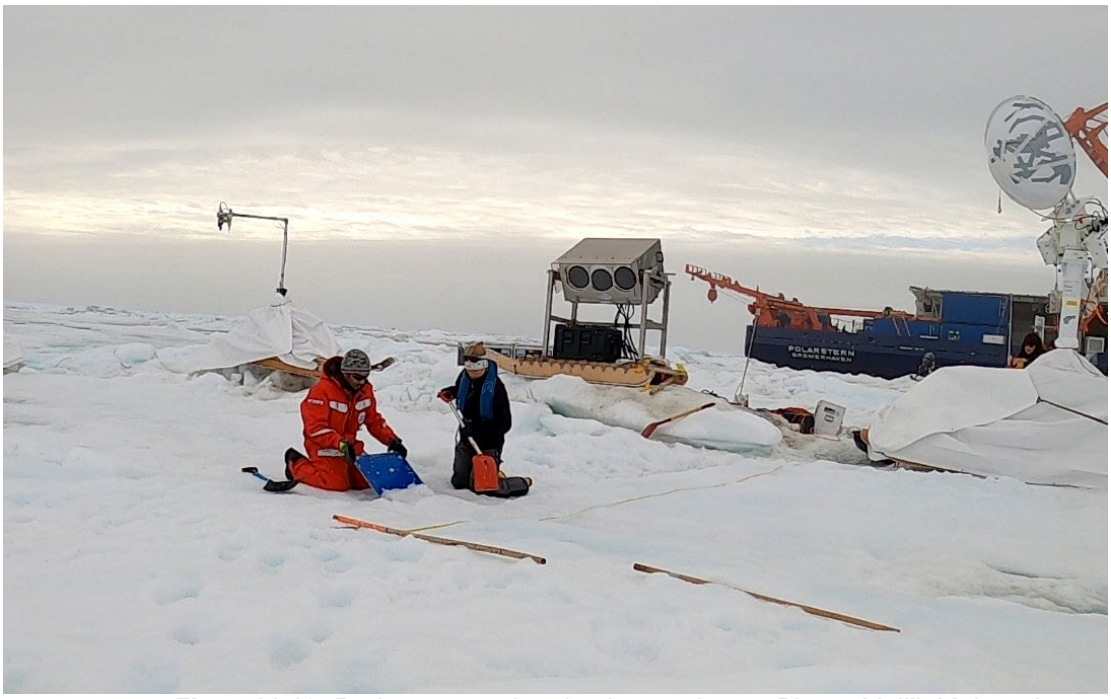

Fig. 4.11.16: *Radar penetration depth experiment. Photo: Mallik Mahmud.*

Extensive destructive snow sampling was performed to aid the radar measurements during the experiments. A continuous NIR photographs and SMP measurements were taken along the 7-m snow transect/wall (at the experiment area) along with snow thickness measurements (Figure 4.11.17). In addition, a ‘B’ type snow pit was done at the center of the destructive sampling site. Coincident snow electrical property (e.g., dielectric) measurements were also acquired. To characterize the snow surface layers, samples were taken for microCT scans. The snow characterizations will be highly valuable for interpreting the observed variability in the radar signal during our last experiment at the remote sensing site.

Fig. 4.11.17: *Destructive snow sampling experiment. NIR photographs and SMP measurements were taken along the 7-meter snow wall. Photo: Mallik Mahmud.*

We also performed a snow-removal experiment to record the radar signature over bare sea ice (Figure 4.11.18). Our goal was to observe the changes in radar backscatter response on an hourly basis over a bare ice surface in warm weather conditions. We ran the experiment for 18 hours. During this period, L-scat acquired measurements from 15 to 65 degrees incidence angles with an azimuth range from 15 to 45 degrees covering the snow-removed ice surface. Before removing the snow, we also observed the same area from radar instrument with identical settings. This experiment with/out snow on sea ice will aid our understanding of the influence of wet snow on radar signals and scattering mechanisms during the Arctic melt season.

Fig. 4.11.18: *Snow-removal experiment at the remote sensing site. Photo: Aikaterini Tavri.*

4.11.2.6 Challenges

Instrument repair was one of the major tasks for the remote sensing team on Leg-4. We struggled to allocate time on repair effort and operations of instruments. We successfully repaired and deployed KuKa radar and L-scat. Substantial time was spent on C-scat and X-scat for repair. We could not fix the C-scat during Leg-4; therefore, the PI suggested to ship the instrument back after Leg-4. We made substantial progress on X-scat. After replacing broken parts, the X-scat data acquisition box started working. However, the communication between radar and data acquisition box could not be established. Relevant information was shared with Leg-5 team for further actions. The L-scat motor repair was successful, and the instrument was operational continuously.

Logistical challenges were a major concern, especially towards the beginning of the leg while instruments were being deployed. Melt conditions on the ice surface were not favorable for instrument transportation via skidoo. Bad weather and the busy schedule of Heli operations restricted our options for instrument transportation to the remote sensing site. Therefore, with 6 volunteers, we started moving heavy instruments to the site. The moving was challenging, especially due to rough topography (e.g., ridge) and thick snow cover at our site, as we selected a site with larger ice thickness for higher stability.

Site management was a continuous effort for the remote sensing team. We installed ablation shields around all instruments during the set-up phase of the site to slow surface melt. Although we slowed down the melting around instruments from the beginning, we had to keep relocating them for better stability throughout the leg. Especially, GNSS-R was moved around several times due to melt pond formation around it. We also drained melt ponds at the site for better mobility and stability. After two weeks of installation, we had to level a ridge to stabilize the KuKa radar site to avoid the risk of tipping over. Extensive melt and rain for several days forced us to bring the KuKa radar onboard. We also experienced similar challenges for the L-scat and HUTRAD. Although additional supports were installed for instrument stability on ice, HUTRAD

sledge slid down from its position overnight due to extensive rain. Luckily, the instrument was in good condition and no damage was done. To manage the heavy remote sensing instrumentation on the ice, often we required additional assistance from scientists and logistics personnel for relocation and site management.

Power outages were one of the major hindrances to the continuous time-series during Leg-4. Like other major establishments requiring power on the floe (e.g. Met City, ROV oasis), power outages were not uncommon at the remote sensing site. Due to polar bear activity on the floe and sudden ship motion, power was disconnected on several occasions during this leg. As most of the instruments were running on ship power, only battery-powered cameras were operational during the outages. We strictly followed power outage protocol as suggested by PIs to ensure instrument safety from the outage.

Additionally, polar bear visited the remote sensing site on two occasions. No damage was found for any instrument. However, a friendly polar bear did not forget to leave its footprint on the radar scanning area (Figure 4.11.19). We repositioned the instrument to avoid the disturbed area for the reminder of the leg.

Fig. 4.11.19: *Polar bear visit at the remote sensing site on 16 July 2020. Photo: Lianna Nixon.*

4.11.3 Preliminary (expected) results

Leg-4 offered an exceptional opportunity to study radar backscatter, radiometer emissivity and GNSS reflectometry over the melt season as moisture/melt water content increased in the snowpack. Examples are given from multi-frequency (Ka-, Ku- and L-band) radar instruments to demonstrate the variable radar responses over the melt season.

Figure 4.11.20 shows substantial differences in Ka-band radar backscatter between morning and afternoon measurements on 2 July 2020. We found increased moisture content in the snow layers on a diurnal basis. Strong responses were found at Ka-band radar signals corresponding to these changes. A similar pattern was seen in the Ku-band data, albeit with lower intensity (Figure 4.11.21). Coincident measurements from duel frequency KuKa radar will advance our understanding of radar responses during melt season, which is relevant to the following satellite missions: CryoSat-2, Sentinel-3, AltiKa, ERS-1/2, Envisat, and future CRYSTAL altimeters; NSCAT, QuikSCAT, OSCAT, SCATSAT1, CFOSAT scatterometers.

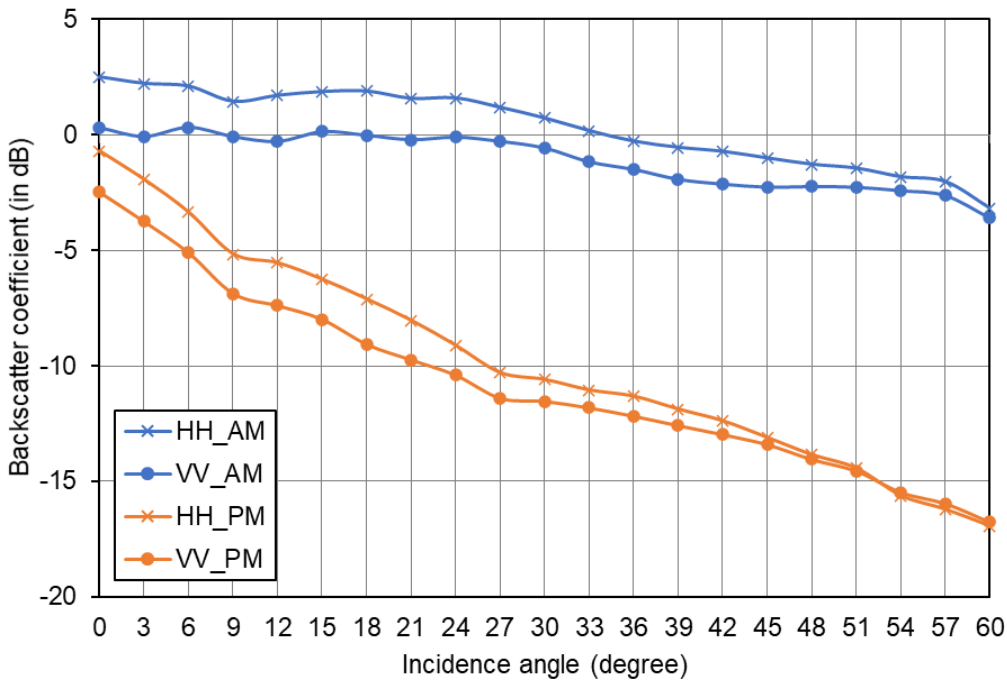

Fig. 4.11.20: *Ka-band radar responses at both HH and VV polarizations during melt season (2 July 2020). AM and PM denote morning and afternoon local time.*

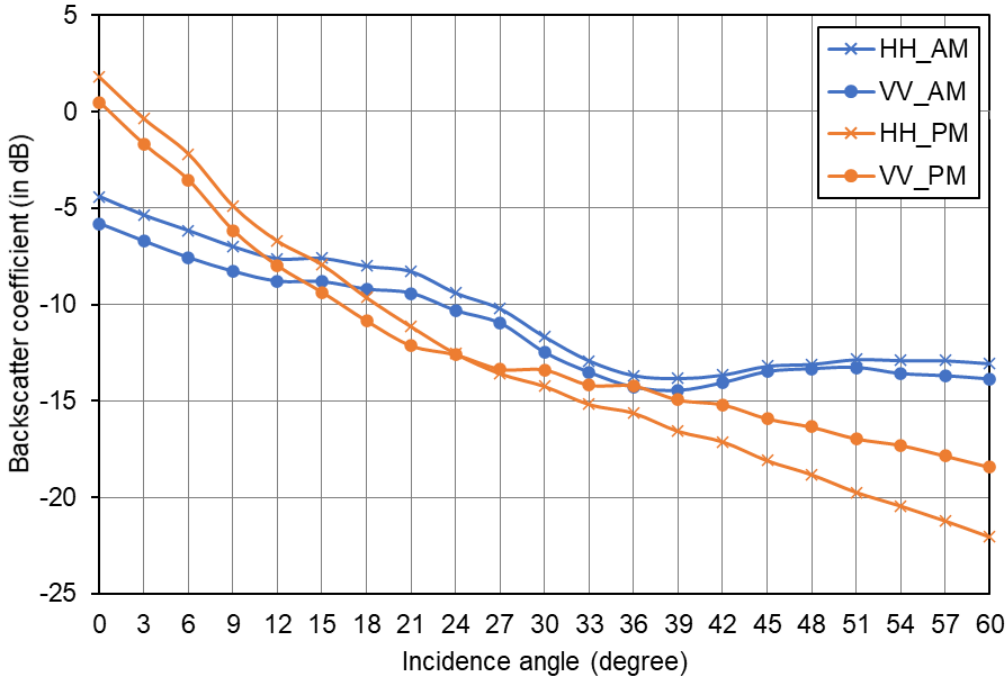

Fig. 4.11.21: *Ku-band radar responses at both HH and VV polarizations during the melt season (2 July 2020). AM and PM denote morning and afternoon local time.*

Besides diurnal variability, radar measurements during Leg-4 showed subtantial variability compared to winter measurements. Figure 4.11.22 shows sustantial changes in L-band backsctter at both HH and VV polarization between the winter (15 January 2020, acquired during Leg-2) and summer seasons (2 July acquired during Leg-4). Due to longer penetration capability into snow/ice volume during cold and dry winter season, radar backscatter was very low. However, increased moisture content in snow during the melt season, reduced the radar penetration capability, and thus, high backscatter response was found. The L-band scatterometer measurements during Leg-4 will be unique and highly valuable for

corresponding L-band SAR satellite missions: ALOS/PALSAR-1, ALOS-2 PALSAR-2, SAOCOM, and upcoming NISAR and ROSE-L.

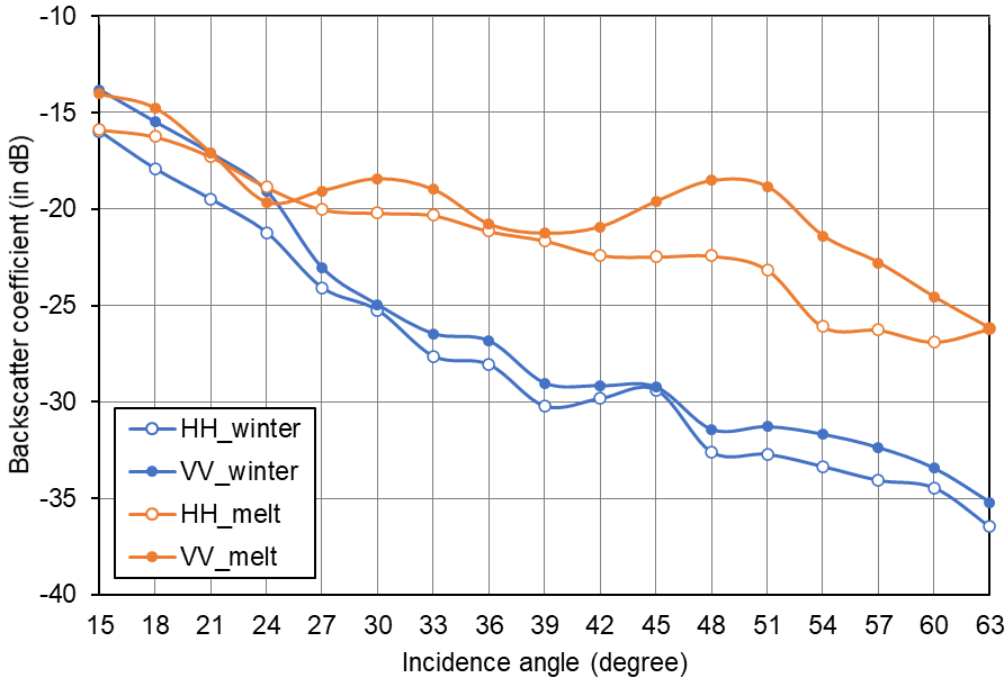

Fig. 4.11.22: *L-band scatterometer responses at both HH and VV polarizations during winter and summer seasons.*

4.11.4 Data management

All data and their availability conform to the MOSAiC data policy (see Chapter 9 APPENDIX). All final data of all on-ice and onboard remote sensing instruments will be stored at the MOSAiC Central Storage (MCS) and at PANGAEA (World Data Center PANGAEA Data Publisher for Earth & Environmental Science (www.pangaea.de)) after post-processing and quality checks. Storage and release of data follow the MOSAiC data policy.

All data are handled, documented, archived and published following the MOSAiC data policy.

4.12 Ponds

Felix Linhardt[1]
Gerit Birnbaum[2]
Natascha Oppelt[1] (not on board)

[1]CAU Kiel
[2]AWI Bremerhaven

4.12.1 Objectives

The overarching goal of the melt pond measurements campaign is to optically characterize melt ponds at in-situ scale and to facilitate upscaling of the gathered metrics to airborne and spaceborne observations.

Parameters of interest are optical properties primarily in the visible and near-infrared wavelength region, as well as physical properties such as pond depth, sea-ice thickness and pond bottom structure.

In the data evaluation phase, the field observations will be coupled with the helicopter measurements, which yielded RGB and hyperspectral images, as well as ice thickness and surface topography data (see chapter 4.4). Moreover, the field measurements will be used to validate satellite derived products such as pond depth and spectral radiance and reflectance of the snow and ice surfaces neighbouring the ponds.

4.12.2 Work at sea

4.12.2.1 Instrumentation

Melt pond spectra were obtained with two different setups. The *Böötle* setup consists of a self-propelled, remotely-controlled measurement platform, primarily carrying three spectroradiometers to obtain downwelling irradiance above and below the waterline, as well as upwelling radiance below the water surface. The *Böötle* further carries an acoustic depth sensor for assessing two-dimensional pond depth data in the field.
The Stick (or *Stickle*) setup is comparable with an ASD setup, i.e. person-mounted, measuring down- and upwelling irradiance (see chapter 4.7 Optics). An additional spectrometer for measuring upwelling radiance is also attached to the stick. The Stick setup can be used on snow and ice surfaces to measure spectral albedo and reflectance, but can also be used to measure reflectance of ponds. When used at pond sites, the setup is usually used together with a ruler for measuring pond depth and sometimes a drill set and thickness gauge to measure sea ice thickness. Accompanying measurements include in situ water temperature, conductivity and chlorophyll concentration. Water samples were taken and analysed in the lab to assess chlorophyll concentration and CDOM (coloured dissolved organic matter).

Fig. 4.12.1: *Böötle on James Pond.*

4.12.2.2 Locations

Pond work was conducted at several sites throughout the Leg 4 MOSAiC floe, including on first-year ice as well as second-year ice (see figure 4.12.2):

- *James Pond* was the first pond to be measured, conveniently located near the spine road to Met City.
- *Mystery Lake* has been boated once before drainage and was drilled extensively afterwards to get an overview of pond bottom thicknesses. Drainage happened during the 24h sampling marathon from 10 to 11 June.
- *Pond No. 1* and *Outer Pond* were located on first-year ice near the *Lemon Drop* albedo line.
- *Root Beer Pond* was surveyed twice with a ruler and GPS device.
- The *EcoLodge Ponds* were only visited once.
- *Starry Lagoon* was the center of attention for the first multi-team destructive pond sampling event.

4.12.2.3 Sampling

In total, Böötle had six deployments, while Stickle had nine deployments. Two surveys were done only with ruler and GPS receiver – no spectra were collected.

Tab. 4.12.1: *Overview of pond work device operations.*

Device Operation	Date	Main device	Location / Comment
PS122/4_44-260	2020-06-14	Stickle	Ice Station 1, albedo line
PS122/4_45-189	2020-07-04	Böötle	James Pond
PS122/4_45-190	2020-07-05	Böötle	James Pond
PS122/4_46-200	2020-07-06	Stickle	Pond No. 1 + Outer Pond
PS122/4_46-201	2020-07-08	Böötle	James Pond
PS122/4_46-202	2020-07-09 AM	GPS + ruler	Root Beer Pond
PS122/4_46-204	2020-07-09 PM	Böötle	Mystery Lake
PS122/4_46-205	2020-07-11	Böötle	Mystery Lake
PS122/4_47-186	2020-07-13 AM	Stickle	Mystery Lake + drilling
PS122/4_47-187	2020-07-13 PM	GPS + ruler	Root Beer Pond
PS122/4_47-188	2020-07-14	Stickle	Mystery Lake + drilling
PS122/4_47-189	2020-07-15	Stickle	Mystery Lake + drilling
PS122/4_47-190	2020-07-18	Stickle	Starry Lagoon, destructive
PS122/4_48-219	2020-07-20	Böötle	James Pond
PS122/4_48-220	2020-07-21	Stickle	EcoLodge Ponds
PS122/4_48-222	2020-07-23	Stickle	Pond No. 1
PS122/4_49-100	2020-07-27	Stickle	Root Beer Barrel line, destructive

Water samples were collected on several occasions. Lab analysis is done with an Avantes spectrometer, with either an integrating cavity or a liquid waveguide capillary setup. The table below shows the samples taken – at the time of this writing, lab analysis is ongoing, but will be logged with reference to the original sampling device operation.

Tab. 4.12.2: *Overview of pond work related water samples.*

Device Operation	Date	Location / Comment
PS122/4_46-203	2020-07-09	Root Beer Pond
PS122/4_46-206	2020-07-11	Mystery Lake
PS122/4_47-191	2020-07-18	Starry Lagoon
PS122/4_48-9	2020-07-20	James Pond
PS122/4_48-223	2020-07-23	Pond No. 1

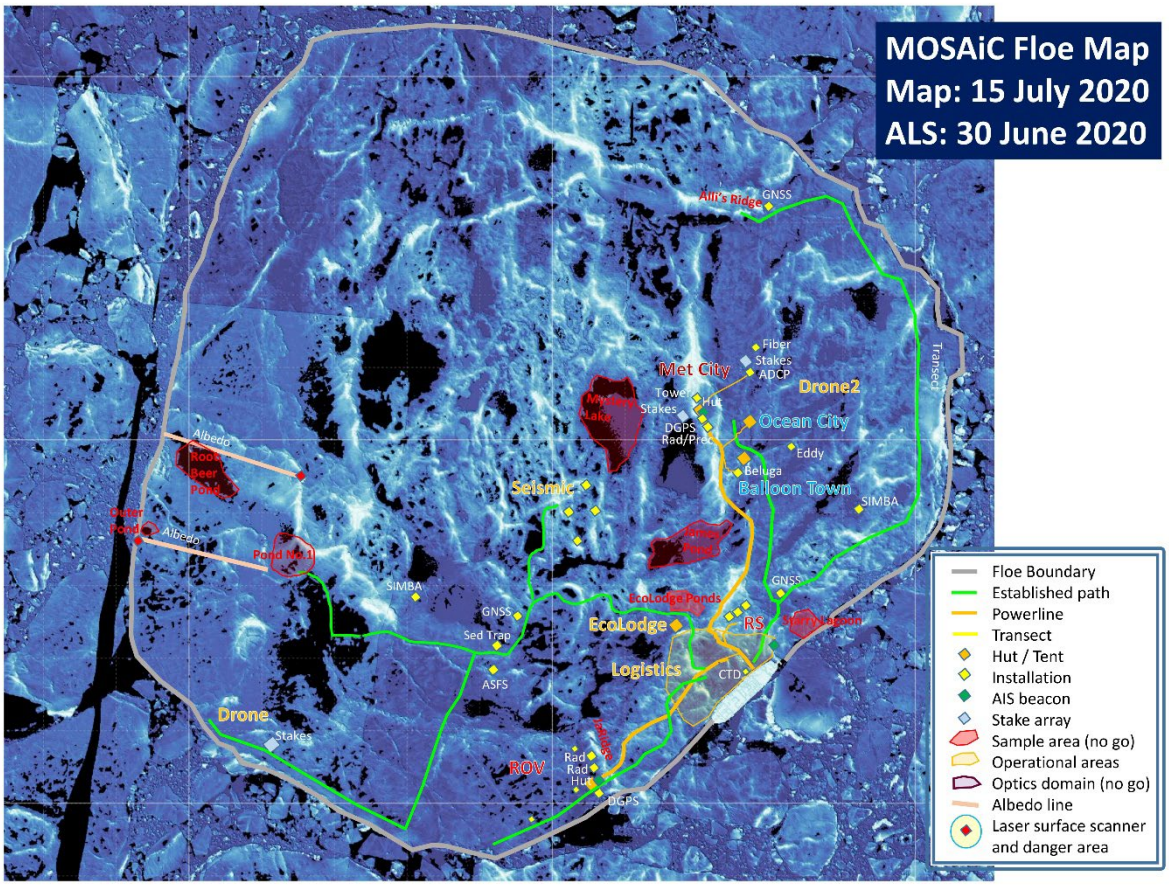

Fig. 4.12.2: *Reduced general floe map with marked out pond areas.*

4.12.3 Preliminary results

An interesting event was the (natural) drainage of *Mystery Lake* during the 24-hour sampling marathon from 10 to 11 July 2020. The pond was surveyed once with *Böötle* before the drainage happened. This allowed for an estimate of the volume of freshwater being discharged to the bottom side of the floe in a relatively short time span and high localization.

The apparent connection between melt pond and ocean also created the opportunity to “non-destructively” (with respect to a possible drainage or salinity-change of the melt pond water) drill the melt pond bottom for thickness measurements. This allowed for the collection of a large number of spectra with collocated water depth and bottom ice thickness measurements.

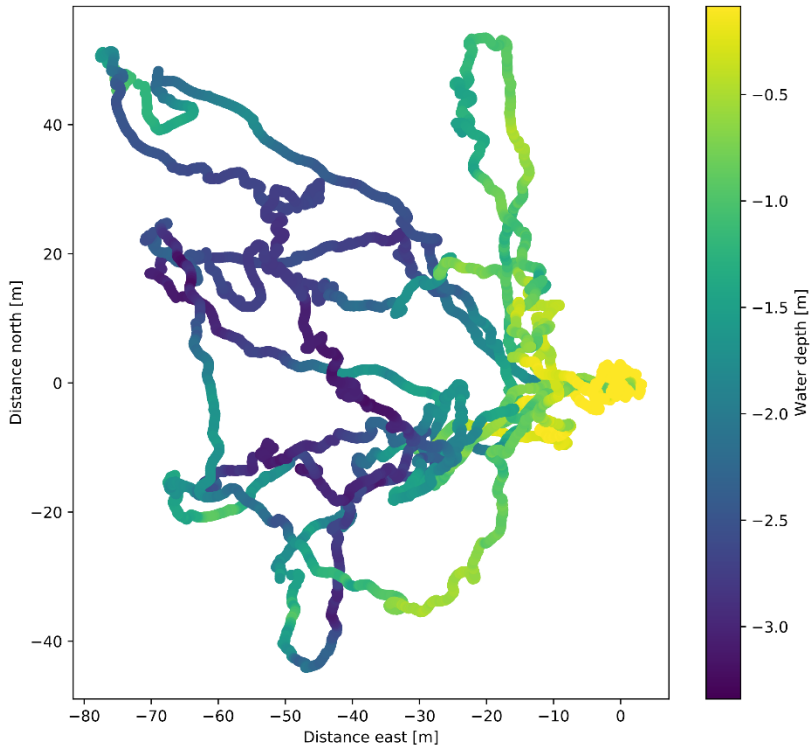

Fig. 4.12.3: *Quick look of depth data of Mystery Lake before drainage. Drift correction of GPS data is only linear between start and end of survey. This leads to substantial positional (horizontal) inaccuracies, but the overall assessment of large portions of the pond being deeper than 2.5m still holds. The track starts and ends on the eastern shore of the pond, but does not extend fully to the other shores, explaining the lack of shallow parts on the west/north/south sides.*

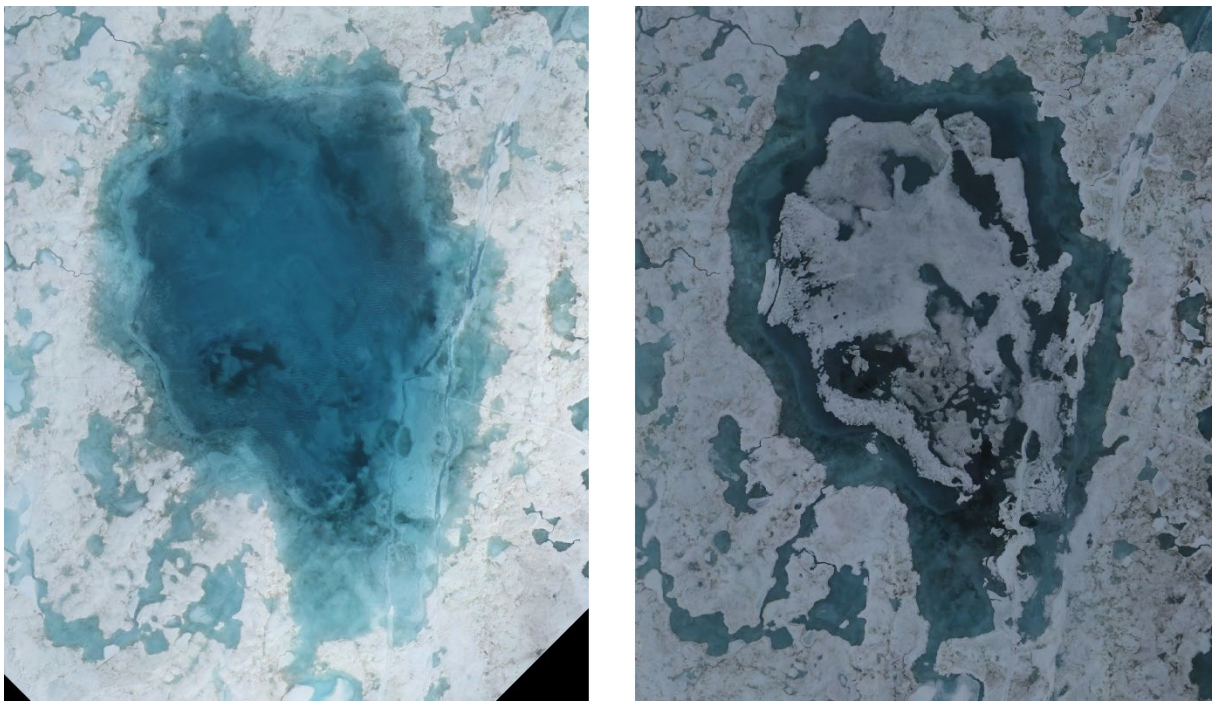

Fig. 4.12.4: *RGB orthomosaics of Mystery Lake, (left) before drainage on 07 July and (right) after drainage on 17 July. Photo credit: Gerit Birnbaum.*

4.12.4 Data management

All data and their availability conform to the MOSAiC data policy (see Chapter 9 APPENDIX).

All instrument deployments were logged in DShip, and all data, including notes and documentation photographs were uploaded onto MCS.
The data of each half day (AM/PM) was zipped, and uploaded under the respective device operation folder of the main instrument (mostly cau_boeoetle_1, cau_stickle_1). All other instruments are either SensorWeb-child-devices of the main instrument (e.g. spectrometers), or co-deployed (e.g. cameras). Co-deployments have a readme-file in their respective device operation folders, pointing the user to the collective *.zip.
Data will be stored at the PANGAEA data repository (World Data Center PANGAEA
Data Publisher for Earth & Environmental Science www.pangaea.de. All data are handled, documented, archived and published following the MOSAiC
data policy.

4.13 Events: Freshwater Lens and False Bottom

Luisa von Albedyll[1], Maddie Smith [2], Ian Raphael [3], Ilkka Matero[1], Benjamin Lange[4]

[1]AWI
[2]UW Seattle
[3]Dartmouth
[4]NPI

4.13.1 Objectives

Ice ablation during spring and summer results in substantial amounts of freshwater that gathers in ponds at the ice surface. Drainage of those ponds releases freshwater into the ocean, which is then entrained into the mixed layer. There is, however, evidence that a part of this melt water re-freezes underneath the ice due to double diffusion at the interface between the seawater and the freshwater, which are both at their respective freezing points (Eiken 1994). Those "false bottoms" contribute to summer ice growth and can affect the colonization of the ice by sea-ice organisms. In addition, they are evidence for a pronounced freshwater lens whose presence strongly reduces gas exchange between ocean and atmosphere. Therefore, the temporal and spatial abundance of of freshwater and false bottoms under the ice and in leads are of great interest for all groups present on MOSAiC. This event-based research focuses on two main questions:

- How abundant are freshwater lens' and false bottoms under the MOSAiC floe?
- What parameters control their occurrence?

In addition, we will analyse how the presence of freshwater affects the ice mass balance measurements conducted with instruments based on the strong conductivity difference between ice and seawater (GEM2, EM-Bird).

4.13.2 Leg 4 Under-ice freshwater lens and false bottom

We first observed false bottoms at the ablation stakes installation close to Met City (Reunion stakes; section 4.8) and in the first-year ice (FYI) cores taken at the FYI site (see Section 4.1 Coring). Thick, freshwater lens were reported from the ROV and ADCP hole. Based on those observations, we selected three areas of the floe in which to perform systematic drill hole transects (Fig. 1). The first area (Lines 0-2) was located close to Met City and was enclosed by larger ridges at two sides, but was primarily relatively level first year ice. The second area (Lines 3-4) was in the FYI part of the floe and extended from almost the floe edge towards the center of the floe. The third area drilled was an albedo line dominated by second-year-ice. In addition, coring activities included sampling and sectioning of false bottoms of FYI weekly. For details on their activities, see Section 4.1 and Chapter 6.

4.13.3 Data sets

In order to understand the abundance of the false bottoms, we conducted drilling transects along 6 lines, spanning 900 m in total (Fig. 1, Table 4.13.1). Point spacing varied between 5 and 30 m, resulting in 130 total thickness measurements. In each drill hole, we measured the thickness of the sea ice, gap, and false bottom using a thickness tape and an aluminum snow probe with an angle bracket attached to the bottom. The hook allowed us to determine the depth of the interfaces between the sea ice and gap layer, gap layer and false bottom and false bottom and ocean.

We used a YSI Professional temperature and salinity probe to measure temperature-salinity profiles of the water within and below the ice in 34 holes. The YSI probe was attached to a measuring tape that was used to determine the measurement depth. In some cases, we measured temperature and salinity of the gap water before breaking through the false bottom. This way, we could differentiate between gaps created due to rafted blocks filled with sea water and freshwater lenses occurring due to false bottoms.

The temporal evolution of the freshwater layer close to Alli's Ridge was captured by a DTC (Digital thermistor chain) unit with a vertical resolution of 2 cm. A DTC unit has the ability to record air, snow, ice and ocean temperatures, as well as recording the temperature change after a period of active heating. The latter functionality allows for determining the state of the medium (liquid, solid, gas), and thus for tracking the vertical evolution of snow, ice and water interfaces in addition to estimating the thickness changes of each layer. The DTC unit in question was installed on 7 February, and seven other DTCs (see section 4.8 and 4.8.2.2) that were deployed at the former MOSAiC central observatory were still recording data in July. Together, these units allow for evaluating the temporal evolution of the freshwater layer and potential freshwater lenses at remote sites in addition to the unit at Alli's Ridge.

In addition to those three main data sets, we collected complementary data, including six ice cores and water collection (under-ice and void space) for salinity and dO18 analysis and two for optics. We conducted GEM surveys over the drill lines and recorded snow and surface properties. GoPro videos through core holes provide visual records of freshwater lenses and false bottoms. Castaway profiles in some of the coring holes provide measurements of temperature and salinity deeper than possible with the YSI. The combination of these data sets will allow us to characterize the freshwater lens and false bottoms, understand their spatial abundance, and analyze the influence of parameters such as ice thickness or ponding on the formation of the false bottom.

***Tab. 4.13.1**: An overview of the sampled lines sets to the drill hole transects*

Line	Description	Length	Data sets	Sampling Dates
0	Reunion Stakes to Bean Pole Stakes	109	• 20 drill hole measurements • YSI • GEM • Cast away	14/07/2020 16/07/2020
1	Across MetCity Meltpond, perpendicular to line 1,	28 m	• 3 drill hole measurements • YSI • Cast away	16/07/2020
2	Reunion Stakes to Alli's ridge	250 m	• 23 drill holes • YSI • GEM • Magna-Probe	19/07/2020
3	Simba buoy to Drone Bones Stakes	280 m	• 35 drill holes • GEM • Surface thickness measurements + photos • 5 Cores • Go-Pro Videos	25/07/2020
4	Simba, perpendicular to line 3	20 m	• 5 drill holes • GEM • 1 core	25/07/2020
5	Albedo line (Root Beer Barrel) extended to floe edge	207 m	• 44 drill holes • GEM • YSI • 2 cores	27/07/2020 29/07/2020

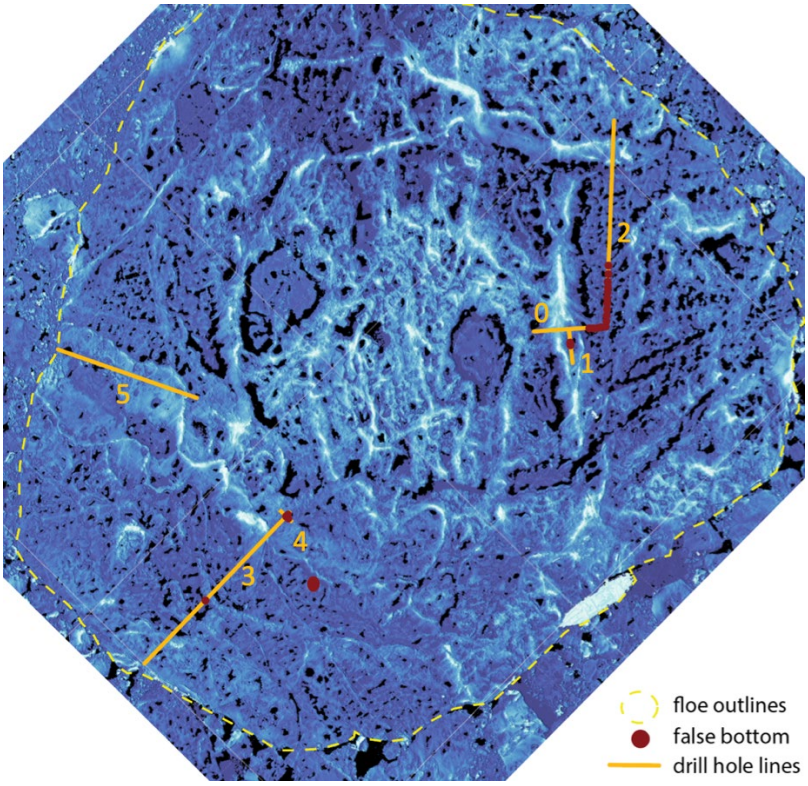

Fig. 4.13.1: *Location of drill lines 0 – 5 and the occurrence of false bottom.*

4.13.4 Preliminary results

4.13.4.1 False Bottoms

In total, 20% of the surveyed drill holes had false bottoms. To differentiate between false bottom associated with freshwater and gap layers resulting from ridging, we made salinity and temperature measurements within the gap layer prior to drilling all the way through. In case those observations were not available, we excluded all outliers of false bottom thickness that were thicker than 40 cm.

Figure 4.13.1 shows the spatial distribution of false bottoms on the MOSAiC floe. False bottoms were spatially concentrated in two areas: close to Met City, and along line 3 and 4 in the first year ice area. No false bottoms associated with a freshwater lens were present along Line 5. The majority (60%) of false bottoms occurred under ice between 1 and 1.6 m thickness.

Figure 4.13.2 shows an example of false bottom thickness along line 2 measured on 19 July. False bottoms were observed at nearly all holes along the first 100 m of the line. We hypothesize this may be related to trapping of freshwater due to the thicker ice around 120 m, but further investigation is necessary to understand the controls on freshwater and false bottom growth.

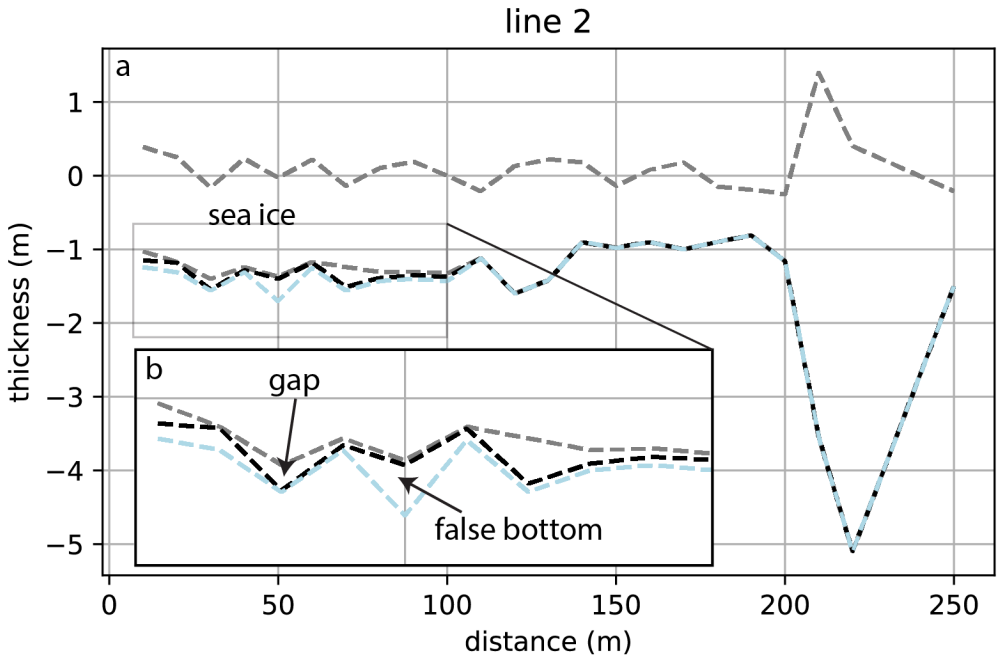

***Fig. 4.13.2**: Sea ice, gap and false bottom thickness along line 2. Sea ice surface (grey line), sea ice bottom (black) and false bottom (blue), when present, are shown relative to sea level. Panel b shows a zoom-in of a for the section of the line where a false bottom was found.*

4.13.4.2 Freshwater Lens

Figure 4.13.3 shows an example of YSI measurements along a drill line (Line 0) to observe the distribution of the fresh lens. In future analysis, these measurements will be used to calculate the thickness of the layer. We will investigate the relationship of the fresh layer's presence and thickness with other parameters such as ice type, thickness, and pond proximity, as well as the false bottom observations.

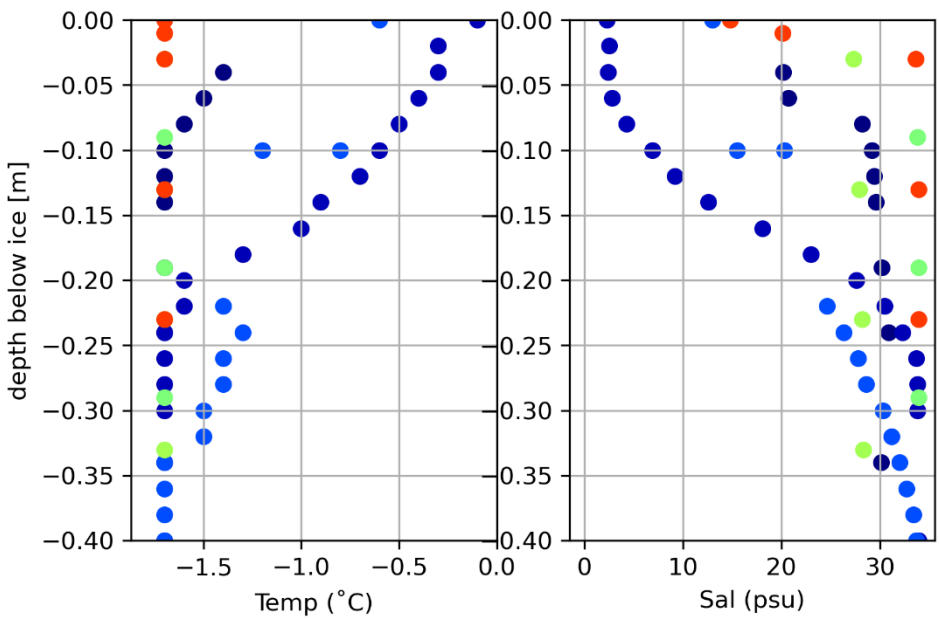

***Fig. 4.13.3:** Example of results from YSI transect on Line 0. Temperature (left) and salinity (right) are shown as a function of the depth below the ice bottom (excluding false bottom, if present). Points are colored by the position on the line.*

Bottom-ice salinities were higher for the three cores taken from the bottom of ice with no false bottom present compared to bottom-ice salinities from the three cores taken where the false bottoms were present (Fig. 4.13.4). Void water samples had lower salinities than the under-ice water indicating the presence of freshwater (Fig. 4.13.4), which is consistent with results from the YSI profiles (Fig 4.13.3.).

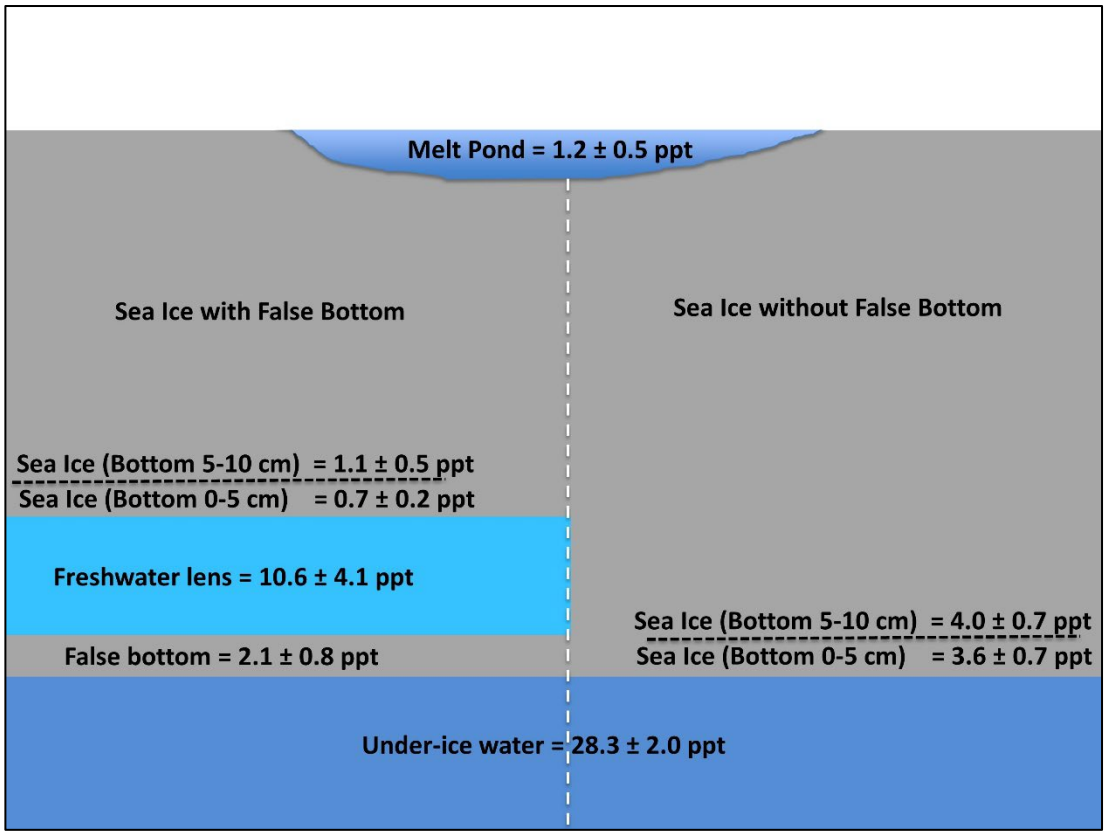

Fig. 4.13.4: *Schematic of false-bottom ice (left) and sea ice without false-bottoms present. Also, shown are the mean ± sd of salinities for three ice cores at false bottom locations and three ice cores from locations without false bottoms. Cores were taken along lines 3 and 4. False bottom samples and void water samples were taken from 3 locations. Under-ice water from four locations and melt ponds from four locations.*

GoPro videos provided visual confirmation of the presence and extent of the fresh layer. Figure 4.13.5 shows an example of this, observed on 29 July at Line 5. The halocline at the bottom of the fresh lens is seen as a shimmer, and appears to be extensive under the level ice in the vicinity.

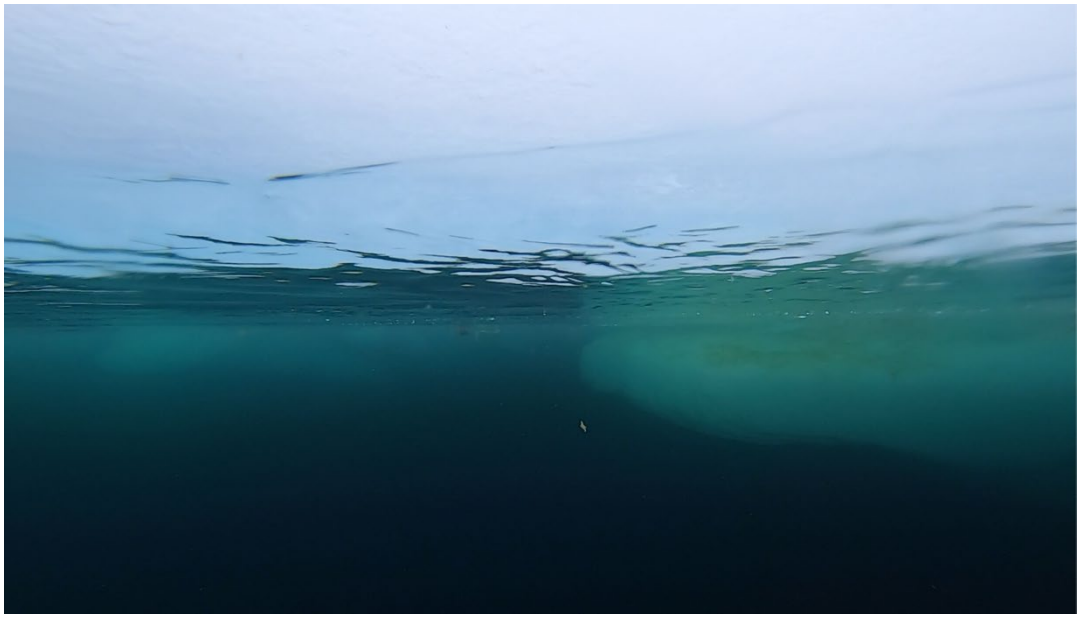

Fig. 4.13.5: *Screenshot from GoPro video taken on 29 July through core hole on Line 5.The shimmer indicates the halocline of the fresh lens, as seen from below.*

4.13.5 Data management

All data and their availability conform to the MOSAiC data policy (see Chapter 9 APPENDIX). All device operations were logged in the AWI sensorweb portal and all sensor raw data files are stored in platform section of MCS. Final geophysical parameters will be made available via the workspace section of MCS and archived in the PANGAEA data repository according the MOSAiC data policy. All drill hole and YSI data is found in one excel sheet archived under PS122_4_47-174.

Device URNs:

GoPro: **camera**:uw_gopro

YSI: **pack_ice:ice_ps**:dart_ysi

Castaway: **pack_ice:ice_ps**:uw_castaway_cc1415003

Thickness drill: **pack_ice:ice_ps**:si_2iauger

References:

Eiken (1994): Structure of under-ice melt ponds in the their effect on the sea-ice cover, Limnol. Oceanography, 39(3), 694-702

4.14 Supporting observations - Sea Ice observations

Ilkka Matero[1], Madison Smith[2], Luisa von Albedyll[1], Gerit Birnbaum[1], Melinda Webster[3], Igor Sheikin[4], Julia Regnery[1], Felix Linhardt[5], Ian Raphael[6], Marcel Nicolaus[1] (not on board), Jennifer Hutchings[7] (not on board)

[1]AWI
[2]UW Seattle
[3]Uni. of Alaska Fairbanks
[4]AARI
[5]CAU Kiel
[6]Dartmouth College
[7]Oregon SU

4.14.1 Objectives

Visual observations of ice from airplane or ship are an integral part of sea ice monitoring for operational and research support [1]. These observations provide information about sea ice morphology that is not obtainable or ambiguous in remotely sensed data [1].

4.14.2 Work at sea

During MOSAiC, the ice observations are done hourly while RV *Polarstern* and the support vessels are moving through ice, in contrast to daily measurements while they are stationary. The aim of these observations is to describe the surrounding conditions over a 10-minute period within a radius of 1.5 nautical miles around the vessel. The list of conditions that are recorded is comprehensive, and includes for example ice concentration, floe size, fraction of ridged ice, ice thickness, amount of ice algae present and melt pond coverage. In addition, several parameters describing the weather conditions and macrofauna present are also included as part of the procedure. Due to the subjective nature of the observations, new observers were initially paired with people with more experience in order to ensure consistency throughout the MOSAiC drift.

4.14.3 Preliminary results

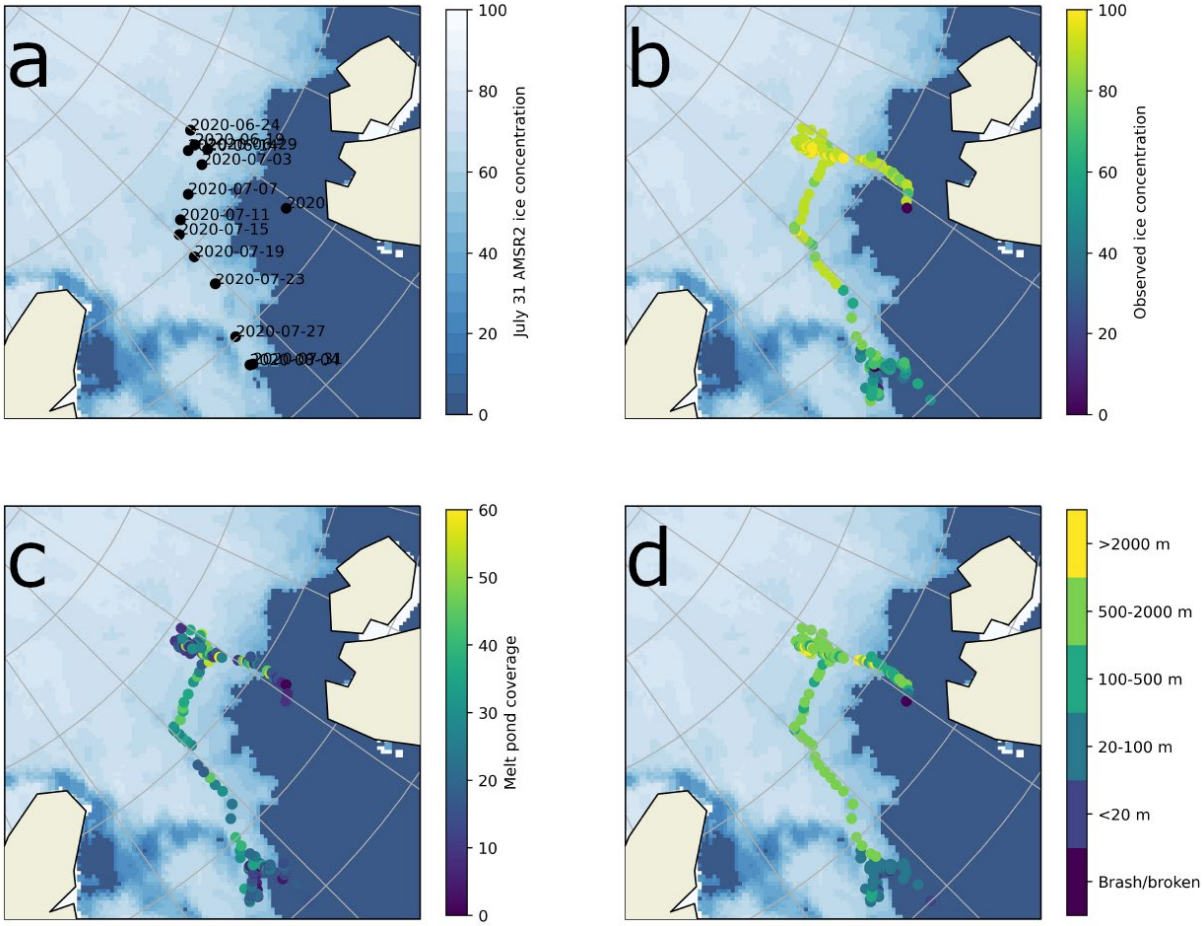

Fig 4.14.1: *Summary plots of ice observations done throughout Leg 4 of MOSAiC (PS122-4). Overlain on AMSR2 ice concentration map from 31. July, 2020. (a) Vessel locations in 4 day intervals. (b) Observed total ice concentration. (c) Total melt pond coverage. (d) floe size category of the observed primary ice type.*

4.14.4 Data Management

All data and their availability conform to the MOSAiC data policy (see Chapter 9 APPENDIX). Data will be stored in the PANGAEA data repository: World Data Center PANGAEA Data Publisher for Earth & Environmental Science www.pangaea.de. All data are handled, documented, archived and published following the MOSAiC data policy. DOIs will be communicated to PANGAEA for later access via the future MOSAiC Data Portal.

References

[1] Hutchings, J., Delamere, J., Heil, P. (2018), The Ice Watch Manual (draft on board)